UNIVERSITY OF ZULULAND

Synthesis of VO_2 Nanostructures for Infrared Modulation Applications

Dissertation presented in fulfillment of the requirements for the degree of Magister Scientae to the:

Department of Physics & Engineering

Faculty of Science and Agriculture

University of Zululand

Supervisor: Prof. M. Maaza
Materials Research Department
IThemba LABS

Co-supervisor: Prof. O. Nemraoui
Department of Physics and Engineering
University of Zululand

By

Hastings Mthobisi Cele

November 2009

DECLARATION

I, the undersigned, hereby declare that the work contained in this thesis is my own original work and that I have not previously in its entirety or in part submitted it at any university for a degree.

Signature: ……

Date: ……

ABSTRACT

Vanadium pentoxide (V_2O_5) is a thermochromic material, meaning it can change is colour upon heating. It has potential application in the fields of lithium-ion batteries, actuators, catalysis (mostly in organic reactions and a precursor for the other vanadium salts) and sensors. In this project, the V_2O_5 sol-gel is used as a precursor of producing thermochromic vanadium dioxide (VO_2) thin films. The consolidated nano- and microcrystal materials based on vanadium (IV) oxide have attracted various fundamental and applied interest due to its unique optical properties related to the Mott's type 1st order transition exhibited at about 68°C. The most interesting property of VO_2 coatings is to transmit in the visible light region as well as infrared region. This makes the good coating for smart windows such as windscreens of the cars, windows of the dwellings as well as infrared shutter in laser laboratories.

In synthesis of the film, ultrasonically cleaned normal glass and silicon (111) substrates were used for the deposition of V_2O_5 film. The low cost method used in synthesis of the film is soft chemistry, which is well-known as *valence reduction method.* The reduction of V_2O_5 was done using three techniques: reduction using 10 % ***H_2*** mixed with 90 % of Ar, reduction using 50 % of ***CO*** mixed with 50 % with CO_2 and reduction using laser ablation. During valence reduction, V_2O_5 was reduced into different vanadium oxides before VO_2: **V_2O_5**; V_3O_7; V_4O_9; V_6O_{13}; **VO_2**. The produced V_2O_5 films were studied under atomic force microscope (AFM) and scanning electron microscope (SEM) techniques to see the surface morphology and compare roughness, the changes of the pure V_2O_5 crystals with VO_2 crystals. There are some other characterization techniques used in this project including: EDX, XRD, RBS, ERDA, FTIR, UV-Visible, and Raman. The main aim of producing VO_2 films was to study them for FTIR modulation applications.

ACKNOWLEDGEMENTS

First and foremost, I express my sense of gratitude to the almighty, the Lord, my provider for extending my days of living and experience my challenges.

It is with a feeling of sincere gratitude that I acknowledge the financial assistance which I received from the NRF, iThemba LABS and the Research Committee of the University of Zululand.

I cannot afford not to acknowledge my flexible supervisor, Prof. M. Maaza, iThemba LABS, especially for being always available and show me the light when I lose hope.

I would like to deeply thank my co-supervisor, Prof. O.M. Ndwandwe, Head of Physics Department, University of Zululand, for fruitful ideas of obtaining good results.

I greatly appreciated a support from Prof. O. Nemraoui, helping in synthesis of the samples.

I greatly appreciated a support from Dr. A. Nechaev during write up of this dissertation.

I would also like to use this opportunity to express my gratitude to people from iThemba LABS:

- Dr. R. Nemutudi, Head of Materials Research Group, iThemba LABS-Cape Town, for making the facilities at MRG available for some of the experiments.

- Dr. R. Butcher, for helping me with XRD measurements.
- Mr. P. Sechogela, for helping me with RBS and ERDA measurements.
- Dr. M. Nkosi, for helping in AFM imaging.
- Dr J.B Kana Kana, for helping in UV-Visible and new ideas.

I would like to thank Timothy Lesch, UWC, for helping with FTIR measurements.

I would like to thank Miranda Waldron, UCT, for helping with SEM measurements.

I greatly appreciate the support, endless encouragement from the mother of my son: Nokwazi Ntuli.

I would definitely like to thank my fellow students: C. Mtshali, C.L Ndlangamandla, B.P. Zulu, Z.M khumalo, C.J. Masina, J. Sithole, B.D. Ngom and A. Malape.

I like to express my gratitude to Takalani Madima for her love, friendship and inspiration; nothing was possible without her encouragement and support.

I would like to thank my best friend Ndabenhle Mbali, for his encouragement, love and friendship.

Finally, I would like to express my extreme gratitude to my precious family for giving me endless love and support: My grandmother, the late grandfather, my mother, my aunt, my uncle, my two brothers; Nhlanhla and Nkos'khona, my cousin Mlondi. My children: Senamile and Esihle.

Ngibonge koNdosi, oMagaye, Dubandlela…ngithi nje Vico!

TABLE OF CONTENTS

LIST OF FIGURES

List of Tables

CHAPTER 1 –Literature Review

1.1 Introduction

Nanotechnology is the design, fabrication and use of nanostructured systems, and the growing, shaping or assembling of such systems either mechanically, chemically or biologically to form nanoscale architectures, systems and devices. This project is based on reduction of V_2O_5 sol-gel to VO_2 nano structures for infrared application applications. Vanadium exists in a number of oxide forms, the di-, sesqui- and pentoxides (VO_2, V_2O_3 and V_2O_5). Vanadium oxygen systems (V_2O_5, VO_2) have been studied extensively by theoretical and experimental techniques. They show metal-semiconductor transition, which implies an abrupt change in optical and electrical properties. That is why this oxide is used in thermal sensing and switching. Especially vanadium oxide (V_2O_5), as a wide band gap and n-type semiconductor material, was widely investigated because of its interesting electrochemical performance, is integration in lithium secondary batteries, and its thermochromic and electrochromic properties [1].

Focusing on VO_2, it is a material that displays thermochromic properties, in that it undergoes a thermally induced, semiconducting- to-metallic phase transition that results in a dramatic change in optical transmittance and reflectivity in regions of the spectrum that are major contributors to solar heating. As such, thermochromic VO_2 coatings have potential application in the area of energy-efficient glazing, as well as other applications that exploit thermally driven changes in dielectric constant. Considering the specific nature of the thermally driven phase transition, at a temperature of 68 °C, bulk, crystalline, semiconducting VO_2 in a monoclinic form undergoes a structural change to a metallic state that possesses a tetragonal rutile structure characterized by chains of equidistant V atoms along the tetragonal *c*-axis. The phase change results in a

high transmittance of infrared (IR) below T_c and a high reflectance of IR above T_c [1, 2].

Research problem:

According to the investigations of smart materials, vanadium dioxide thin film is one of the promising coatings to conserve energy. In this project, vanadium dioxide thin films are prepared for the infrared radiation (IR) studies because of its properties such as electrical, electronical, optical and technological applications which will be discussed also in this chapter. Many researchers tried to produce VO_2 coatings under vacuum condition which is difficult to have large vacuum in industries. The aim of this project is the synthesis and optimization of an intelligent nano-VO_2 coatings for solar radiation self modulation. The synthesis of these coatings should be of low cost to reduce expenses and effective to industries.

The VO_2 films will be produced from $V_2O_5.nH_2O$ (Sol-gel). The bare glass will be used as the main substrate to deposit V_2O_5 thin films. According to literature, the VO_2 is known as a thermochromic material-meaning it can change its color upon heating. This kind of material can change its crystal structure during temperature transition. Normally, VO_2 is monoclinic and changing to tetragonal after satisfying some condition related to transition temperature. Therefore, VO_2 coatings keep rooms and offices cool and excessive electricity use during the summer months which can lead to ESKOM load shedding.

1.2 Physical properties of V_2O_5 and VO_2

Vanadium is a transition metal with an atomic number 23 and atomic mass of 50.9414g.mol^{-1}. The melting point of vanadium is 1910 ^{0}C and its boiling point is 3407 ^{0}C. There are five isotopes of vanadium. The vanadium is a rare, soft, ductile gray-white element found combined in certain minerals and used mainly to produce certain alloys. The protective film of oxide on the surface of vanadium makes it to resist. The common oxidation states of this element include +2, +3, +4 and +5 [3]. After vanadium has been oxidized, it produces all the vanadium oxides with different colours, transition temperature, melting point and boiling point.

1.2.1 Vanadium pent-oxide

Vanadium (V) oxide is a yellow to red crystalline powder with the chemical formula V_2O_5 and also known as vanadic acid [4]. The V_2O_5 is thermochromic material a transition temperature of about 375 ^{0}C, melting temperature of 690 ^{0}C. It is a poisonous orange solid, because of its high oxidation state, is both an amphoteric oxide and an oxidizing agent. This thermochromic material has orthorhombic crystal structure [5]. It is used as a catalyst in various organic reactions and as a starting material (*precursor*) for other vanadium salts. It has been shown that upon heating V_2O_5 reversibly loses oxygen [4].

1.2.2 Thermochromic Vanadium dioxide

The word thermochromic can be broken into two Greek words *thermos* and *khroma* meaning "warm" and "colour", respectively. Thermochromic vanadium dioxide is the kind of material that changes its colour upon heating. Its optical

properties also changes with temperature [3]. In this project, vanadium is chosen because of the tendency of changing in the infrared radiation wavelength region.

There are other vanadium oxides except vanadium dioxide. These oxides are shown in Table 1-1 with their transition temperature T_t, melting temperature T_m, color, and crystal structure. Phase diagram in Figure 1-1 is also giving the clear understanding of vanadium oxides and in which temperatures can they change one phase to another. In the entire oxides only vanadium dioxide which has the transition temperature 67 ^{0}C near the room temperature (25 ^{0}C). The other vanadium oxides are much less than the room temperature and others are much greater.

The behavior of VO_2 at room temperature is semiconducting and highly IR transparent [1-3]. When VO_2 is heated above its transition temperature, it changes its properties becoming metallic-electrically conducting and IR reflecting or absorbing.

Material	System	T_t (^{0}C)	T_m	Color
$VO_2(M_1)$	Monoclinic	67	1967	Dark blue
V_2O_3	Monoclinic	-105	1970	Black
$V_5O_9(R)$	Tetragonal	-138		
V_6O_{13}	Monoclinic	-123	700	
VO		-147		Grey
V_3O_7	Monoclinic			
V_2O_5	Orthorhombic	375	685	Yellow

Table 1-1-1: *The different types of vanadium oxides [3].*

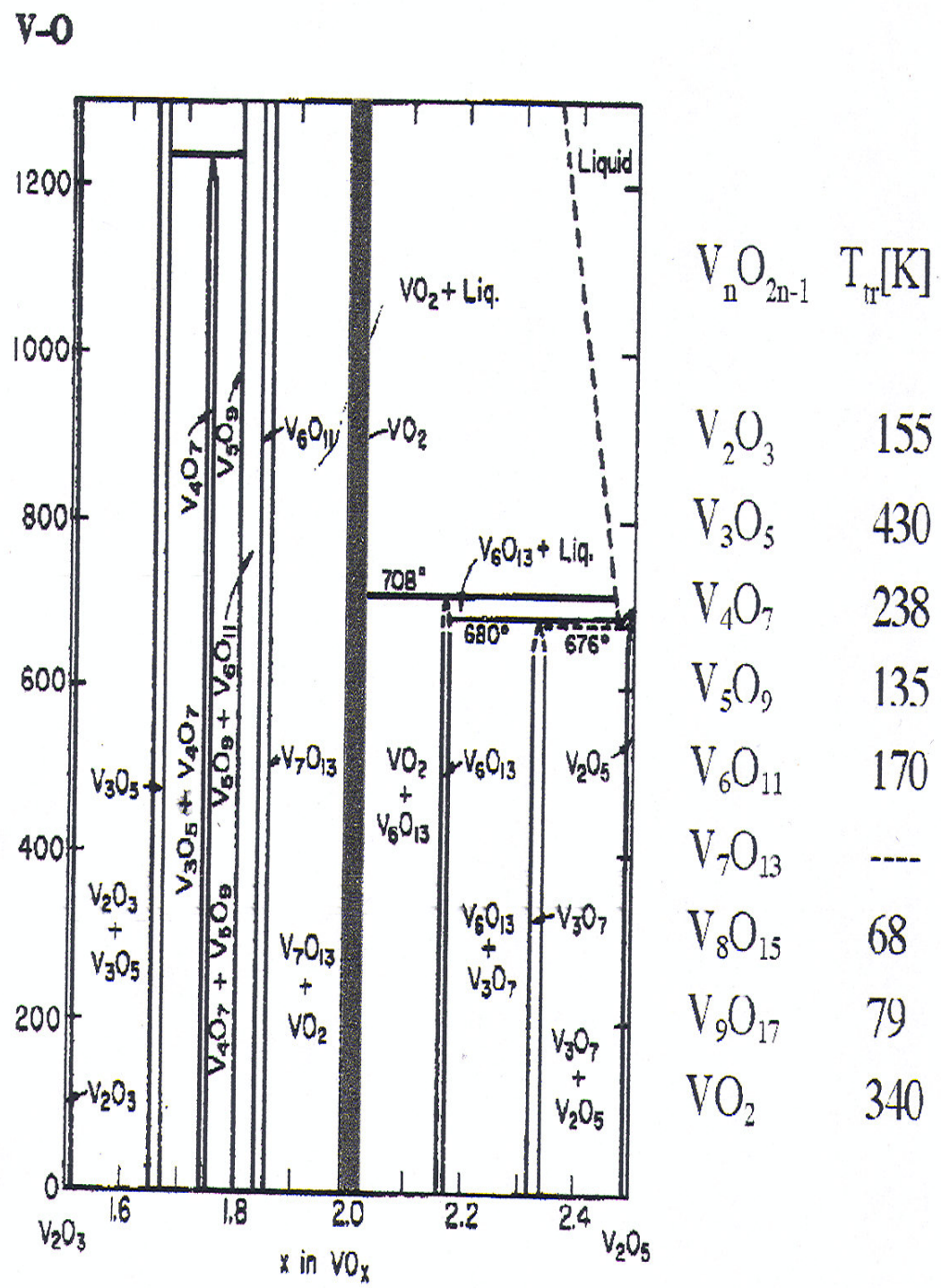

Figure 1-1: *Phase diagram of vanadium oxides with the corresponding transition temperatures* [6]

1.3 Methods of Preparing Pure Vanadium (IV) Oxide Films

The deposition of vanadium dioxide can be done using the following methods:

- Chemical vapor deposition (CVD)
- Sol-gel method
- Physical vapor deposition (PVD)
- Atmospheric pressure chemical vapor deposition (APCVD)

The produced thin films can be used as IR shutter (in blocking some of infrared radiation). The advantage for using thin films is that they resist or survive the stresses caused in cycling between the two polymorphs of vanadium oxide involved in the in metal-to-semiconductor transition (MST), which is known to cause single crystals to crack and disintegrate after few cycles [7]. The experiment done by [7] in sol-gel method showed that a vanadium (IV) oxide thin film could be cycled 10^8 times without any degradation in electrical contrast.
Sol-gel spin or dip coated takes more application –based approach while VO_2 films prepared by PVD methods are generally used for fundamental studies of the properties of the thin films. In addition, CVD can be used in preparation of thin films of vanadium (IV) oxide for commercial applications.

1.3.1 Chemical Vapor Deposition (CVD) method

This method is considered as the final method for thin films preparation of VO_2. The model method that can be used in producing thin films on high throughput glass substrates is atmospheric pressure chemical vapor deposition (APCVD). Un-doped (pure) vanadium (IV) is produced onto glass substrates by CVD [8]. Vanadyl tri (*iso-propoxide*) or vanadyl tri (*iso butoxide*) [9] have been used as a

single source precursors for the CVD of vanadium(IV) oxide films, usually if the resultant of vanadium(V) oxide thin films has been reduced.

Some of the vanadium oxides can be deposited by using two compound; VCl_4 or $VOCl_3$ with an oxygen source such as water (H_2O) or ethanol (CH_3CH_2OH) [10] with carbon dioxide (CO_2) [11]. The vanadium oxides, which are produced from the precursor VCl_4 or $VOCl_3$, can be reduced to form vanadium (IV) in a suitable atmosphere. Other precursors which can be used in preparing vanadium(IV) oxide films from APCVD are acetylacetonate, $V(acac)_3$ and APCVD method followed by slow post deposition cooling [12], from vanadium(IV) acetylacetonate, $V(acac)_4$, by a pyrolysis method in a controlled atmosphere [13]. The two materials vanadyl acetylacetonate and $VO(acac)_2$ have been used to prepare the metastable VO_2 and their crystal structure can be converted into tetragonal phase by annealing in argon at 500 ^0C [14].

1.3.2 Sol-gel method

This method thin film is formed by dip or spin coating substrates with solutions of metal alkoxides. The coatings are suitably treated to form a thin film of the required metal oxide. The initial vanadium (IV) oxide has partially hydrolyzing in the initial coating and this can be reduced by heating the film in a reducing atmosphere to form crystalline vanadium (IV) oxide. The addition of extra layers easily achieves the control of the thickness of the film. Sol-gel has been used extensively to prepare vanadium (IV) oxide thin films in a pure or doped form due to its simplistic nature. Most researchers regard vanadyl tri (iso-propoxide) as the most widely used precursor for sol-gel preparation of vanadium (IV) oxide, followed by vanadyl tri(tertamyloxide). The whole of the first row d-block elements and much of the second and third row d-block elements have been doped into vanadium (IV) oxide using sol-gel method [15].

Takahashi et al [16] reported that there is a new method using polyvanade sols that can be used in metallic vanadium dissolved in 30% H_2O_2 and heated to form

a hydrosol. The hydrosol could then be spin coated onto a suitable substrate and then reduced in a hydrogen atmosphere. There are two elements (Tungsten and Molybdenum), which could be introduced in metallic form at the initial dissolution stage [15, 16].

1.3.3 Atmospheric Pressure Chemical Vapor Deposition (APCVD) Method

This method uses mechanical or thermodynamic means to produce a thin film of solid. In APCVD some of the steps are associated with the one of CVD process:

- *Transport of the reactive species to the reaction site*
- *Gas-phase reaction*
- *Adsorption onto the substrate surface*
- *Nucleation on the substrate surface*
- *Reaction and desorption of byproducts*
- *Film growth*

In the APCVD experimental setup, the reaction chamber must be at or near the atmospheric pressure. The required precursors must be low-melting solids or volatile liquids and they can be transported to the reaction by hot, inert carrier gas [17]. The high temperature of the substrate is required in order to initiate the deposition.

In the reaction chamber two types of reactions may occur: homogenous reactions occurring entirely in the vapor phase and heterogeneous reactions occurring at the vapor solid surface interface [18]. In the cold wall reactors, the homogenous reactions and heterogeneous reactions at the reactor walls are suppressed owing to the lower heat input to the system. Vapor-substrate reactions are regarded as the most important process [19].

1.4 Reduction of V_2O_5 to VO_2 using gases

This kind of method requires the reducing agent which will reduce the excess oxygen by forming another by product (e.g. H_2O, CO_2). In this case, hydrogen and carbon monoxide are the most suitable reducing agent. Vanadium (V) oxide with it properties can be reduced to vanadium (IV) oxide with different properties and applications.

1.4.1 Reduction of V_2O_5-VO_2 in Mixture of Hydrogen with Argon

Hydrogen is the one of the gases used to reduce oxygen content from the metal oxides. In this project, hydrogen was used to remove excess oxygen from V_2O_5 in order to produce VO_2 film. The produced V_2O_5 film can be reduced to VO_2 at 500 ^oC in argon gas, containing 4% hydrogen. Under these conditions, the brown film turns brown film turns grey and converts to mainly V_2O_3. In order to obtain VO_2, a second heat treatment is carried out at 450 ^oC in argon gas, bubbling through water. The water vapor treatment provides a slightly oxidizing atmosphere, which leads to the formation of a stable blue colored VO_2 **[20]**.

1.4.2 Reduction of V_2O_5-VO_2 Mixture of carbon monoxide with carbon dioxide

The mixture of carbon monoxide with carbon dioxide was used in this project as a second gas to reduce excess oxygen from V_2O_5. The use of V_2O_5 for the oxidation of SO_2 is part of a well established industrial process. The oxidation process may be understood in terms of the redox reaction given by:

$$V_2O_{4(s)} + \frac{1}{2}O_{2(g)} \rightarrow V_2O_{5(s/l)} \qquad (1.1)$$

The V_2O_5-V_2O_4 system is ill-defined. On the V_2O_5 side of the V_2O_5-V_2O_4 subsystem, a eutectic temperature is indicated at 660°C and at a composition of 15 mol% V_2O_4. Liquidus temperatures at compositions 28.5, 35, 36.6, 37.8, and 40.0 mol% are respectively 685°C, 700°C, 750°C, 800°C and 850°C [21]. The flow rate of the gas should be between 15 and 110 ml/min [21].

1.4.3 Valence reduction of V_2O_5 to VO_2 and the phase formation

Yuan Ningyi [22] managed to convert highly orientated V_2O_5 film to VO_2 film by using sol gel method. The V_2O_5 films were annealed at 400 ^{0}C and the pressure was below 2Pa in air. It has been mentioned that vanadium has four oxidation states (+2, +3, +4, +5) and vanadium in vanadium (V) oxide has valence of five while vanadium in vanadium (IV) has valence of four. This implies that V_2O_5 can be converted to VO_2 by reducing the oxygen content, and valence of vanadium is reduced from +5 to +4. Vanadium pentoxide can form other phases before VO_2 is produced.

$$\mathbf{V_2O_5} \rightarrow V_3O_7 \rightarrow V_4O_9 \rightarrow V_6O_{13} \rightarrow \mathbf{VO_2}$$

The general formula for the phases between V_2O_5 to VO_2 is given by: V_nO_{2n+1}; (n=*2-4, 6*).The series of phase between V_2O_3 to VO_2 (and V_2O_5 to VO_2) are called Magneli phases and their general stoichiometry formula [22]:

$$V_nO_{2n-1} = V_2O_3 + (n\text{-}2)\ VO_2 \qquad \text{where} \quad 3 \le n \le 9 \qquad (1.2)$$

1.5 Structural properties of V_2O_5 and VO_2

Vanadium oxides have different crystal structures with different space group. In this investigation, two crystal structures of vanadium (V) Oxide as a precursor and vanadium (IV) Oxide will be studied. This includes the lattice parameters and the V-O bonding.

1.5.1 Orthorhombic structure of V_2O_5

This thermochromic material has orthorhombic crystal structure; and belongs to P_{mnm} space group with a lattice parameters a=11.510Å, b=3.563Å, c=4.369Å, where the b and c axes are often interchanged [5]. The vanadium atoms form five bonds with oxygen V-O bond lengths vary from 1.585 Å to 2.021 Å: one with O_1 atoms, one with the O_2 atom and three with the O_3 atoms [23].

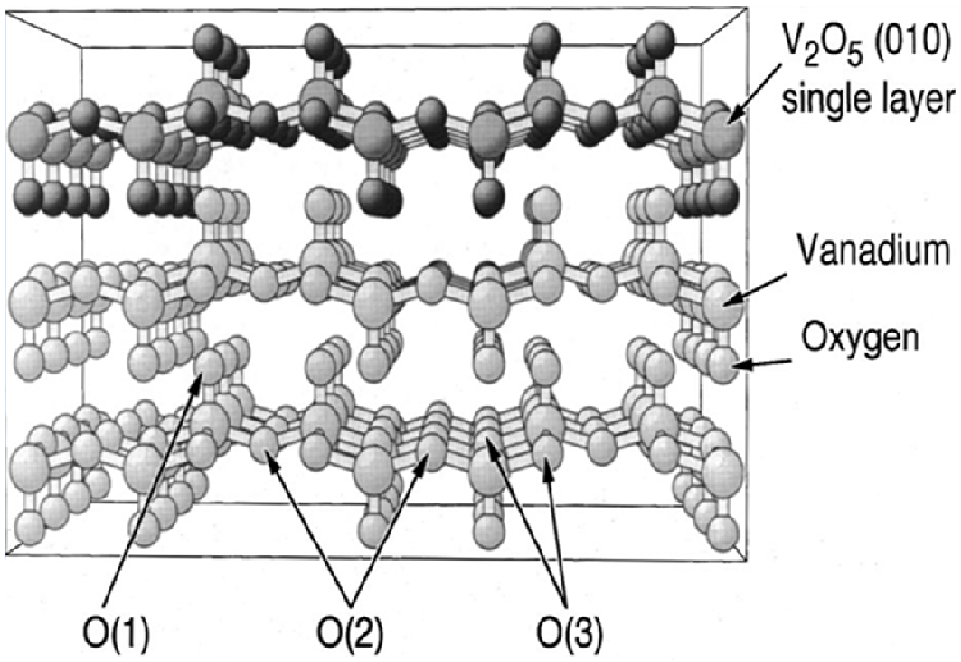

Figure 1-2: *Crystal structure of the orthorhombic V_2O_5 with netplane stacking along the (010) direction. Vanadium and inequivalent oxygen centers, singly coordinated O (1), doubly coordinated O (2), and triply coordinated O (3), are marked accordingly. All atoms of the V_2O_5 (010) single-layer slab at the top are emphasized by darker shaded balls [23].*

1.5.2 Rutile structure of VO_2

The metal VO_2 is regarded to have a rutile structure if it is a simple tetragonal lattice with space group $P4_2/mnm$ [6]. The metal atoms are located at the Wyckoff positions (2a): (0,0,0), (1/2,1/2,1/2) and the oxygen atoms are located at the positions (4f): ±(u,u,0), ±(1/2+u, 1/2-u,1/2). According to McWhan the lattice constants and the internal oxygen are: a = 4.5546 Å, c = 2.8514 Å [6]. The rutile structure is shown in Figure 1-3.

1.5.3 Monoclinic M_1 structure of VO_2 ($T<T_t$)

At room temperature, the monoclinic M_1 VO_2 has a simple monoclinic lattice with space group $P2_1/c$ [6]. In the IR-transparent low temperature, Vanadium (IV) oxide has a monoclinic crystal structure and semiconducting. According to Andersson the monoclinic lattice parameters are a = 5.743 Å, b = 4.517 Å, c = 5.375Å and the angle is β = 122.61 °. Lateron, Longo and Kierkegaard reported that the lattice parameter and monoclinic angle are a = 5.7517 Å, b = 4.5378 Å, c = 5.3825Å and β = 122.646 ° respectively. The crystal structure is shown in Figure 1-4. The unit cell consists of four formula units. The metal atoms and the two kind different oxygen atoms occupy the general Wyckoff (4e): ±(x, y, z), ± (x, 1/2-y, 1/2 +z). Anderson, Longo and Kierkegaard in Table 1-2 and 1-3 [6] give the atomic positions.

Wentzcovitch [6] determined the lattice parameters and monoclinic angle as a = 5.629 Å, b = 4.657 Å, c = 5.375 Å and β =122.646° respectively; and the crystal structure parameters which were derived from the variable cell shape molecular dynamics calculations are listed in Table 1-4.

1.5.4 Monoclinic M_2 structure

The monoclinic M_2 phase differs from monoclinic M_1 since VO_2 in this phase crystallizes in a centered monoclinic lattice space group C2/m [6]. In M_2 phase,

the monoclinic angle distorts the basal plane of the original rutile cell hence the setup of the new primitive translations is different from that of the M_1 phase. There are two different types of metal atoms and three types of oxygen atoms and this occupy subsets on the general Wyckoff position: ±(x,y,z), ±(x,-y,z), (1/2,1/2,0)±(x,y,z), and (1/2,1/2,0)±(x,-y,z). The crystal structure is shown in Figure 1-5, and this only happen when VO_2 is doped with small amount (few percent) of Al, Cr, Fe and Ga [6].

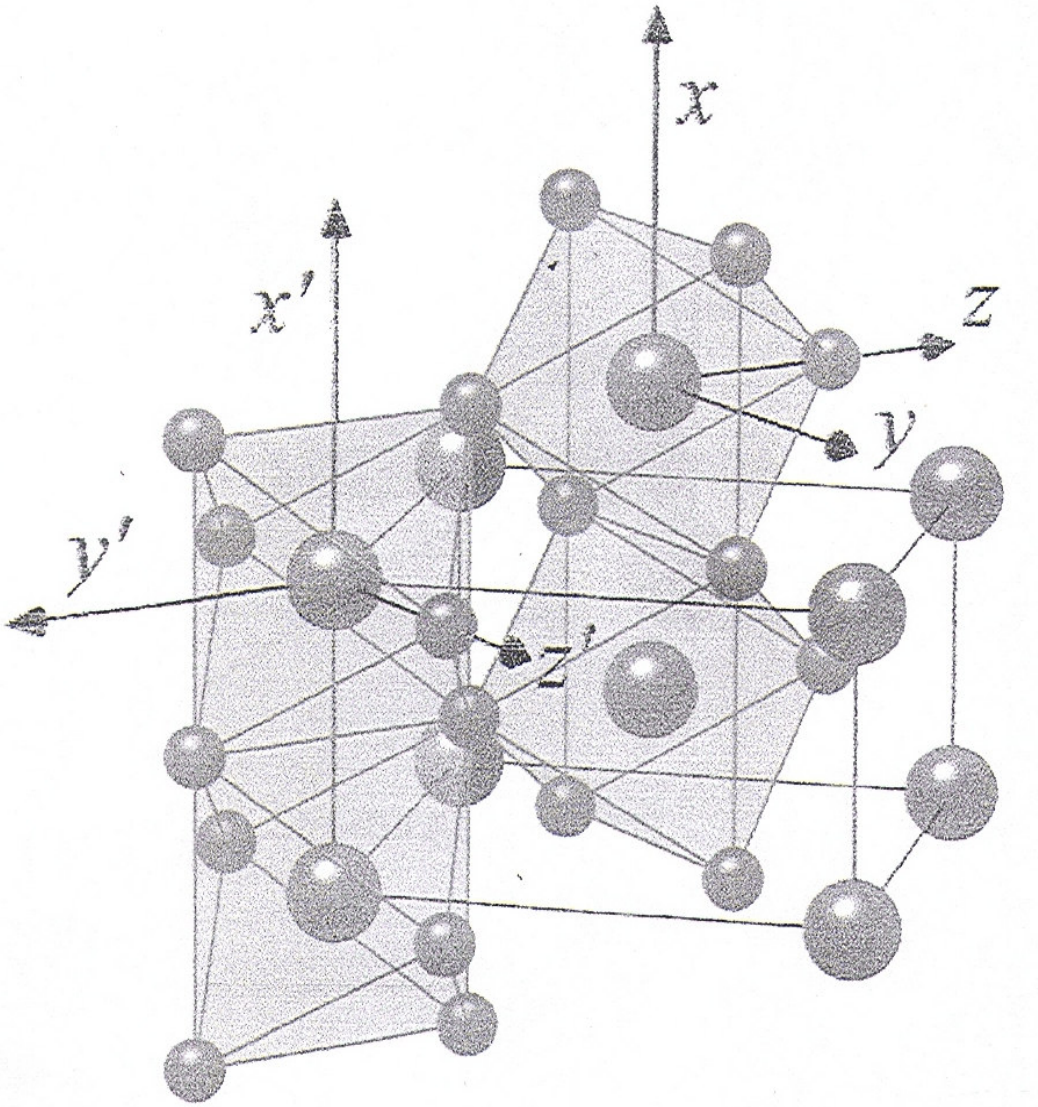

Figure 1-3: *The rutile structure of VO_2 showing the location of metal atoms and oxygen* [6].

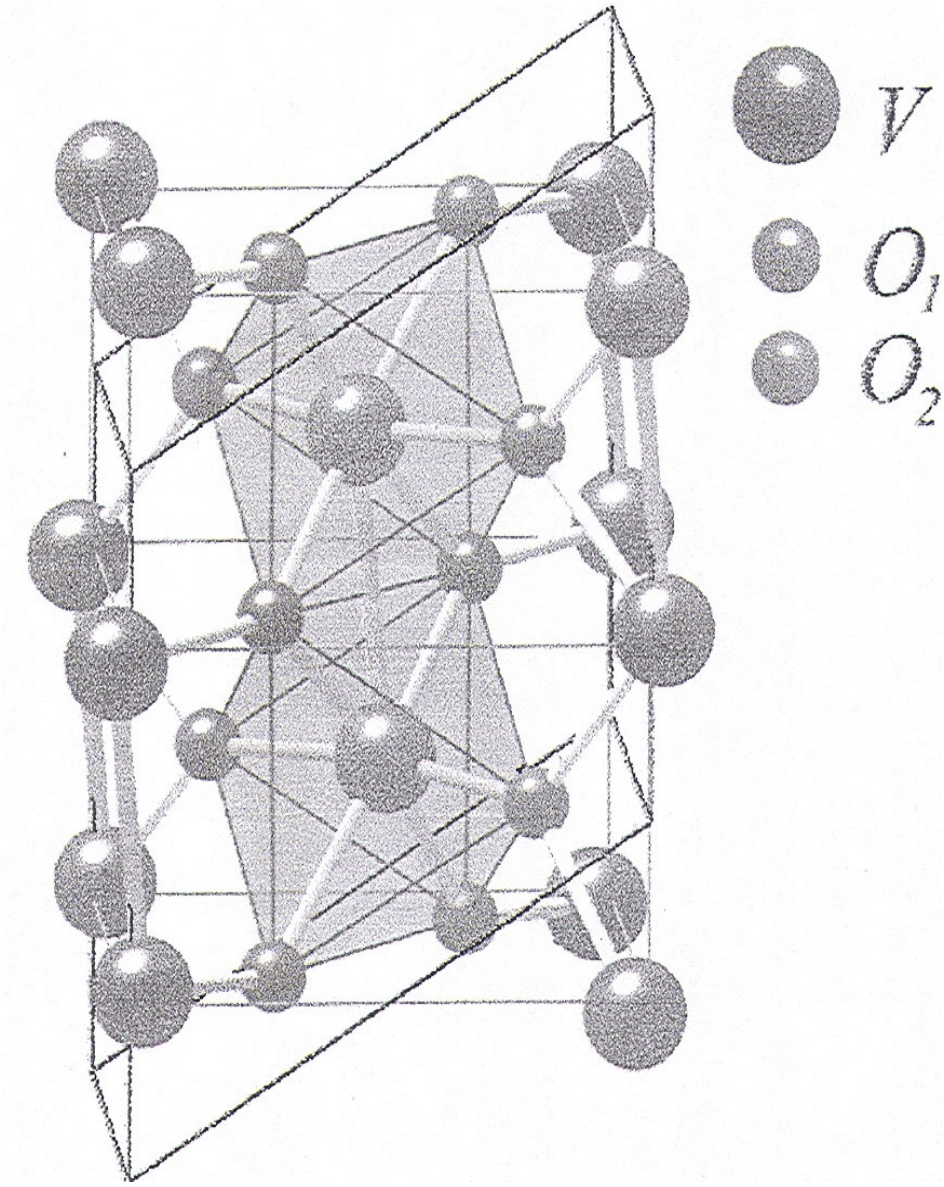

Figure 1-4: *The monoclinic M_1 phase of VO_2* [6].

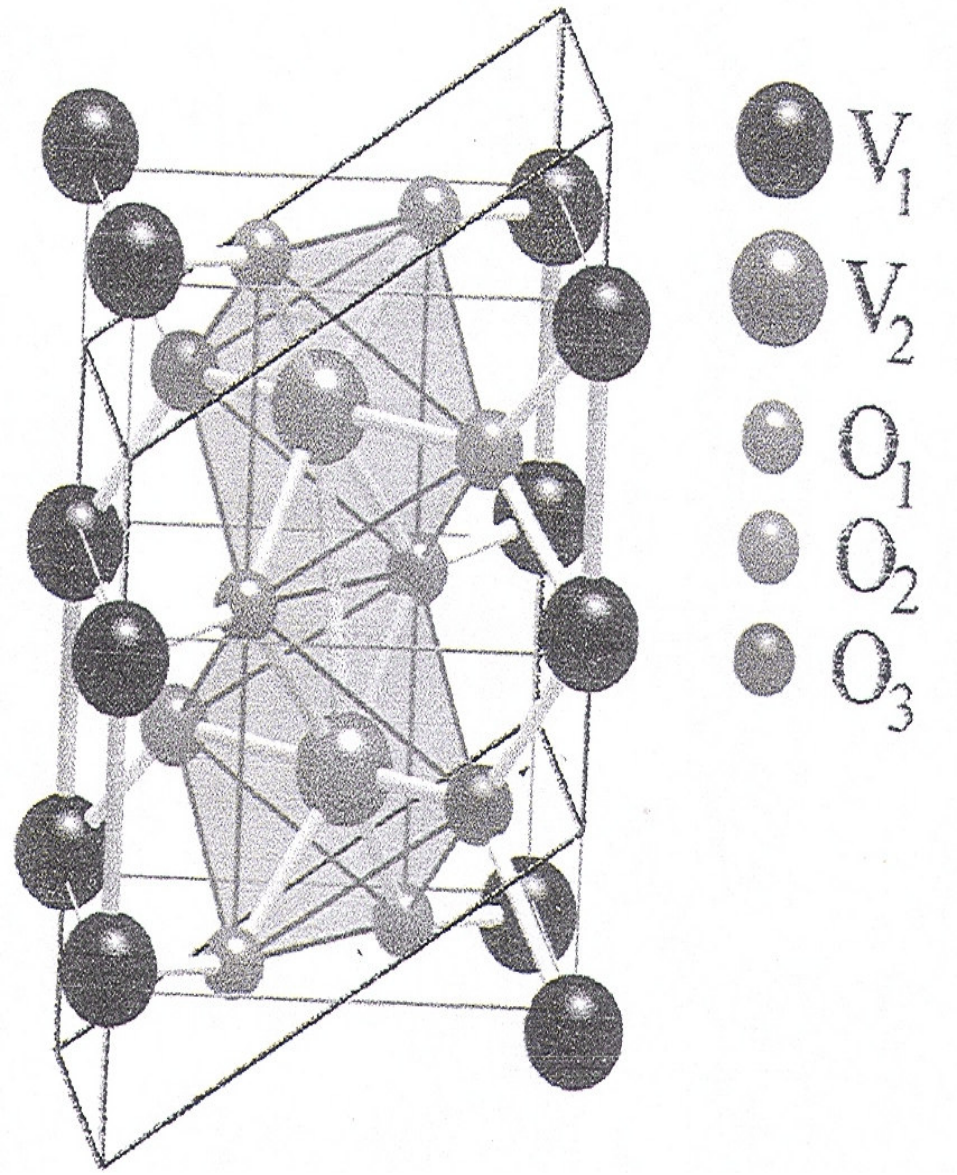

Figure 1-5: *The monoclinic M_2 phase of VO_2* [6].

Atom	**W**yckoff positions	**P**arameters		
		X	**Y**	**Z**
V	(4e)	0.242	0.975	0.025
O1	(4e)	0.1	0.21	0.2
O2	(4e)	0.39	0.69	0.29

Table 1-2: The Anderson's crystal parameters of M_1-VO_2 [6].

Atom	**W**yckoff positions	**P**arameters		
		X	**Y**	**Z**
V	(4e)	0.23947	0.97894	0.02646
O1	(4e)	0.10616	0.21185	0.20859
O2	(4e)	0.40051	0.70258	0.29884

Table 1-3: Crystal structure parameters of M1-VO_2 as given by Longo and Kierkegaard [6].

Atom	**W**yckoff positions	**P**arameters		
		X	**Y**	**Z**
V	(4e)	0.233	0.976	0.021
O1	(4e)	0.118	0.212	0.228
O2	(4e)	0.399	0.685	0.293

Table 1-4: Wentzcovitch's crystal structure parameters of M1-VO_2 [6].

1.6 Electronic properties of VO_2

1.6.1 Tetragonal structure of VO_2 ($T>T_t$)

In tetragonal structure shown in Figure 1-7a, VO_2 is meant to be in metallic state and it has V^{4+} ion at the center of an O octahedron. For the fact of symmetry, the degenerate five 3d atomic orbitals of V are split in doubly degenerate e_g (d_{3z2-r2}, d_{xy}) levels and triply degenerate t_{2g} (d_{x2-y2}, d_{xz}, d_{yz}) levels [6]. The e_g orbitals are directed towards O ligands and hybridized with the O2p orbitals. They form the σ and σ* bands with the O2p orbitals. The π and π* bands, and the $d_{||}$ band are formed from the t_{2g} orbitals which point in between the ligands and this results from the V3d_{xy} orbitals along the c-axis.

The high temperature phase forms a metallic properties of VO_2 due to the overlap of the $d_{||}$ and π* bands at Fermi level. The low temperature phase causes the V-O hybridization to change and V-V bonding is stronger an π* rises above Fermi level. The $d_{||}$ band separate into an empty and filled band due the doubling of the unit cell, thus VO_2 has semiconductor properties with a band gap of about 0.7eV. The semiconductor phase of VO_2 can have anomalous effects due to the doping of magnetic impurities and it is in the boundary of being a magnetic insulator. The metal-semiconductor transition of VO_2 is shown in Figure 1-8 (a,b) [6].

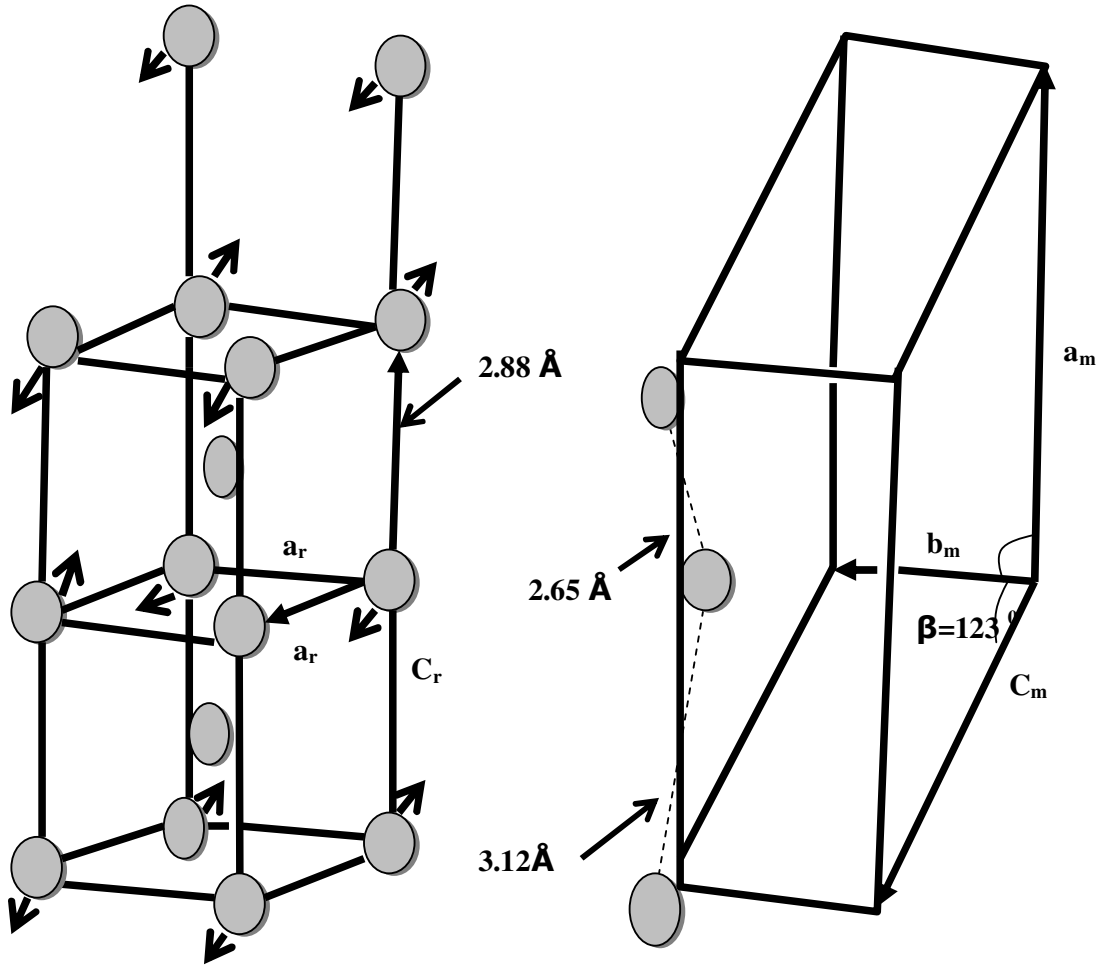

Figure 1-6: *The unit cell for VO_2 and its metal-semiconductor transformation. (a) tetragonal structure of VO_2, (b) Monoclinic structure of VO_2* [3,6].

VO_2

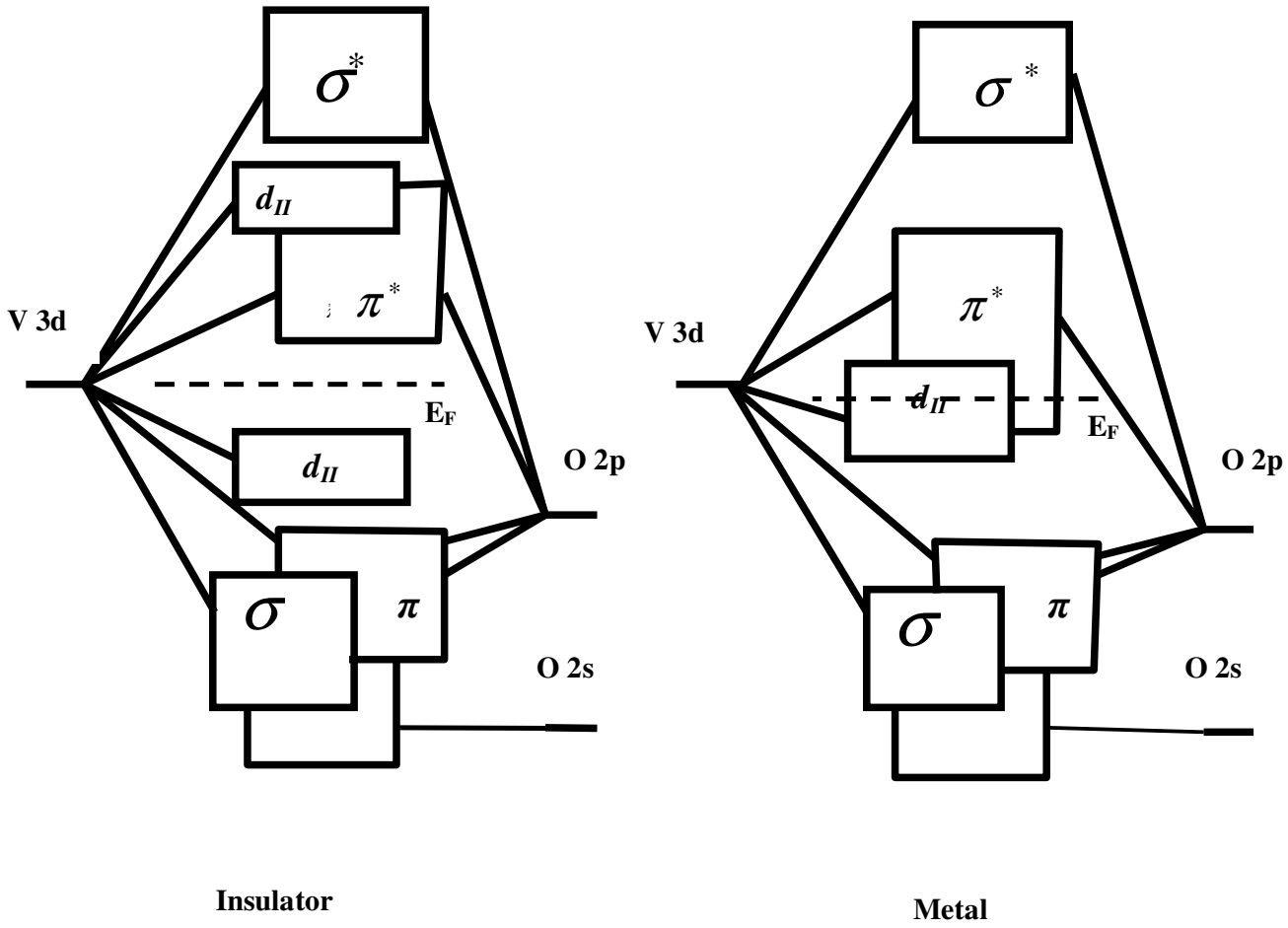

Figure 1-7: (a) *The insulator showing a band gap, and (**b**) metallic phase of VO_2 showing no band gap* [3, 6].

1.7 Electrical properties of VO_2

During semiconductor-metal transition, VO_2 undergoes a $\sim 10^5$ decrease in resistivity (Figure 1-6) when switching to the metallic state. The sharpness or the lack of thereof, of these changes in electrical properties has been related to disorientation between grains, and grain size and other morphologic faults [24].

It has been determined that the variations in the VO_2 switching are due to the level of internal or external stress, which can be modified by mismatch between lattice constants, expansion coefficients on different substrates, or even by ion bombardment [25-27].

The effect of hydrostatic pressure on the transition temperature (T_c) in VO_2 has been examined, and the results showed that T_c increases linearly with pressure at a rate of 0.082K/bar [28].

It has been shown that the effect of some impurities (e.g. F, Fe, Co, Ni, Ti, Nb, Mo, Tc, Ta, Re and W) lowers the T_c while Al, Cr, and Ge can raise it appreciably [29]. Nevertheless, the doping of VO_2 has some deterioration of the switching characteristics.

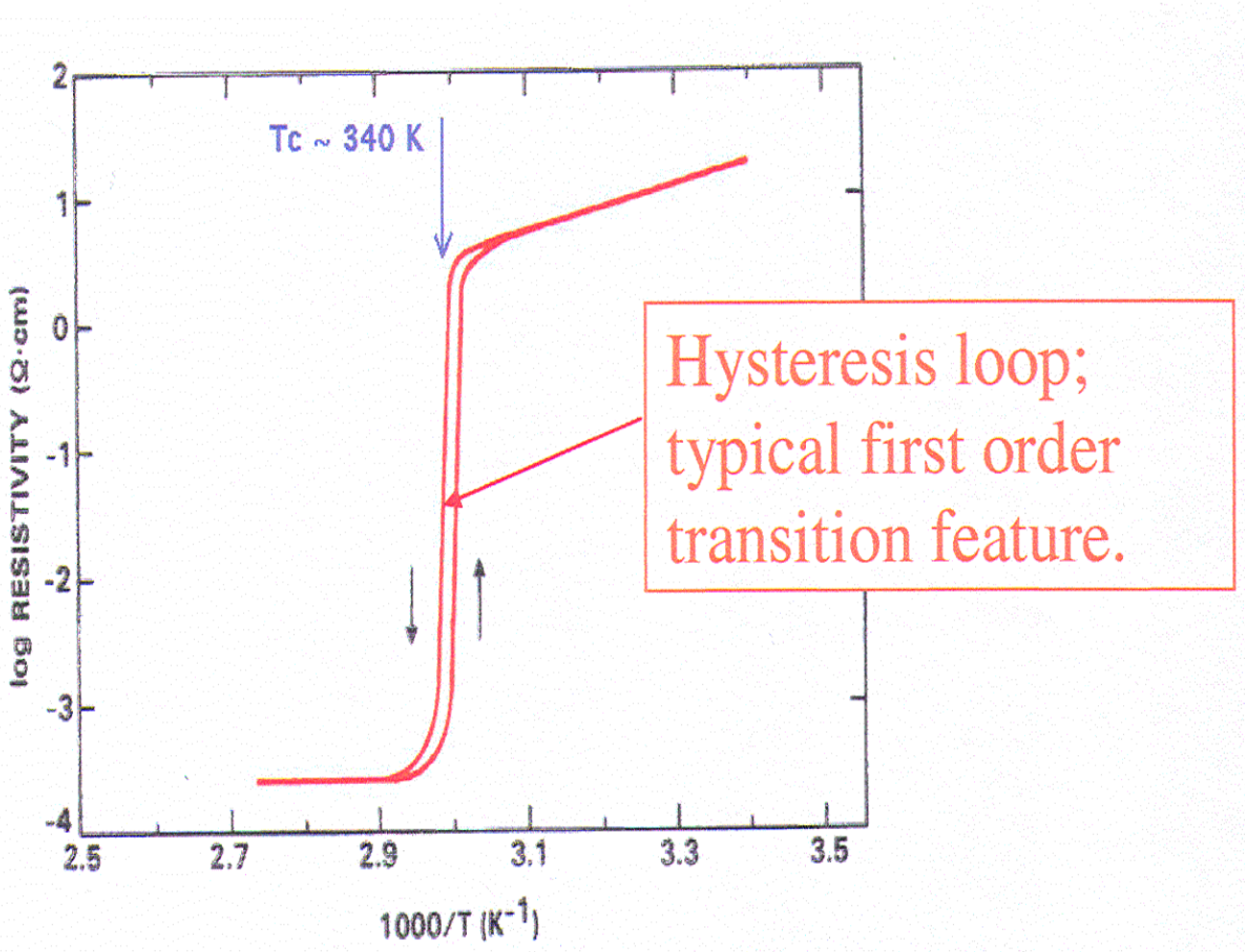

Figure 1-8: *The variation of VO_2 electrical resistivity with temperature* [24].

1.8 Optical properties

1.8.1 General optical properties of coated material in Infrared Region

The optical properties of the material change if the light passes through [30]. The most important optical properties are the refractive index *n* and the extinction coefficient *k*. In other books, authors' extinction coefficient is called the attenuation or absorption coefficient α. This chapter is going to explain how infrared radiation (IR) is transmitted on the glass with vanadium dioxide (VO_2) film.

This project is based mostly on IR, visible light and ultra violet. In the spectrum below (see Fig. 1-9), the wavelength of Ultra violet (UV) ranges between 10nm to 100nm, visible light ranges from 400nm to 750nm and IR ranges between 750nm and 1 mm.

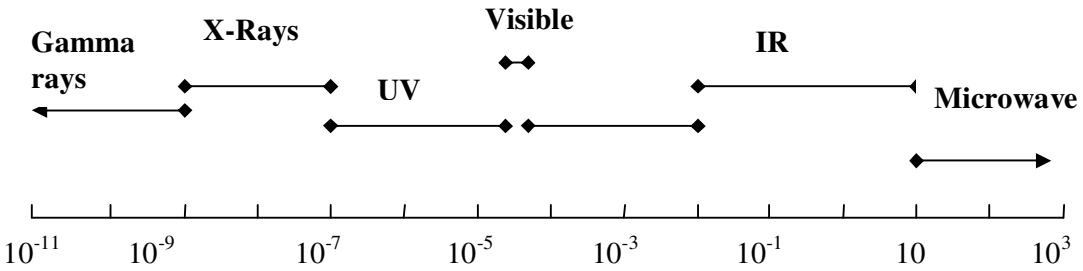

Figure 1-9: *Light wavelengths within the electromagnetic spectrum.*

1.8.2 Transmittance, reflectance and absorption

If the light passing through the material, three things happen: transmittance, reflectance, absorption [3].

The light depends on the thickness and the absorption coefficient of the material to get transmitted. It is not easy for the light to get transmitted if the sample is too thick, small percentage will be transmitted, and also small percentage will be absorbed but the rest will be reflected. If the light is not transmitted at all, the minimum transmittance is zero. Theoretically, the probability of light transmitted in the thin material is 1; meaning 100% of light is transmitted.

The incoming intensity for incident light is called incident intensity I_0, I_r for the reflected light and I_t for the transmitted light. The transmittance T, and reflectance R are defined as follows:

$$T = \frac{I_t}{I_0} \qquad (2.1)$$

$$R = \frac{I_r}{I_0} \qquad (2.2)$$

The transmittance and reflectance are given in percentage. The addition of the two (transmittance and reflectance) should give 100% for all [3]. Except from the frequency-dependent refractive indices of both materials at the interface, T and R also depend on the incident angle and on interference effects [3].

1.8.3 Optical properties of VO_2

Vanadium (IV) oxide has vital and interesting optical properties since the switching also affect the optical constants of the material. The effect is accentuated in the IR region of the smaller changes occurring in the UV-Vis spectral region (see Figure 1-10). The optical constants have been an object of study long before any theoretical explanation of the transition, but the disagreements between authors still persist [31]. This may arise strongly because of the small change in stoichiometry can result in somewhat different behavior. By inspection, the VO_2 can exist in different colors ("blue" VO_2 "brass" VO_2,

"brown" VO_2) with slightly difference in their oxygen content as well as their optical properties in the 1-2 eV region [32].

Doping VO_2 also changes the transition temperature, which also modifies the VO_2 optical properties, but like the transport properties, they also deteriorate somewhat [33] in the process (see Figure 1-11).

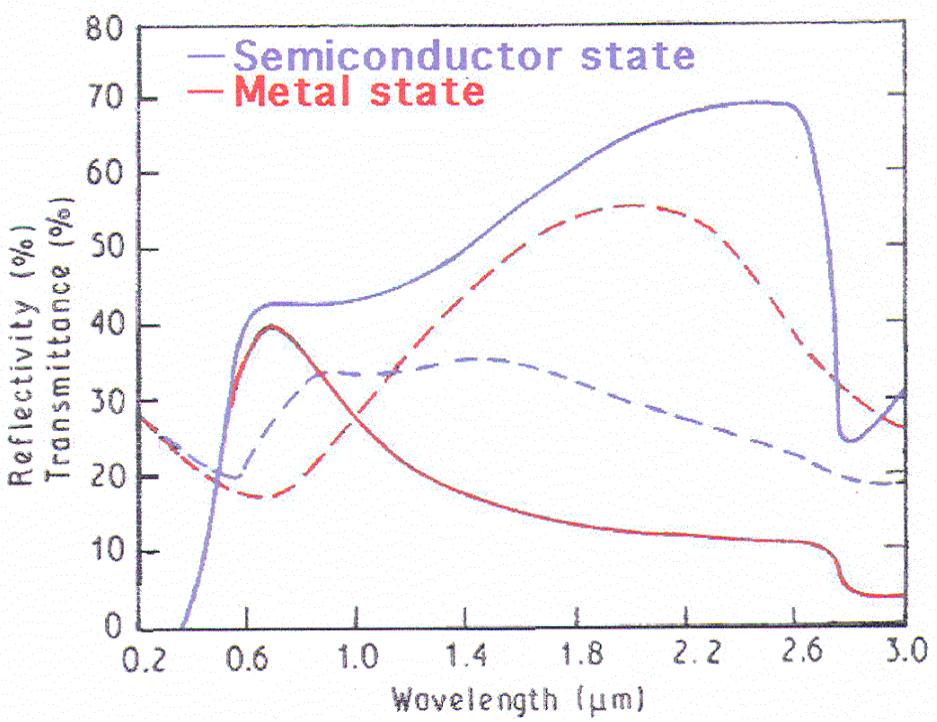

Figure 1-10: *Optical transmittance (-) and reflectivity (--) of a VO_2 85 nm thin film [6] deposited on a silica substrate. (a) room temperature, (b) 100°C.*

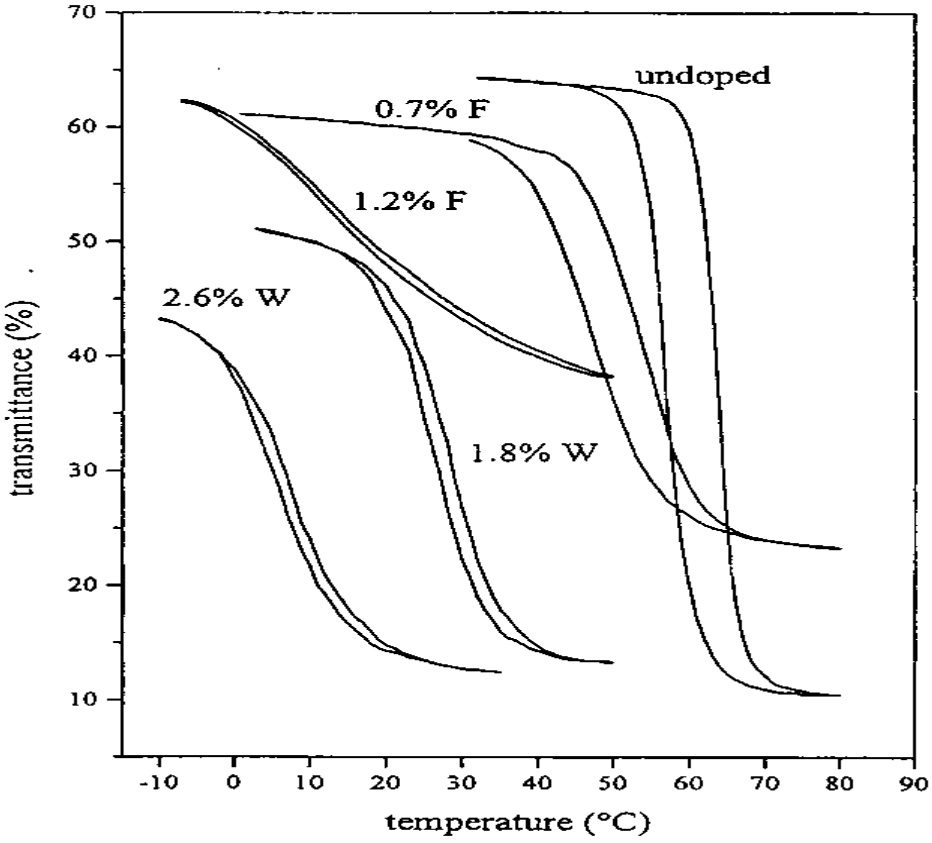

Figure 1-11: *Hysteresis loops of optical switching recorded from undoped and tungsten and fluorine doped films* [33].

1.9 Doping of Vanadium (IV) Oxide

1.9.1 Tungsten (W) Doping

Out of all the dopants that have been investigated in single crystals and PVD or sol-gel prepared thin films, tungsten seems promising in reducing the transition temperature of vanadium (IV) oxide by the greatest extent. The vanadium (IV) oxide films containing two atom percent tungsten which have been shown to have a thermochromic transition temperature of 25 ^{0}C (see Fig. 1-12), and this is the ideal transition for nano- VO_2 smart window coatings [34].

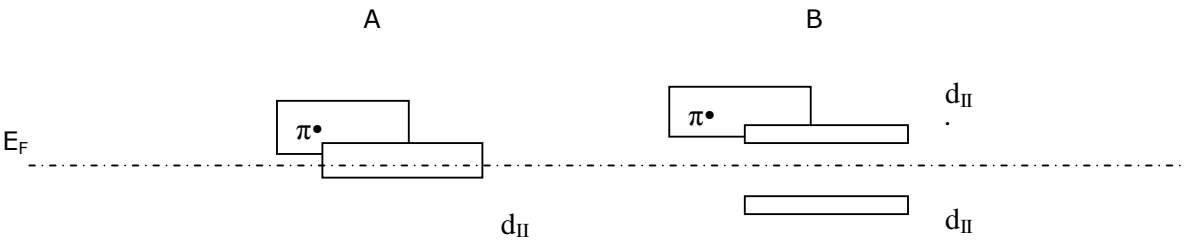

Figure 1-12: *Schematic drawing of two materials, (a) showing no band gap in metallic structure and (b), showing band gap in semiconductor material* [34].

1.9.2 Other Dopants

With the exception of tungsten as a dopant, some other metal ions can be introduced into vanadium (IV) oxide lattice as dopants. These metal ions have an ability to affect the metal-to-semiconductor transition (MST) temperature of vanadium (IV) oxide [34].

In the methods that have been mentioned in [34] for preparation of thin films, sol-gel have seen greatest variety of dopant ions used most with most of the first-row transition metals having been used [35-37]. By using sol-gel method vanadium

(IV) oxide have been doped with metal ions namely gold [38], molybdenum [39], niobium [8], and aluminium [40].

It has been investigated that co-doping of vanadium (VI) oxide with tungsten and titanium displayed almost no hysteresis width for infrared switching**.** Low thermochromic transition temperature in VO_2 can also be given by the co-doping molybdenum and tungsten, or titanium and tungsten [41].

The doping of VO_2 lattice using physical vapor deposit method is not quite so extensive compared to sol-gel method and have mostly have been limited to those that are known to bring about the largest decrease in MST temperature like tungsten and molybdenum[42-44]**.** The poor doping in VO_2 that have shown by PVD method is the one of iron (Fe) when showing a minimum thermochromic transition temperature with 1.4 atom percent Fe at 59 ^{0}C on heating cycle [45, 46]**.**

1.10 Technological applications

1.10.1 Applications of V_2O_5

According to the research done, lithium-ion batteries have become the most popular power sources for consumer electronic devices, such as cell phones and laptop computers, due to their high specific energy and long cycle-life. In addition, lithium-ion batteries have tendency of being major breakthrough in the hybrid electric vehicle field. In defiance of their successful commercial application, further improvement in the performance of the lithium-ion battery is still required for large scale applications [24-27].

Vanadium pent-oxide (V_2O_5) is the most commonly used material as a cathode in lithium-ion batteries to improve capacity, voltage (versus the anode material), reversibility, and stability.

Nanostructured V_2O_5 has potential application in the fields of lithium-ion batteries, actuators, catalysis (in organic reactions and as a *precursor* for other vanadium salts), and sensors [4]. The performance of a V_2O_5 cathode is heavily dependent on its crystallinity and morphology. Crystalline V_2O_5 has a high specific capacity, but during deep charge and discharge cycles, it undergoes with structural modification which is induced by mechanical stress and this result in decrease of specific capacity and specific energy. Amorphous or low crystallinity V_2O_5 is inherently low. It has investigated that upon heating V_2O_5 reversibly loses oxygen [4, 24-27].

1.10.2 Applications of VO_2

The applications of VO_2 can be divided into two, civilian and military application. The example of civilian application is VO_2 as window coating. The second application is where VO_2 is used as a laser protective device [32].

If VO_2 is used as window coating, this can help in regulating heat transmission (IR) in buildings or vehicles and this coated window (see Figure 1-13) might not need external control system. By doping VO_2 that can creates chances of reducing its transition temperature from 68 ^{0}C to room temperature (25 ^{0}C). Transition temperature can be made less sharp and this making the heat transmission easier to control [32].

Daniel Johansson [32] focused the laser light to heat a metallic VO_2 and the incident light was reflected. The VO_2 phase transition also contributes in reflectance changes, which means IR emissivity of a surface can be controlled. The decrease in emissivity of hot surface of a material also decreases the initial transparent of the material.

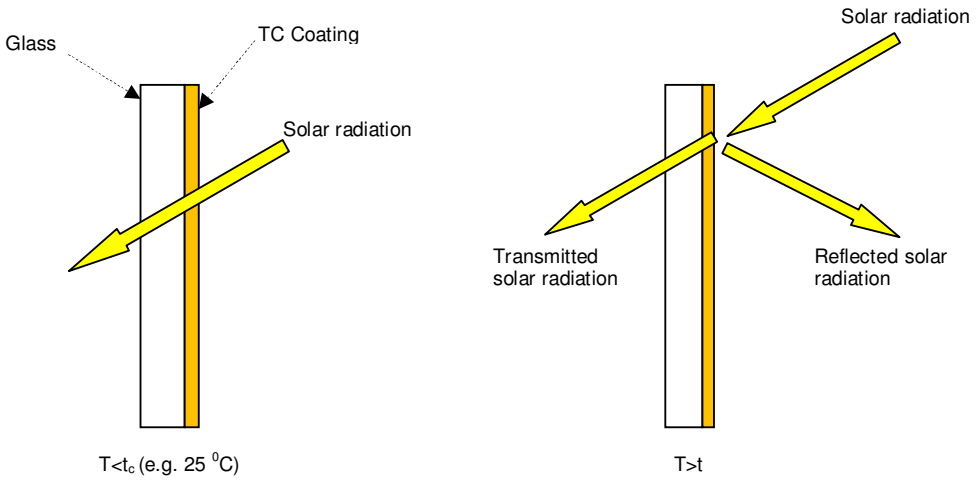

Figure 1-13 : *Schematic drawing showing how the light has been reflected or absorbed by a material.*

1.11 Conclusions and the scope of investigations

Preparation of VO_2 thin film, metal oxides, compounds and superfine-grained materials, intended for various areas of science and engineering, is one of the challenges faced in modern nanotechnology such as car windscreens and IR-shutter. The consolidated nano- and microcrystal materials based on vanadium (IV) oxide have attracted fundamental and applied interest due to its unique optical properties.

In this investigation, we are focusing on the synthesis VO_2 coatings from V_2O_5 sol-gel and the characterization of the film. VO_2 was selected as one of the promising materials in the window-coating industries. A wide range of physical and optical properties VO_2 thin film, especially metal-semiconductor properties, have to be well investigated. The film synthesis method, based on the use of reduction gases (e.g. H_2 and CO) and laser irradiation as a reduction technique, is currently used for synthesizing consolidated vanadium oxides. These methods allow the fabrication ensembles of nano- and micro structured VO_2 rods consisting of metal-semiconductor properties, which is crucial in infrared modulation.

The objectives of this research are the following:

The main goal of this research is to produce VO_2 coatings which will be marketable because of its technological properties. Vanadium dioxide thin films on a glass can be useful in smart window-the window which can change one or more of its properties in the response to some external stimulus. Smart windows can be the window panes for the houses or the car windscreens. The glass coated with vanadium dioxide changes its properties in such a way that becoming more reflective in the infrared wavelengths at elevated temperature and transmitting at room temperature. Thus, air conditioners and fans can be substituted by these

windows, which reduce the electricity cost. These VO_2 coatings can be useful in workshop or laser laboratories by acting as an IR shutter. This prevents the laboratory users from getting injured which might lead in losing sight.

a) To deposit V_2O_5 thin film on a glass substrate and silicon wafer, reduce it to form VO_2 nano-structures. To design and develop the installation for reduction of V_2O_5 sol-gel using hydrogen gas as a reducing agent. To investigate the influence of temperature in crystal structure of the target material when annealing at high temperatures using. In order to characterize the film, SEM and AFM were used to study the surface morphology of nano consolidated structure. The XRD technique was used for the analysis of crystallography.

b) The V_2O_5 film will be also reduced in the presence of carbon monoxide gas. During reduction parameters such as temperature, annealing time and gas flow rate have to be varied. In this investigation, the focus is to study and optimize the influence of temperature in the film during reduction treatment. The reduced film will be also studied its physical properties using the analytical techniques.

c) To reduce V_2O_5 film using laser treatment and the support for this experiment will be corning glass. The film will be reduced with different shots to compare the influence of shots in the film. The influence of shots versus intensity will be studied. The prepared film will be analyzed their physical properties using analytical techniques such as AFM, SEM, XRD, RBS, ERDA, EDS, Raman, UV-Visible and FTIR.

d) To use ion beam technique (RBS) for the study of impurities of the film. To use the ERDA technique for the detection of hydrogen concentration.

Each and every technique is used according to the information behind the investigation of the target material. The whole overview is further discussed in **chapter 2**. In the experimental section a short summary of the V_2O_5-VO_2 film reduction and deposition techniques is given in **chapter 3**. The most important of result and observations, discussion of results is also included in **chapter 4**. The results discussion is divided into three parts since the reduction of the film was done with three reduction methods. The results of the three different methods will be presented and the physics/mechanism through the reduction process will be discussed.

CHAPTER 2 - Characterization Techniques

2.1 X-Ray diffraction

2.1.1 Background

X-Ray diffraction (XRD) is a versatile, non-destructive technique that reveals detailed information about the chemical composition and crystallographic structure of natural and manufactured materials [47]. The X-ray diffraction methods have qualitative and quantitative analysis.

Qualitative analysis involves the identification of phase or phases in a specimen by comparison with the reference pattern (i.e. data collected by someone else), and relative estimation of proportions of different phases in multiphase specimens by comparing peak intensities attributed to the identified phase. The quantitative analysis of diffraction data involves the determination of amounts of different phases in multi-phase samples.

In quantitative analysis, an attempt is made to determine structural characteristics and phase proportions with quantifiable numerical precision from the experimental data itself. The most successful quantitative analysis usually involves modeling diffraction pattern such that the calculated pattern(s) duplicates the experimental one. All quantitative analysis requires precise and accurate determination of the diffraction pattern for a sample in terms of both peak positions and intensities. In some kinds of analysis (i.e. particle shape and clay structure) rely on the existence of preferred orientation, most require a uniformly sized, randomly oriented fine (ideally 1-2 μm) powder specimen to produce intensities which accurately reflect the structure and composition of the phase(s) analyzed [47].

2.1.2 Generation of X-ray

X-rays are short-wavelength with high-energy electromagnetic radiation and having the properties of both waves and particles. They can be described in terms of photon energy (E) or wavelength λ and frequency ν. The relation of between energy, frequency or wavelength can be defined as follows:

$$E = h\nu = \frac{hc}{\lambda} \qquad (2.1)$$

By substituting the values of the constants in equation (2.1), therefore the energy can be defined as:

$$\lambda = \frac{12.4}{E(KeV)} \qquad (2.2)$$

X-rays are produced from the interaction of high energetic electrons with the metal target. The X-ray tube must contain (a) a source of electron, (b) a high accelerating voltage, (c) a metal target. The x-ray tubes contain two electrodes, an anode (the metal target) usually maintained at ground potential, and cathode maintained at negative potential. The diffraction work is normally in the order of 30 KV to 50 KV. If the beam of electrons interacts with target, this results in loss of energy. The continuous spectrum is formed when the high energy electrons are slowed rapidly by multiple collisions with the anode material, which gives rise to white radiation called Bremsstrahlung [47, 48].

2.1.3 Constructive interference

When a monochromatic X-ray beam with wavelength *lambda* is projected onto a crystalline material at an angle *theta,* diffraction occurs only when the distance traveled by the rays reflected from successive planes differs by a complete number *n* of wavelengths.

2.1.4 Bragg's Law

Since atoms are arranged periodically in a lattice, x-rays scattered from a crystalline solid can constructively interfere and produce a diffracted beam through these atoms. In 1912, W.L. Bragg recognized the predictable relationship among several factors and those factors were combined in Bragg's Law:

$$n\lambda = 2d \sin\theta \qquad (2.3)$$

n=an integer 1, 2, 3…etc [n=1 for calculations]

λ= the wavelength of the incident X-radiation, symbolized by the Greek letter lambda (equal to 1.54 angstroms)

θ=the diffraction angle in degrees

d=the distance between similar atomic planes a mineral, which called d-spacing and measured in angstroms.

By varying the angle theta, the Bragg's Law conditions are satisfied by different *d*-spacings in the polycrystalline materials. Plotting the angular positions and intensities of the resultant diffracted peaks of radiation produces a pattern, which is characteristic of the sample. Where a mixture of different phases is present, the resultant diffractogram is formed by addition of the individual pattern.

Based on the principle of X-ray diffraction, a wealth of structural, physics and chemical information about the material investigated can be obtained. A host of application techniques for various material classes is available, revealing its own specific details of the sample studied.

2.1.5 Crystal lattice

A crystal lattice is a regular three-dimension distribution (cubic, rhombic, etc.) of atoms in space. The arrangement of the atoms form a series of parallel planes separated from one another by a distance *d,* which varies according to the nature of the material. For any crystal, planes exist in number of different orientations and each with its own specific *d spacing*. The lattice parameters can be calculated from the following equation:

$$(1/d^2_{hkl}) = \{(h^2/\mathbf{a}^2) + (k^2/\mathbf{b}^2) + (l^2/\mathbf{c}^2)\} \qquad (2.4)$$

where *hkl* and d_{hkl} are the planes and d-spacing between the planes, respectively.

2.1.6 Crystallite size measurement

The phase identification using x-ray diffraction depends on the positions of the peaks in the diffraction profile with relative to intensities at some extent. Another important aspect of the diffraction from the material is to consider how diffraction peaks change through the presence of various types of defects such as small number of dislocations in crystals with dimensions in millimeters. The defects can be caused by the small grain size, which can change diffraction peak widths. The crystallite size is calculated as a function peak width (i.e. full-width at half maximum peak intensity, FWHM) peak position and wavelength [49].

2.1.7 Scherer's formula

Suppose that a material has a thickness δ measured in a direction in the direction perpendicular to a particular set of Bragg planes as shown in Figure 2-2. Let there be (m+1) planes in this set. Let the Bragg's angle be variable and let θ_B the angle which satisfies Bragg's law for the particular values of λ and d-spacing involved:

$$\lambda = 2d \sin \theta_B \qquad (2.5)$$

The rays **A, D**...**M** make the angle with θ_B the diffraction planes, shown in Figure 2-2. Incident x-rays that make angles with slightly difference with θ_B produce incomplete destructive interference. For example, ray **B** makes a slightly larger angle θ_1, such that **L**′ from *m*th plane below the surface is (m+1) wavelengths out of phase with **B**′, the ray from the surface plane. The intensity of the diffracted beam at an angle $2\theta_1$ is equal to zero. The angle $2\theta_2$ is also equal to zero, where θ_2 is such that ray **N**′ from the *m*th plane below the surface is (m-1) wavelengths out of phase with ray **C**′ from the plane. This defines that the two limiting angles, $2\theta_1$ and $2\theta_2$, at which the diffracted intensity must drop to zero.

The curve of diffracted intensity vs. 2θ shown in Figure 2-3**a** and contrast in Figure 2-3**b**, which the hypothetical case of diffraction occurring only at the exact Bragg angle. The width of the diffraction curve of Figure **a** increases as a thickness of the crystal decreases, because the angular range ($2\theta_1$-$2\theta_2$) increases as m decreases. The width B is usually measured, in radians, at an intensity equal to half the maximum intensity (FWHM). The estimated grain size is calculated from the measured width of the diffraction by using the Scherer's formula:

$$\delta = \frac{\lambda}{B \cos \theta_B} \qquad (2.6)$$

or,

$$\delta = \frac{0.9\lambda}{B \cos \theta_B} \qquad (2.7)$$

a value 0.9 or 1 is used depends on shapes of the crystallites [49]. The XRD instrument used in the phase analysis is shown in figure 2-3.

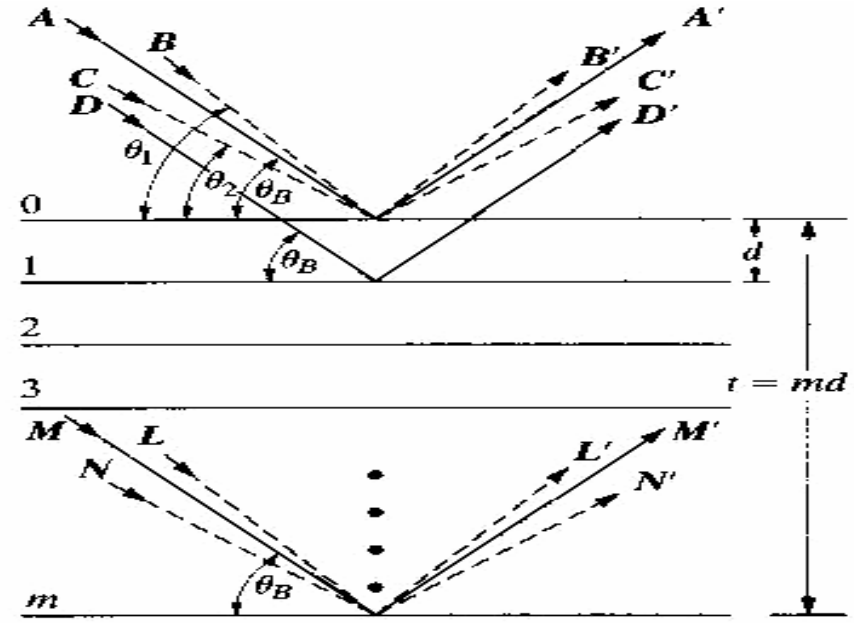

Figure 2-1: *The effect of crystal size on diffraction* [49].

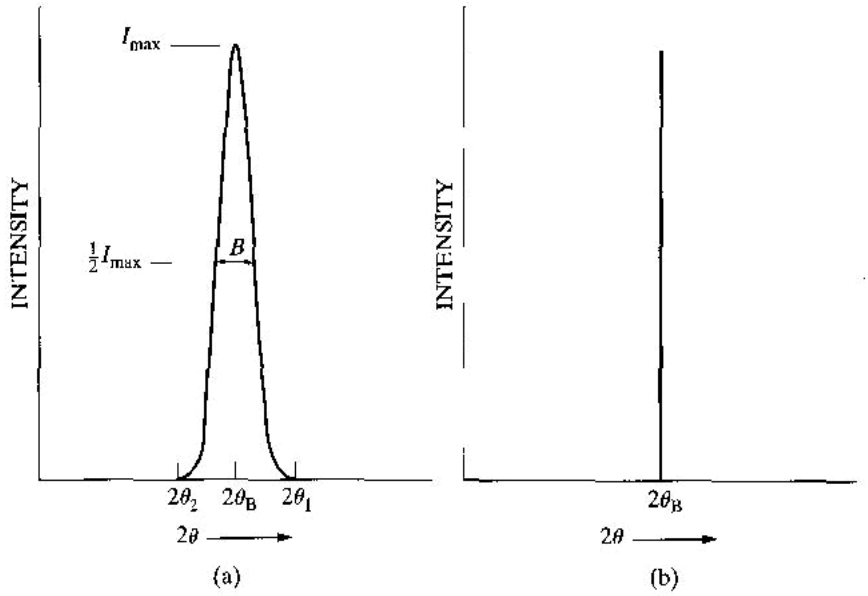

Figure 2-2: *The effect of fine crystallite size on diffraction curves* [49].

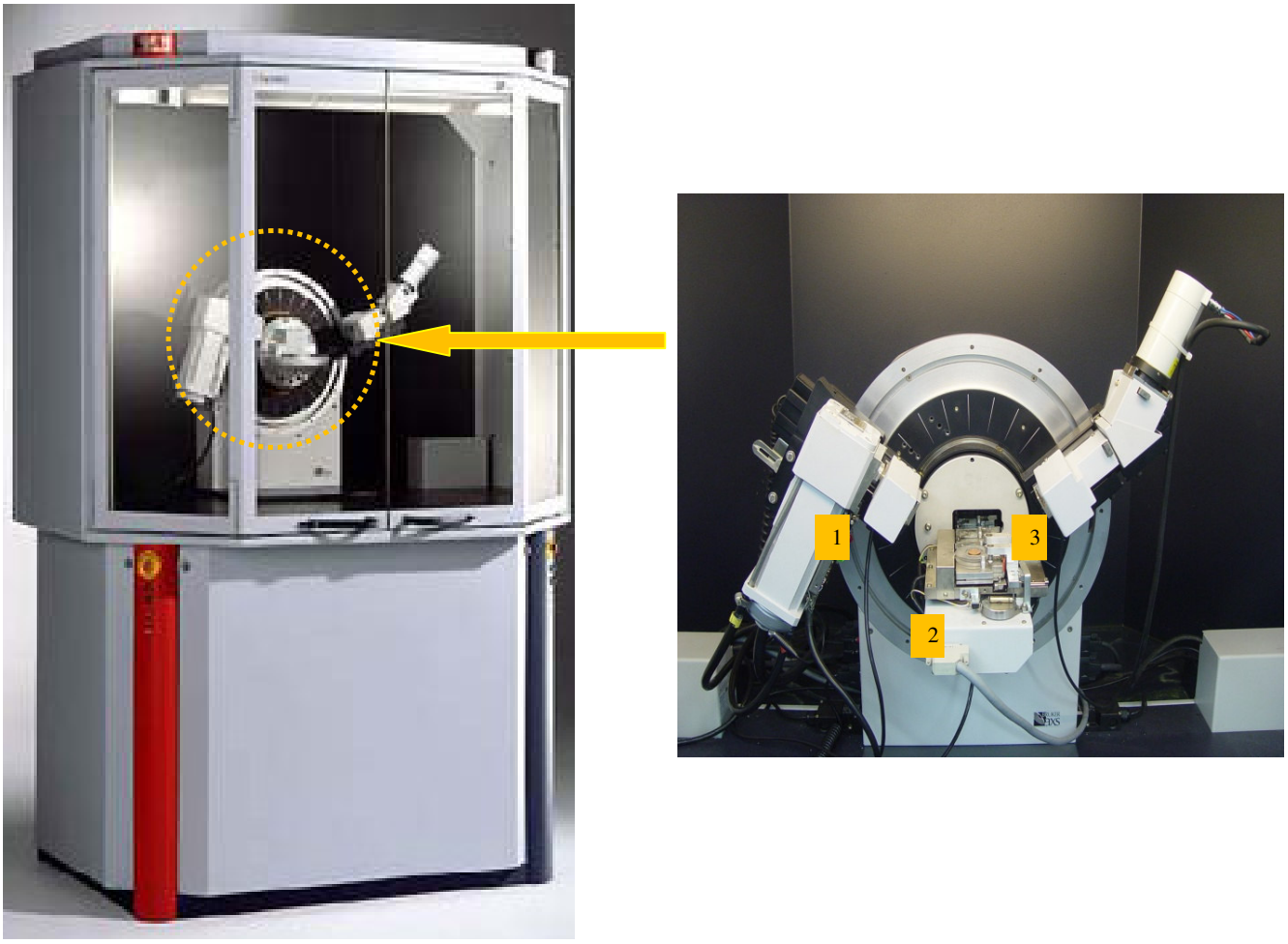

Figure 2-3: *The Bruker D8 Advance XRD instrument at IThemba Labs. (1) X-Ray source, (2) sample stage and (3) position sensitive detector.*

2.2 Atomic Force Microscope

The atomic force microscope (AFM) or scanning force microscope is a very high resolution type of scanning probe microscope, with the demonstrated resolution of fractions of nanometer and it is more than 1000 times better the optical diffraction limit. In tapping mode the cantilever is driven to oscillate up and down at near its resonance frequency by a small piezoelectric element mounted in the AFM tip holder [50].

2.3 Advantages and disadvantages of AFM

The AFM has many advantages compared to scanning electron microscope (SEM). The electron microscope provides a two-dimensional projection or a two-dimensional image of a sample, the AFM provides a three-dimensional surface profile.

The AFM has the disadvantage in image size compared to SEM. The SEM can image an area approximately millimeters by millimeters with a depth of field about millimeters. The AFM can only image a maximum height approximately micrometers and a maximum scanning area of around 150 by 150 micrometers [50-53].

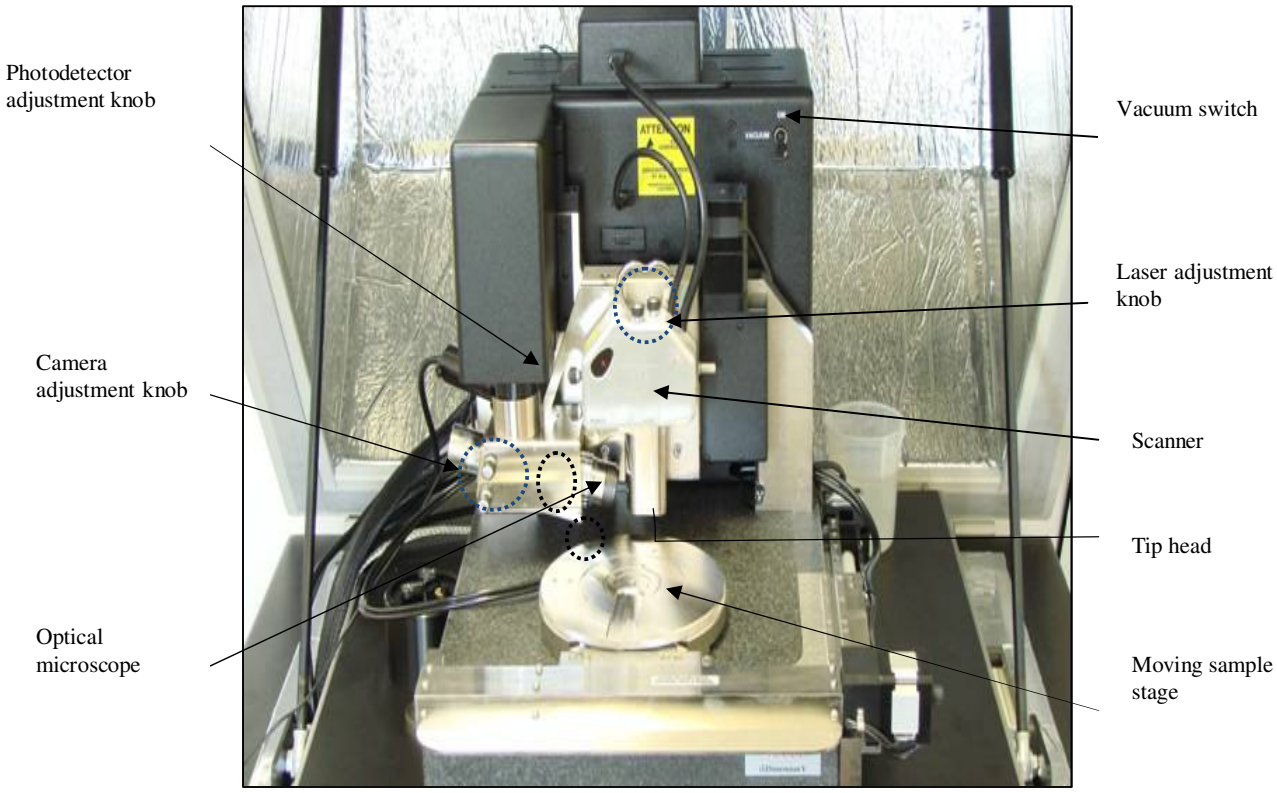

Figure 2-4: *The Nano-man V AFM machine photograph taken from IThemba LABS.*

2.4 Scanning Electron Microscope (SEM)

Scanning electron microscopy (SEM) is a type of electron microscope which is used for various purposes;

- Topographic studies
- Microstructure analysis
- Chemical composition
- Elemental mapping
- Elemental analysis if equipped with appropriate detector (energy/wavelength dispersive x-rays)

For the SEM analysis, focused beam of high-energy electrons is required to generate a variety of signals at the surface of solid specimens. The signals that derive from electron sample interactions reveal the hidden information about the sample including external texture (morphology), chemical composition, and crystalline structure, and the orientation of materials making up the sample [49].

In SEM, primary electrons are filled emitted by cathode filament (W or LaB6) or filed emission gun (W-tip) and after that accelerated with high energy typically 1-30KeV. Electron beam is steered with scanning coils over the area of the interest. During the interaction of the beam with material, the primary electrons decelerate and lose their energy by inelastic transfer to the other atomic electron and to the lattice. Due to continuous scattering events the primary beam spread up with different energies depending on origin source shown in Figure 2-5a. The interaction volume with the various electrons emitted and their respective energy is shown in Figure 2-5b [49, 54-55].

Secondary electrons of about 1-50eV are mostly used for the imaging the topographically contrast and reproduce the surface. High energy elastically backscattered electrons depends on the atomic number (Z) of the element, which is useful to obtain Z-contrast. For the qualitative and quantitative analysis of the

elemental composition and distribution in the sample, the X-ray characteristic is commonly used.

2.4.1 Applications

The SEM is used to generate high-resolution images of shapes of objects (SEI) and to show spatial variations in chemical compositions, usually cathodoluminescence (CL) and backscattered electrons (BSE) and energy dispersive spectroscopy (EDS) [54,55].

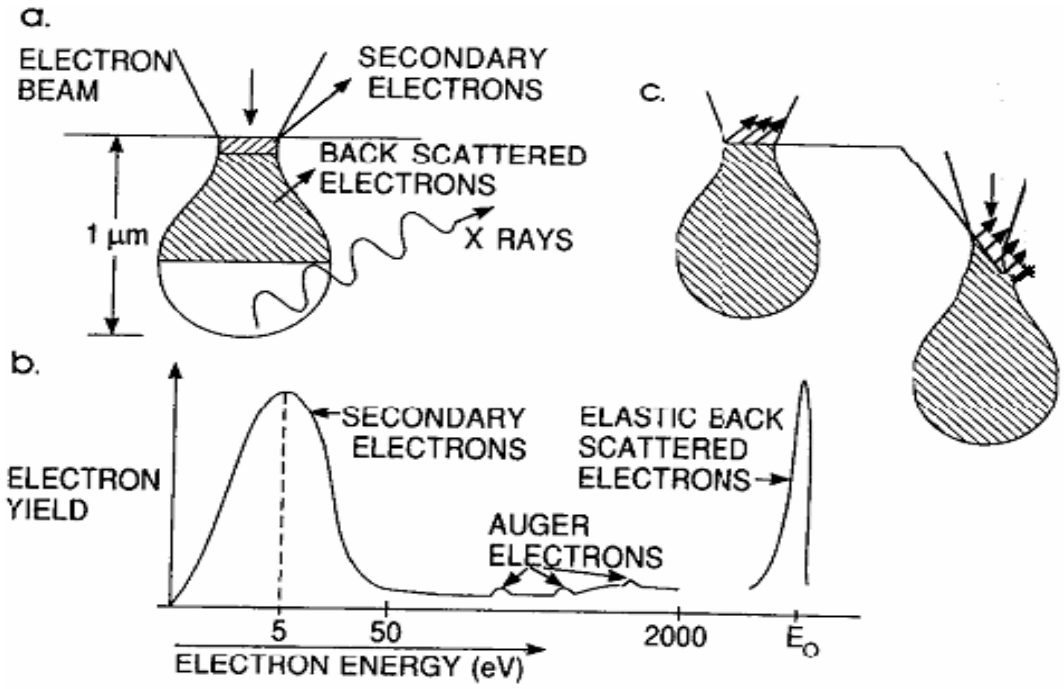

Figure 2-5: (a) *The interactions of electrons with the surface during bombardment. (b) Type of electrons and corresponding energies of the emitted electrons after element interaction. (c) Showing the effect of surface topography on electron emission* [49].

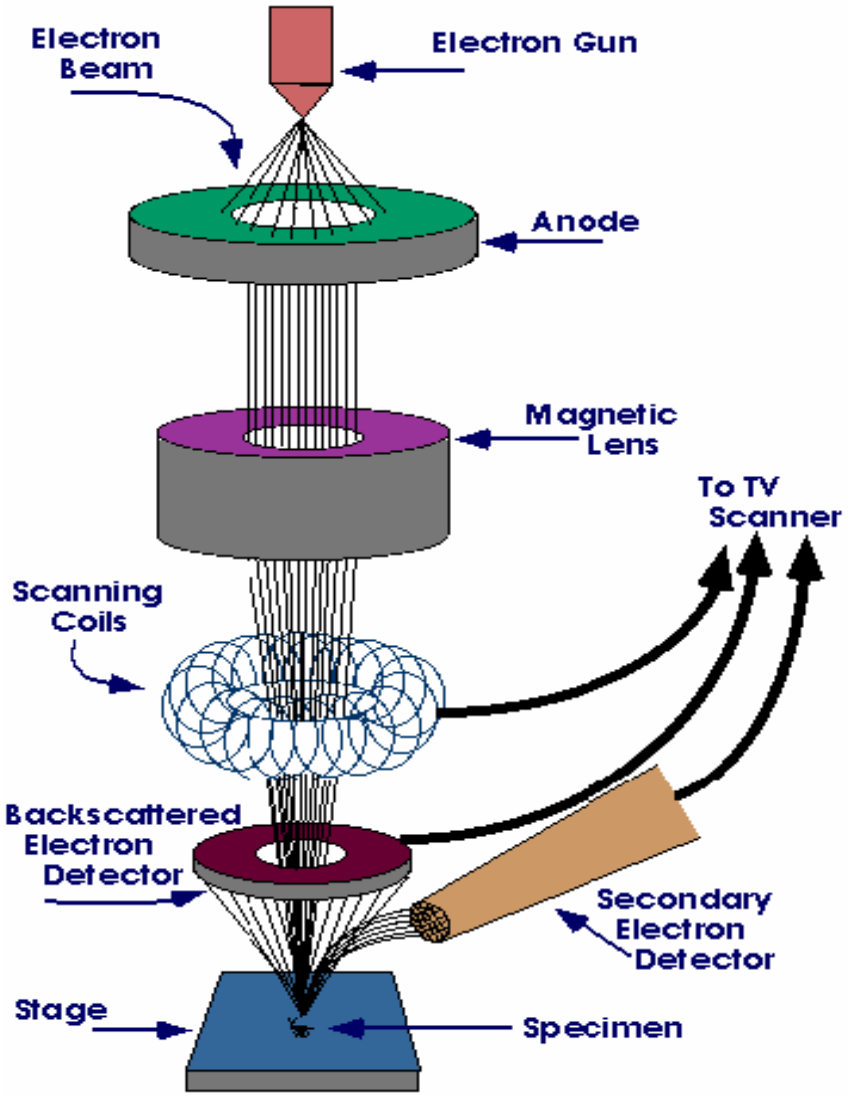

Figure 2-6: Schematic illustration of the SEM [49].

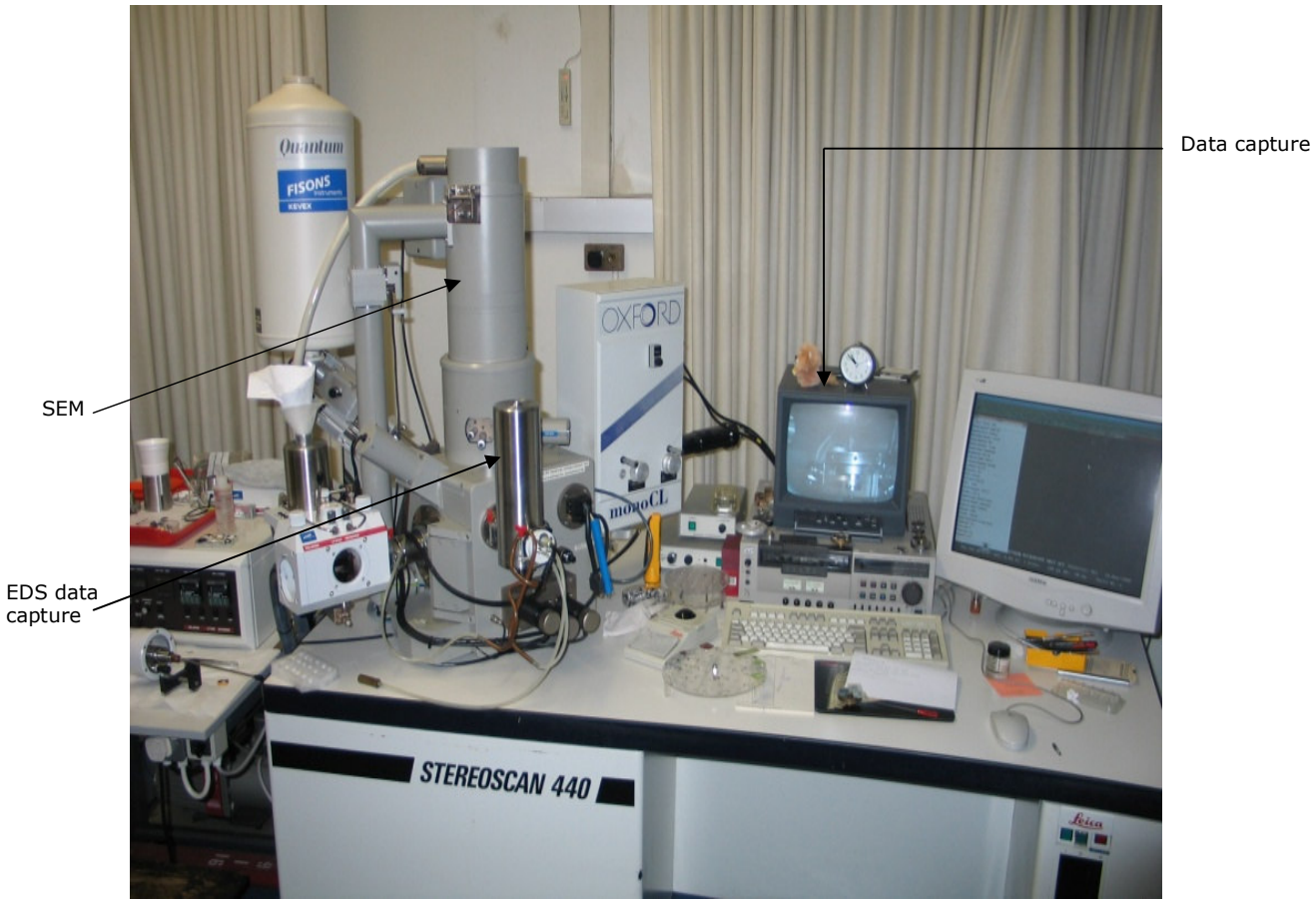

Figure 2-7: *The SEM (LEO S 440) picture which was taken from UCT.*

2.5 Energy-Dispersive X-Ray Spectroscopy (EDX)

The EDX system is connected to electron microscopes such as SEM, FE-SEM and HR-TEM. EDX spectra of the corresponding elements of the sample are obtained by measuring the energy of x-rays emitted from the sample during e-beam bombardment.

X-rays are produced as a result of ionization of an atom when an inner shell electron has been removed by the incident electrons. When an ionized atom returns from its excited state to its ground state, an electron from a higher energy outer shell fills the vacant inner shell and then releases an amount of energy equal to the potential energy difference between the two shells. This energy, which is unique for every atomic transition, will be emitted either as an x-ray or as Auger electron. In EDX analysis, the detector analyzes these emitted x-ray photons from the sample, which can be utilized for quantitative and qualitative composition analysis [54, 55].

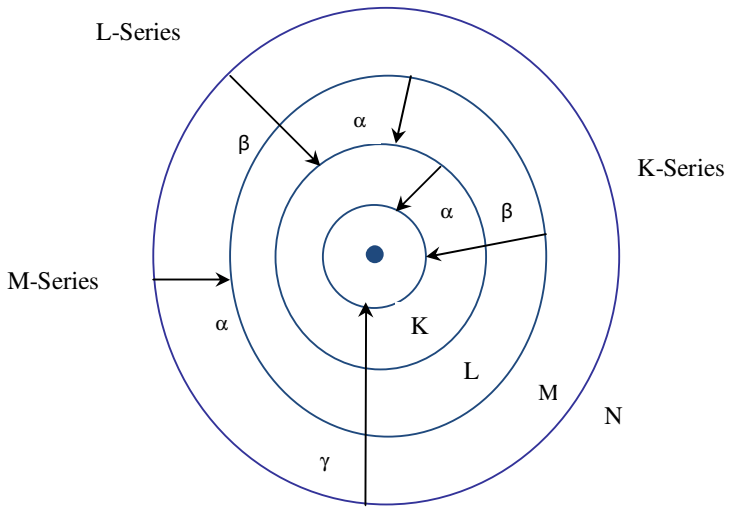

Figure 2-8: *A schematic representation showing how X-rays are produced which are used by EDX to analyze samples [49, 54-55].*

2.6 Rutherford Back-scattering (RBS)

Rutherford backscattering spectrometry (RBS) is an analytical technique used in material science. This is a non-destructive technique since the erosion and the radiation degradation of the sample material by the particle impact is negligible. Sometimes referred to as high-energy ion scattering (HEIS) spectrometry, RBS is used to determine the structure and composition of materials by measuring the backscattering of a beam of high energy ions impinging on a sample [56].

In RBS, ions of a high kinetic energy (typically 1-3MeV) are directed at the sample. The incident ions are elastically scattered from the atoms in the sample. The number of scattered ions and their energy is measured. The data obtained from the spectrum gives the information on the composition of the sample, the distribution of the components and the thickness of the sample. The incident ions from a Van der Graaf are positively charged He+ atoms or protons [56].

In order for the signal from the detector to be processed, common nuclear electronics and the particle energy spectra are stored in a computer based multi channel analyzer. The data evaluation is accomplished using standard procedures and computer codes. The advantage of the RBS analysis depends in the quantitative analysis of major and minor constituents lying in the first 0.5 to 2.0 micrometers of a material. The detection limits vary from 10^{11} to 10^{15} at.cm^{-2} for heavy and light elements depending on the sample structure and composition respectively. The best solution for improving the detection limits of some light elements is to use resonant scattering. The depth distribution of constituents can be reconstructed with a depth resolution approximately 10-20 nm.

2.6.1 Kinematic factor

The interaction between the projectile ion and the target atom can be properly described by a simple elastic collision of two isolated particles when the conditions below are fulfilled.

1. The projectile energy E_o must be larger than the binding energy (in order of eV) of the atom in the target.
2. Nuclear reactions and resonances must be absent. For H^+ beam, nuclear effects can appear below 1 MeV; with He^+, nuclear effects begin to appear at relatively higher energies.

From the assumptions, we consider the collision between two particles. The projectile of mass M_1 has an incident energy E_o and the target of mass M_2 is initially at rest. After the elastic collision, a part of projectile energy transfers to the target.

The kinematics of the simple elastic collision can be fully solved by applying the principles of conservation of energy and momentum. The ratio K of the scattering energy to the incident energy can be defined as:

$$K = \frac{E_1}{E_0} = \left[\frac{(M_2{}^2 - M_1{}^2 \sin^2\theta)^{0.5} + M_1 \cos\theta}{M_1 + M_2} \right]^2 \qquad (2.8)$$

The ratio K is also called *kinematic factor.* The scattered angle θ, which is defined as the angle between the projectile incident direction and the scattered angle is shown in Figure. Using kinematic factor formula, M_2 can be determined from the known incident particle mass M_1, the initial energy E_o, scattering angle θ and scattering energy E_1.

The small mass difference ΔM_2 produces a small energy change ΔE_1 in the measured energy ΔE_1 of the projectile after the collision. The relation between ΔM_2 and ΔE_1 is given by:

$$\Delta E_1 \approx E_0 \left(\frac{dK}{dM_2} \right) \cdot \Delta M_2 \qquad (2.9)$$

Therefore, the mass resolution can be estimated from the overall resolution δE of RBS as:

$$\delta M_2 = \frac{\delta E}{E_0} \left(\frac{dK}{dM_2} \right)^{-1} \qquad (2.10)$$

If the mass difference of two elements in the target falls below the limit mentioned above, the distinction between two elements is lost [56-57].

2.6.2 Scattering Cross Section

Scattering cross section σ is the likelihood of occurrence of a two-body collision. This leads to the capability of quantitative analysis of atomic composition. The differential scattering cross section dσ/dΩ can be used to estimate how frequently a collision actually occurs and ultimately the scattering yield at a certain angle θ.

In most cases, the force between the projectile ion and the target atom is very small described by Coulomb repulsion of the two nuclei as long as the distance of closest approach is large compared with nuclear dimensions, but small compared with the Bohr radius $a_B=\hbar/m_e.e=0.53Å$. The assumptions made came out with the differential scattering cross section given by Rutherford formula:

$$\left[d\sigma / d\Omega\right]_c = \left(\frac{Z_1 Z_2 e^2}{4E_0}\right)^2 \times 4 \frac{\left[\sqrt{\left(M_2{}^2 - M_1{}^2 \sin^2\theta\right)} + M_2 \cos\theta\right]^2}{M_2 \sin^4\theta \left(M_2{}^2 - M_1{}^2 \sin^2\theta\right)^{0.5}} \quad (2.11)$$

where Z_1 and Z_2 represent nuclear charge of the incident particle and target atom, respectively. For a target of a thin film with thickness *D,* the scattering yield *Y(θ),* detected by a finite acceptance solid angle $\Delta\Omega$ at particular scattering angle *θ,* which can be given by:

$$Y(\theta) = N.D \times \frac{d\sigma}{d\Omega} \times \frac{\Delta\Omega.Q}{\cos\alpha} \quad (2.12)$$

where *Q* represents the number of incident ions impinging into the target, *N* is the atomic density of the target and is the incident angle [56-57].

2.7 Elastic Recoil Detection Analysis (ERDA)

ERDA uses high energy of about 1MeV/amu, heavy ion beam to kinematically recoil and depth profile low atomic number target atoms. The heavy ion projectile only requires a greater mass than the target atom. Alpha particles (He^+) are commonly used to obtain recoil spectrum for hydrogen and its isotopes. Kapton with four elements ($C_{22}H_{10}N_2O_5$) is used as the standard target for calibration. The composition, the depth profile of the target is determined in this technique [58].

Consider a beam of positive ions strikes a solid target, and then enough energy can be transferred from the incident ion to the target nucleus during their elastic collision to make the latter recoil from the target. There is an energy loss (from scattered particles) which can be determined between the initial beam energy and the final. The heavy elements from the target can be blocked by the Mylar foil, which only allows the light element (such as hydrogen) to pass through and detected, shown in Figure 2-9. The concentration of hydrogen can be calculated using the SIMNRA program [58-59].

Using the momentum and energy conservation laws, the relation between the energy E_r of the recoil particle and the incident energy E_o can be defined as [58-60]:

$$E_r = K_r E_O \tag{2.14}$$

Where K_r is a kinematic factor connected with the recoil particle, defined by:

$$K_r = \frac{4M_1M_2\cos^2\varphi}{(M_1+M_2)^2} \tag{2.15}$$

Where M_1, M_2 and φ are: the mass of the projectile, recoil particles and the recoil angle, respectively. Therefore, it is easy to see that:

$$K_r = 1 - K \tag{2.16}$$

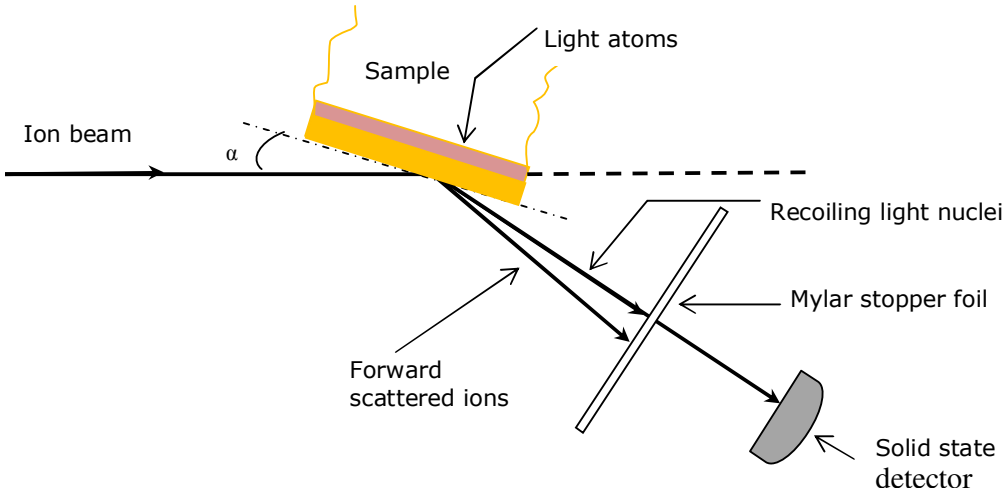

Figure 2-9: *Schematic representation of the irradiation setup in ERDA* [58, 60].

2.8 Visible and Ultraviolet Spectroscopy

Sunlight is seen to be white light or as uniform or homogeneous in color, it is actually composed of a broad range of radiation wavelengths in the ultraviolet (UV), visible and infrared (IR) portions of the spectrum. Different molecules absorb radiant of different wavelengths, but many molecules absorb ultraviolet or visible light. The absorbance of solution is directly proportional to the attenuation of the beam meaning if absorbance increases attenuation of the beam also increases. The absorbance is also directly proportional to the path length, b, and the concentration, c, of the absorbing species [61-62]. *Beer's Law* states that

$$A=\varepsilon bc \tag{2.17}$$

where ε is a constant of proportionality, called the *absorbtivity.*

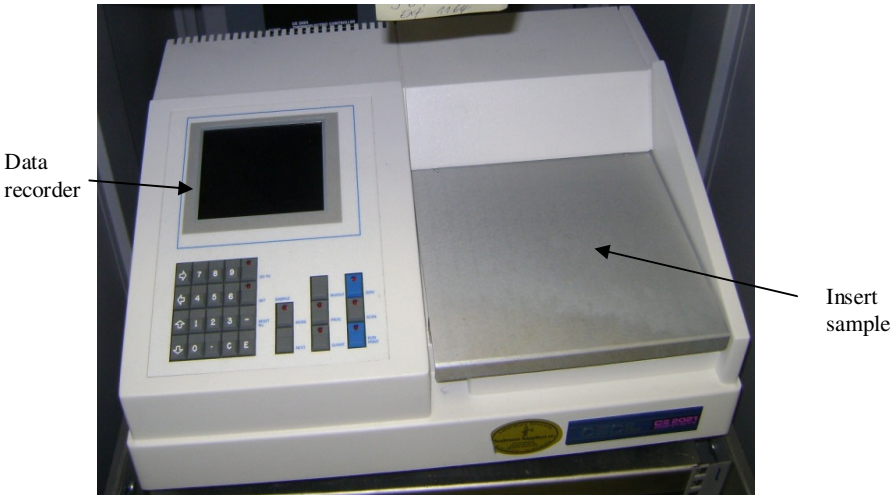

Figure 2-10: *The UV-Visible Spectrophotometer at iThemba LABS.*

2.9 Fourier Transformer Infrared Radiation (FTIR) Spectroscopy

FTIR is the most used techniques in identifying chemicals that are either organic or inorganic. It can be utilized to quantitative some components of an unknown mixture. This technique can be applied to the analysis of liquids, solids and gases. It can also used in identifying chemicals from spills, coatings, paints polymers, drugs and contaminants [63]. The FTIR used in this research is shown in figure 2-11.

By interpreting the infrared absorption spectrum, the chemical bonds in the molecule can be determined. For the most common materials, the spectrum of an unknown can be identified by comparison to a library of known compounds [63].

Figure 2-11: *The FTIR Spectroscopy picture taken from UWC.*

2.9.1 Infrared (IR) Spectroscopy

Infrared (IR) spectroscopy is considered as one of the most common spectroscopic techniques, which is used by organic and inorganic chemists. Others call it the absorption measurement of different IR frequencies by a sample positioned in the path of IR wavelength or beam. The main aim for using IR spectroscopy analysis is to determine the chemical functional groups in the sample, and functional groups can be determined according to its different absorption characteristic frequencies of IR radiation [63-64].

In this technique, there are some general uses; namely:

- *Determination of functional groups in organic materials*
- *Determination of the molecular composition of surfaces*
- *Determination of structural isomers and geometrical isomers (molecular conformation stereochemistry)*
- *Determination of molecular orientation (polymers and solutions)*
- *Identification of all types of organic and many types of inorganic compounds*
- *Identification of chromatographic effluents*
- *Quantitative determination of compounds in the mixtures*
- *It is a nondestructive method*

The common applications are:

- *Identification of compounds in spectrum using the reference spectrum*
- *Identification of functional groups unknown substances*
- *Identification of reaction components and kinetic studies of reactions*
- *Identification of molecular orientation in polymer films*
- *Identification of polymers, plastics, and resins*

- *Detection of molecular impurities or additives present in amount of 1 % and 0.01 % if it is low*
- *Formulation such analysis such as insecticides and copol*

2.9.2 State of samples

Analysis can be done almost in any solid, liquid or gas samples. The amount for the solids expected is 50 to 200 mg, but 10 µg ground with transparent matrix (e.g. KBr) is the minimum for qualitative determinations; 1 to 10 µg minimum amount which is required if the solid is soluble in a suitable solvent.

The analysis of liquids can be done for 0.5 µl if neat and less if pure. Gases only need 50 ppb for its analysis. Some solid samples need to be grinded into KBr matrix or to be dissolve in a suitable solvent (such as CCl_4 and CS_2). Solid sample can use holder to be analyzed and cells if liquids. This technique sensitive in water, therefore water should be removed from the sample if possible. The estimated time to obtain spectrum of one is from 1 to 10 min depending on the type of the instrument and the resolution required. It is investigated that most samples can be prepared in duration of about 1 to 5 minutes for infrared (IR) analysis [63-64].

2.9.3 IR Frequency Range

Infrared radiation is the electromagnetic radiation having a wavelength of between 700 nanometers and 1 millimeter. In the IR spectrum, the Wavenumbers range approximately from 13, 000 to 10 cm^{-1} and its wavelengths longer than visible light but shorter than radio waves [63-64]. The interpretation of spectra is giving the correlation of absorption bands in the spectrum of unknown compound with the known absorption frequencies for types of bonds [63-64]. The

Table 4-1 helps the users in significant for the identification of the source of the absorption band with *intensity* (**w**eak, **m**edium, or **s**trong)*, shape* (**b**road or **sh**arp)*, position* (cm^{-1}) in the spectrum.

IR absorption positions are presented as either wavenumbers ($\bar{v}$) or wavelengths (λ) [64]. Wavenumber defines the number of waves per unit length. Wavenumbers are directly proportional to frequency *f,* as well as the energy of the IR absorption and inversely proportional to wavelength. Wavenumber, frequency and wavelength can be interconverted using the following equations:

$$\bar{v} = \frac{1}{\lambda} \times 10^4 \qquad (2.18)$$

where $\bar{v}$ is measured in per centimeter (cm^{-1}) and λ is in microns (μm).

Bond	Compound Type	Frequency range(cm^{-1})
C-H	Alkanes	2960-2850(s) stretch
		1470-1350(v) scissoring and bending
	CH_3 Umbrella Deformation	1380(m-w)-Double-isopropyl, *t*-butyl
C-H	Alkenes	3080-3020(m) stretch
		1000-675(s) bend
C-H	Aromatic Rings	3100-3000(m) stretch
	Phenyl Ring Substitution Bands	870-675(s)bend
	Phenyl Ring Substitution Overtones	2000-1600(w)-fingerprint region
C-H	Alkynes	3333-3267(s) stretch
		700-610(b) bend
C=C	Alkenes	1680-1640(m, w) stretch
C≡C	Alkynes	2260-2100(w, sh) stretch
C=C	Aromatic Rings	1600-1500(w) stretch
C-O	Alcohols, Ethers, Carboxylic acids, Esters	1260-1000(s) stretch
C=O	Aldehydes, Ketones, Carboxylic acids, Esters	1760-1670(s) stretch
O-H	Monomeric-Alcohols, Phenols	3640-3160(s, br) stretch
	Hydrogen -bonded-Alcohols, Phenols	3600-3200(b) stretch
	Carboxylic acids	3000-2500(b) stretch
N-H	Amines	3500-3300(m) stretch
		1650-1580 (m) bend
C-N	Amines	1340-1020(m) stretch
C≡N	Nitriles	2260-2220(v) stretch
NO_2	Nitro Compounds	1660-1500(s) asymmetrical stretch
		1390-1260(s) symmetrical stretch

Table 2-1: *Characteristic infrared absorption frequencies* [64].

2.10 Theory of Raman Spectroscopy

Vibrational spectroscopy provides functional information on the structure of molecules. Molecules absorb radiation of frequencies, and that matches exactly the frequencies of vibration within the molecule. The frequency at which a molecule vibrates depends upon the forces between the atoms, the masses of the atoms, and the geometry of the molecule. If radiation passes through a transparent medium, the species present scatter a fraction of the beam in all directions. Raman scattering results from the same type of quantized vibrational changes associated with IR absorption, and the difference in wavelength between the incident and scattered visible radiation corresponds to the wavelength in the mid-IR region [65].

In Raman spectroscopy the energies of the same vibration modes can be obtained. Standard Raman spectroscopy is a scattering technique: a molecule is exposed to a light beam and deflects some of this light into different directions. Some of this deflected light obtains a higher or lower energy due to exchange of energy with the molecule, leaving the molecule in a lower or higher vibration state. Deflected or scattered light with the same frequency as the incident laser beam is called ***Rayleigh scattering***, light with higher frequencies is referred to as ***anti-Stokes scattering***, and with lower frequencies as ***Stokes scattering***. (see Figure 2-13). The anti- Stokes lines are weaker than the Stokes lines, since they can only be observed if a vibrational mode is thermally excited. The difference frequency between the incident and the scattered light corresponds to the vibrational energy of the mode involved. The selection rule for a mode to be Raman active differs considerably from that of absorption spectroscopy. For a mode to be Raman active its polarizability has to change during the vibration. Modes that are active in absorption need not be Raman active, and vice versa. Consequently, Raman is a tool that can give additional unique information on molecular vibrations.

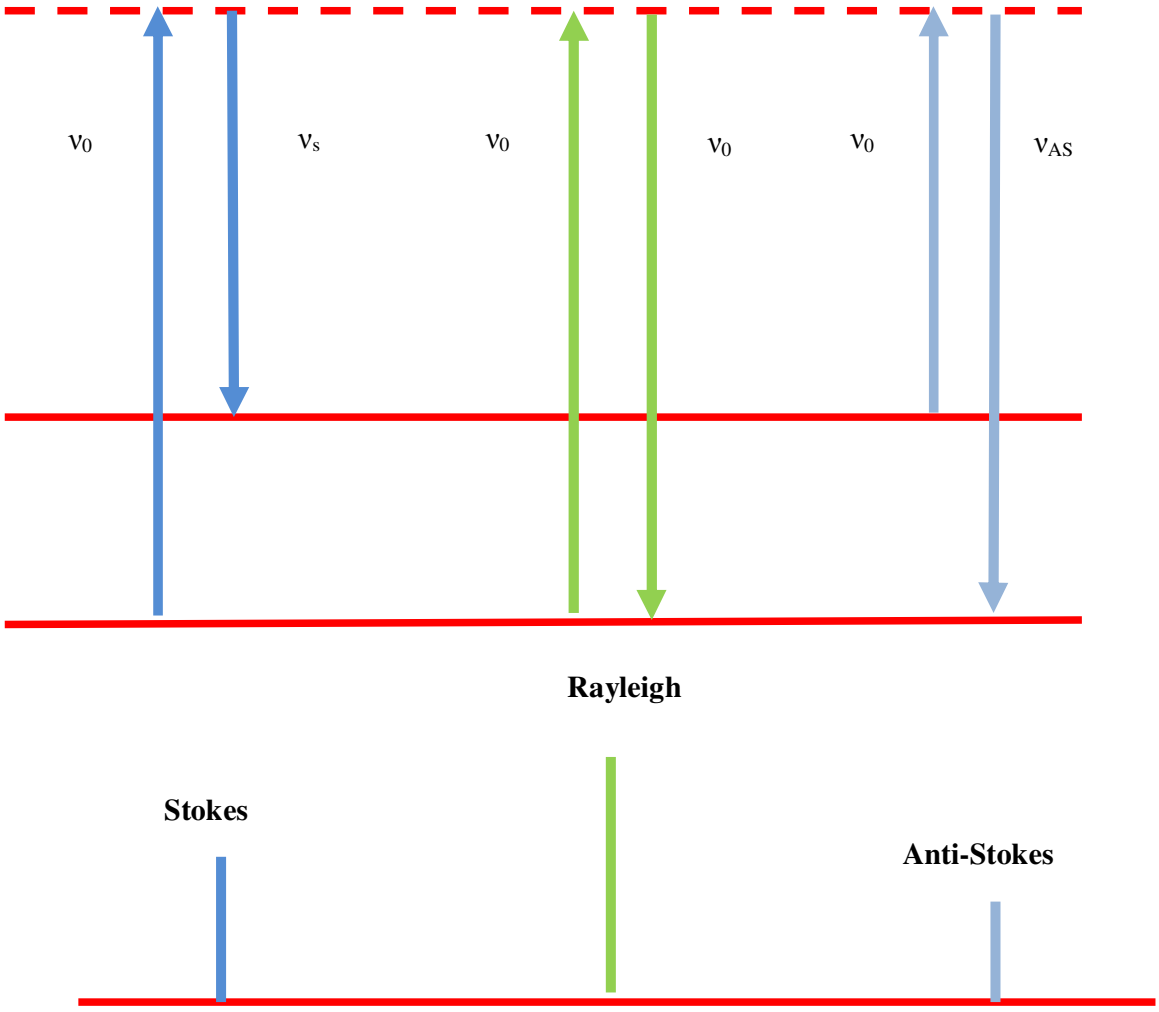

Figure 2-12: *Rayleigh and Raman Scattering* [65].

2.10.1 The Raman experimental setup

Lasers are the mostly used sources in the modern Raman spectrometry shown in figure 2-13; however lasers are used because of their high intensity and they are necessary to produce Raman scattering of sufficient intensity to be measured with a reasonable signal-to-noise ratio. The five types of common lasers used in Raman spectroscopy are listed in table 2-2.

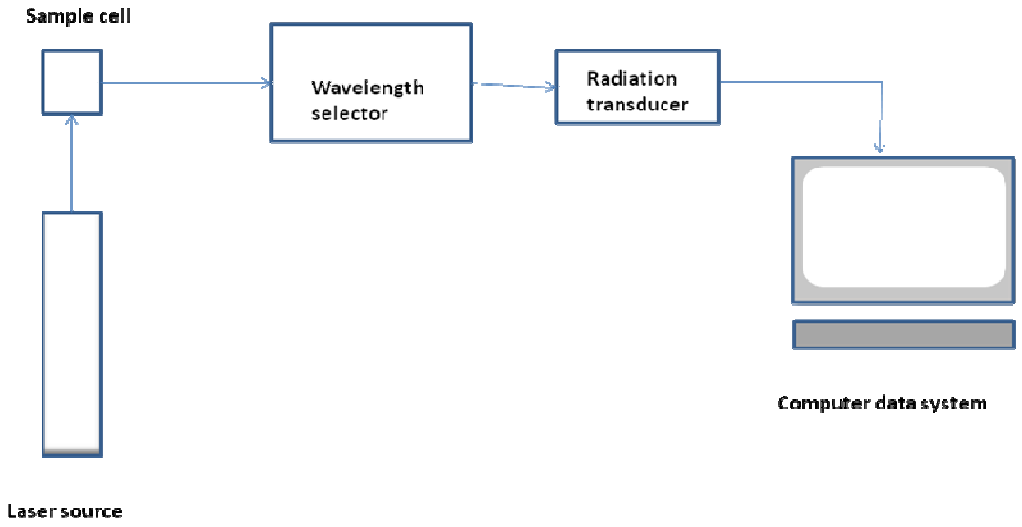

Figure 2-13: *Block diagram of the Raman spectrometer* [50]

Laser Type	Wavelength (nm)
Argon ion	488.0 or 514.5
Krypton ion	530.90 or 647.1
Helium-neon	632.8
Diode	785 or 830
Nd-YAG	1064

Table 2-2: *The common Laser Sources for Raman Spectroscopy* [50].

CHAPTER 3 -Methodology

3.1 Deposition of V_2O_5 film

It has been mentioned in chapter 1 that chemical methods will be used to prepare the VO_2 samples from V_2O_5 precursor. The bare glass was used as the main substrate for the initial preparation of the V_2O_5 film. Silicon (111) was also used as a substrate for the high temperature annealing. The substrates were cleaned using ultra sonic device. They were put in a beaker which containing methanol, acetone and trichloroethylene. After the substrates have been washed, they were rinsed using de-ionized water.

After the substrates were well cleaned, they were cut in 10 mm x 10 mm. The droplets approximately 4.8 ml of vanadium pent-oxide solution were deposited on a bare glass substrates and silicon wafer (Si [100]). In order for the solution to dry up, these substrates were heated in the furnace (oven) at about 95 ^{0}C for two hours. A brownish film grew on the substrates, with a colour which corresponded to that of the V_2O_5 solution. These samples were taken for XRD phase measurements to verify whether V_2O_5 peaks were present.

3.2 Reduction of V_2O_5 to VO_2 using H_2/Ar gas

The deposited samples of V_2O_5 films were annealed to produce VO_2 films in the presence of hydrogen (see chapter 1.4.1). During annealing, the parameters such as temperature, flow rate and time were varied. The first step was to put the samples in a HV furnace. In this case the first parameter to be varied was temperature. In order to reduce the stress on the substrate (glass) and not to consume our precursor completely; the temperature was varied from 200 ^{o}C to 550 ^{0}C. The annealing time and flow-rate of the gas were fixed at two hours and

4.5 litres per minute, respectively. The mixture of 10 % hydrogen-90 % Argon gas was used as the reducing agent of oxygen. The other samples which were deposited on silicon (111) were also annealed at: 200 ^{0}C, 300 ^{0}C, 400^0 C, 500 ^{0}C, 600 ^{0}C, 700 ^{0}C, 800 ^{0}C, and 900 ^{0}C. The reason for using silicon was to heat the sample at high temperatures because of its high melting point compared to the glass. Nevertheless, heating the sample at high temperatures produced various phases and to confirm the phases as well as the melting point of V_2O_5 we used XRD. Thereafter, the annealed samples were taken for XRD measurements to see phase formation. The temperatures at which some VO_2 was observed were 350 ^{0}C and 400 ^{0}C. Therefore, the annealing time was varied from 2 hours to 5 hours in the step size of 1 hour. The temperature was kept fixed at 400 ^{0}C and the flow rate of the gas was still fixed at 4.5 litres per minute.

The same experiment was performed with the 50:50 % mixture of hydrogen to argon. In this case only the film deposited on glass was used. In order to conserve the gas, flow rate of the gas was reduced from 4.5 l/min to 57 ml/min (milliliter per minute). The heated samples were also measured using XRD.

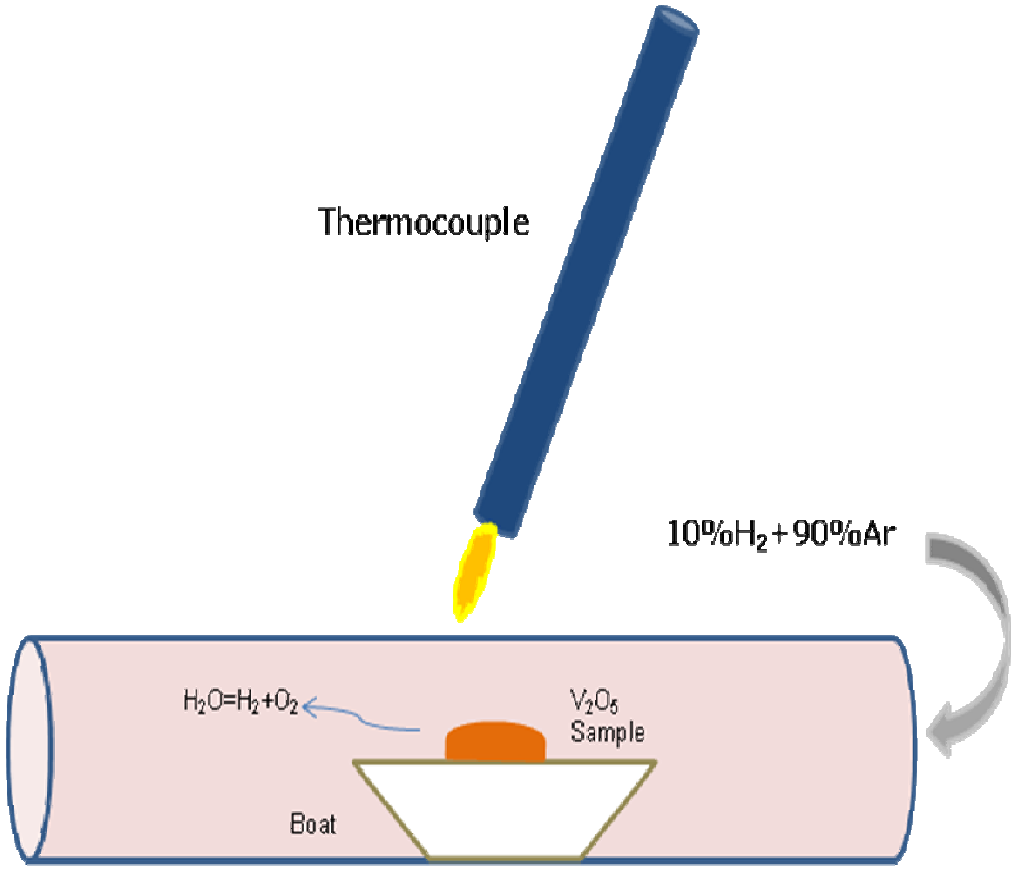

Figure 3-1*: Schematic diagram of V_2O_5 reduction to VO_2 using hydrogen (H_2) gas as reducing agent.*

3.3 Reduction of V_2O_5 to VO_2 using CO/CO_2 gas

In this case, the gas that was used was carbon monoxide (CO) to reduce oxygen from V_2O_5. This idea is from chemistry where CO is mixed with oxygen to form carbon dioxide (CO_2). Three parameters (annealing temperature, annealing time and flow-rate of a gas) were used in this experiment. The V_2O_5 sample was heated under pure carbon monoxide to reduce all the oxygen content. A grayish, silver like film was obtained which indicated a presence of a pure metal. XRD measurements confirmed that indeed we had pure vanadium. After we have seen that CO can convert metal oxide to metal, the mixture of CO-CO_2 from the different gas cylinders were used in a sense of 50:50 % ratios. The samples of V_2O_5 on a glass were put in the furnace and the lid of the furnace was tightly closed. The furnace was switched on; the adjustable temperature was also set. In order for the gas not to spread all over the lab, the fan was switched on. This fan extracts all the gas inside the fume hood and the fume hood was also tightly closed for assurance of the gas used not to spread all over the lab.

The CO_2 was the first gas to let it flow and after five minutes let CO flow. The bubbles were seen in bottle half-filled with water and this was a symbol of gas flow. The annealing time and flow-rate were fixed to 2 hours and 4.5 litres per minute, respectively. The temperature was varied from 300 ^{0}C to 550 ^{0}C. All the temperatures were giving some VO_2 peaks under XRD but 350 ^{0}C was the best. Annealing time was also varied from 30min to 3 hours while flow-rate and temperature were fixed at 4.5 litres per minute and 300 ^{0}C, respectively.

The similar experiment to the one above was performed with the mixture of CO/CO_2 [50:50 %] gas in the same cylinder. The flow-rate of the gas was also changed to 57 milliliter per minute. The produced samples were taken for XRD to identify the phases formed.

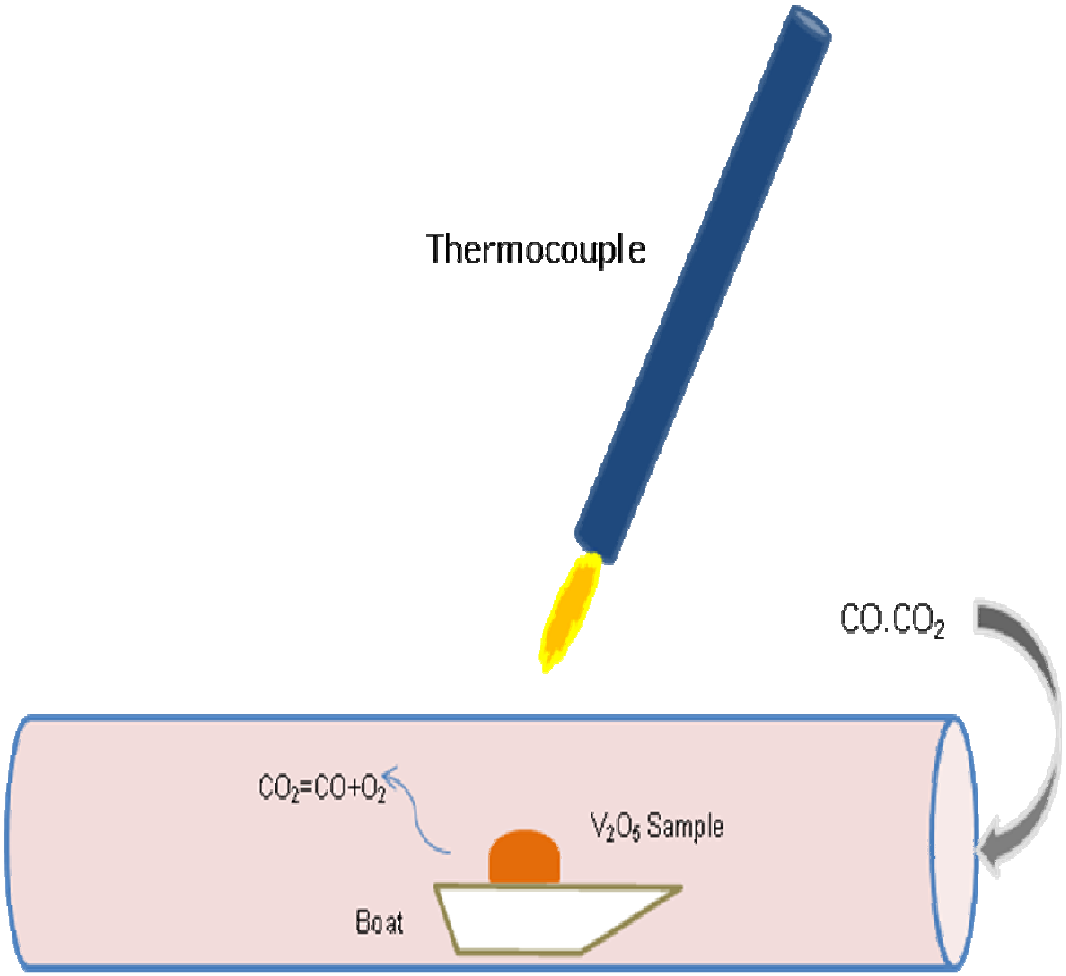

Figure 3-2 : *Schematic diagram showing the V_2O_5 reduction to VO_2 using carbon monoxide (CO) gas as the reducing agent.*

3.4 Reduction of V_2O_5 to VO_2 using laser irradiation

The main idea was to reduce V_2O_5 film to VO_2 thin film using laser pulses. V_2O_5 sol-gel was deposited on corning glass substrate and dried at 95 ^{0}C furnace for three hours. These films were ablated using XPL 200 model machine. The type of laser used is KrF excimer at a wavelength of 248 nm, energy of 272.2 mJ/cm^2, power of 113 mJ and pulse duration of 30 ns. The target-substrate distance was typically 7 cm. in order to compare the effect of laser on the film, different pulses were sent to the V_2O_5 film.

The first heating was done at low pulses of 1, 2, 5 and 10 shots. In comparison, the V_2O_5 film was also irradiated with 25 shots and 100 shots. After the V_2O_5 film had been laser irradiated, the phase and crystallinity were studied by XRD. The films were also studied using analytical techniques; AFM, SEM, FTIR, UV-Vis and Raman.

CHAPTER 4 –Experimental Results

4.1 Introduction

In this section, we present experimental results and discuss further the science behind what we got. This chapter contains results obtained from samples which were annealed under ***hydrogen***, ***carbon monoxide*** and heated using a ***laser***. There is also a presentation of the experimental analysis of correlations between sample surfaces and optical responses (using Raman spectroscopy, FTIR-spectroscopy and UV-Vis spectroscopy) for polycrystalline samples having no preferential orientation. Other analytical techniques discussed in this chapter include XRD, SEM, EDS, RBS, and ERDA.

4.2 SEM surface morphology of H_2/Ar reduced V_2O_5

In this case, SEM was used to study the surface morphology films annealed at various temperatures. The discussion is based on the film which was deposited on silicon (111) wafer as a substrate. We used silicon, because unlike the glass we used in some cases, it is thermodynamically stable at high temperature. These high temperature anneals would hopefully show the change in film morphology from the low temperature anneals. The observed surfaces vary in appearance under SEM observation as a function of annealing temperature. Analysis of the as-deposited V_2O_5 thin film (see Fig. 4-1a) shows that the film surface is not homogenous but is rough. In figure 4-1b, it can be observed that the film which was annealed at low temperature (300 ^{0}C) tends to peel in some places. This could be due to stress that develops during the annealing process, which causes the film to peel off. The sample annealed at high temperature (800 ^{0}C) in figure 4-1c shows the increase of particles on the surface. This shows that as the temperature is increased, the roughness of the film increases as well.

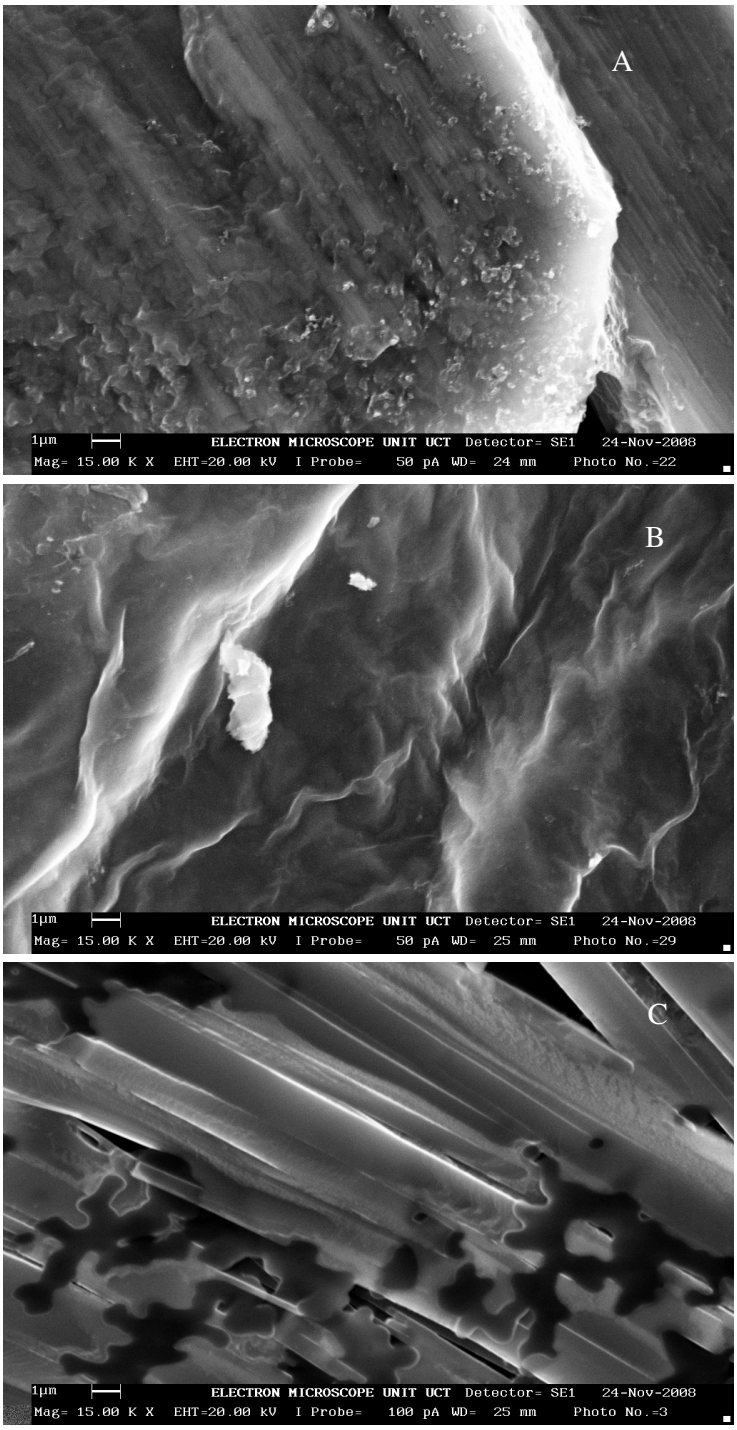

Figure 4-1: *The SEM images of the annealed V_2O_5 samples under H_2/Ar gas. (A) as-deposited film, (B) 300 ^{0}C annealed sample and (C) 800 ^{0}C annealed sample.*

The three dimensional (3D) AFM image (Fig. 4-2a) of the as deposited V_2O_5 film was taken in order to further observe microstructure and confirm the SEM result of Fig. 4-1a. The finer morphology and roughness of the films can be clearly seen. The nanoscope software analysis reveals random growth of grains in the film. The maximum roughness and average RMS roughness is 202 and 18 nm, respectively.

Fig. 4-2b shows the AFM image of annealed V_2O_5 film at 300 ^{0}C for 2 hours. It is seen that there are grains formed in the film, also it has revealed that the growth of these grains is not uniform. Using the nanoscope software, the maximum roughness and the average RMS roughness are 284 and 19 nm, respectively. The film also tends to peel from the substrate due to stress, which confirms the SEM results. The sample which was annealed at 800 ^{0}C for 2 hours is showing an increase in number of grains. The maximum roughness and the average RMS roughness are 97.2 and 6.63 nm, respectively. Comparing Fig. 4-2a and Fig. 4-2c, the roughness of the film decreases as the temperature is increased. This can be caused by an increase in the consumption of the film and the melting of V_2O_5. It can also be caused by partial peeling of the film from the substrate.

In conclusion, after thermal treatments, the increase of roughness can be explained by the grain growth. The randomly distributed grains in the films can be explained by the polycrystalline nature of vanadium or vanadium crystals during the deposition process.

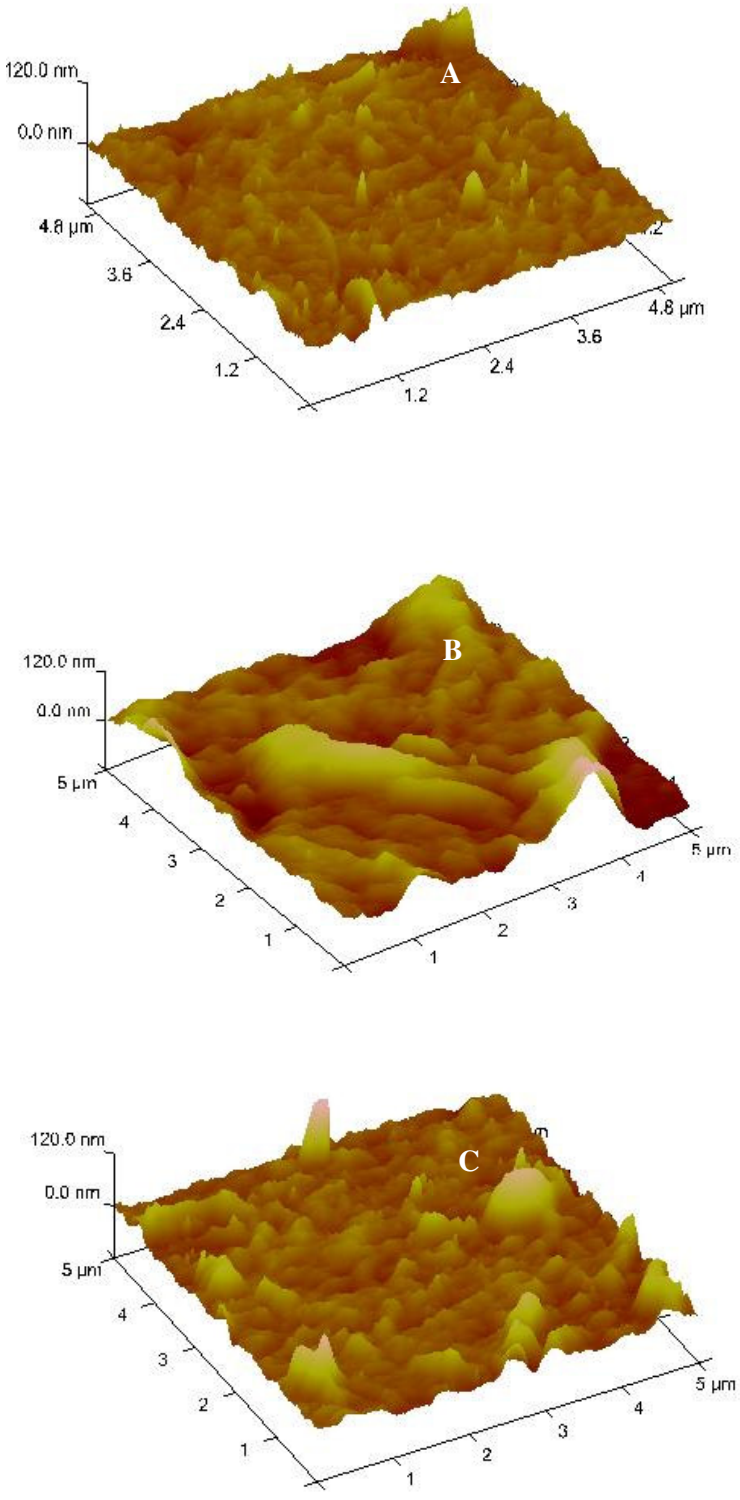

Figure 4-2: *The AFM images of the V_2O_5 film annealed under H_2/Ar gas. (a) as-deposited sample (b) annealed at 300 ^{0}C sample and (c) annealed at 800 ^{0}C.*

4.3 XRD analysis of H_2-treated samples

X-ray diffraction instrument was used to characterize the annealed V_2O_5 samples. Bruker D8 Advance XRD instrument with CuK_α source and wavelength of 1.54 Å was used to analyze calcined sample. This kind of machine uses Vantec 2000 detector to detect wide diffraction angles of the material. Silicon substrate with high melting point was used to anneal V_2O_5 at high temperatures. Vanadium has five oxidation states which make to be difficult to get single phase throughout the XRD spectrum after the sample has been annealed.

In this experiment, hydrogen was used as reducing agent in V_2O_5-VO_2 reduction. The gas flow rate used in this experiment was 1 l/min and time was fixed at two hours. In Figure 4-3, the spectra of the heated V_2O_5 samples under the mixture of 10 % hydrogen with 90 % argon. The V_2O_5 (001) peak seems to appear in all the annealing temperatures. This V_2O_5 (001) peak is decreasing in intensity, its full width at half maximum (FWHM) varies (see table 4-1). The V_2O_5 (001) peak which is found at the approximate 2θ of 41.8 ^{0} is starting to disappear from 500 ^{0}C to 900 ^{0}C.

The V_3O_7 peak was found at the approximate 2θ of 29.1 ^{0} which follows the asdeposited samples. The broadness and intensity of the peaks were varying, not constantly decreasing. Another Magneli phase, V_6O_{13} peak was found from the 700 ^{0}C and 800 ^{0}C samples at the approximate 2θ of 54.7 ^{0}. The V_4O_9 peak was found around 2θ of 31.7 ^{0}. In conclusion, the formation of Magneli phases shows that the V_2O_5-VO_2 reduction can be improved by varying time, temperature and the gas flow rate.

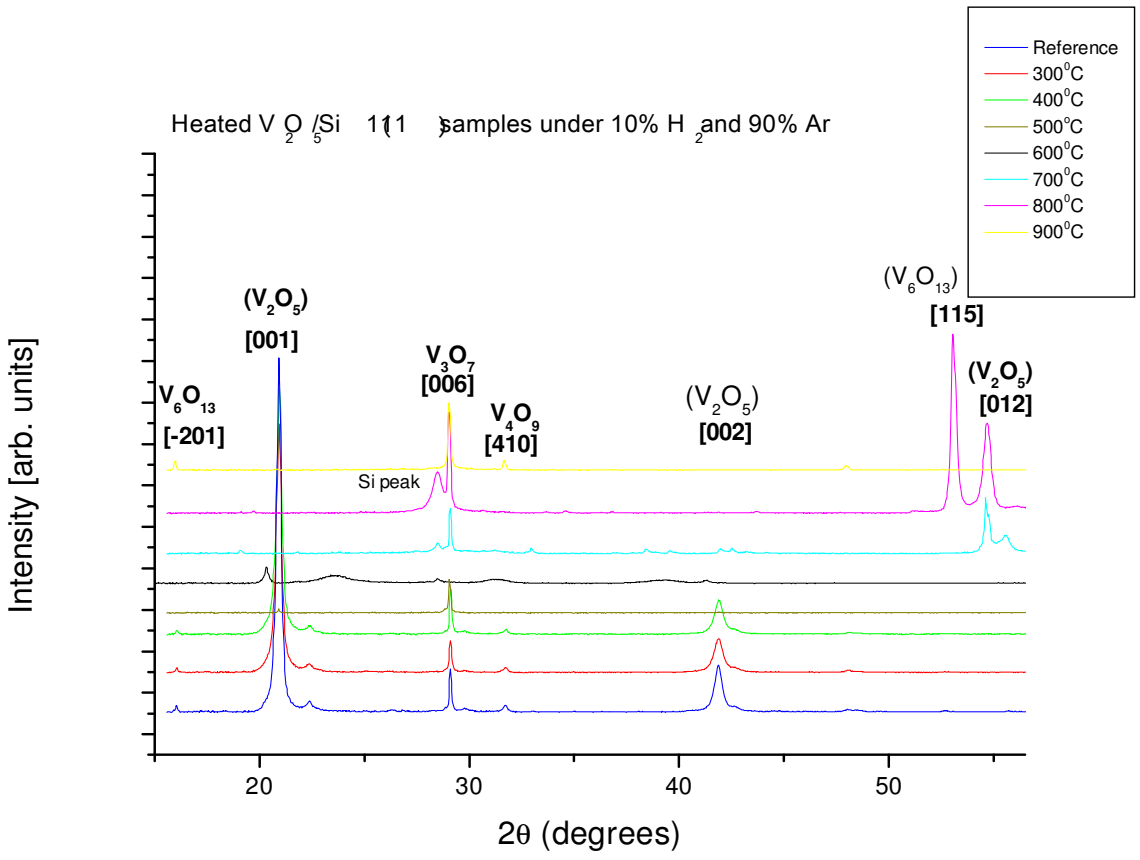

Figure 4-3: *The reduced V_2O_5/Si (111) for 2 hours under H_2/Ar gas. As the sample is heated to 700 ^{0}C and 800 ^{0}C, a new phase appears.*

Sample	2θ (^{0})	Intensity (a.u)	FWHM
Reference	20.929	45695	0.271
300 ^{0}C	20.931	31264	0.306
400 ^{0}C	20.948	30715	0.299
500 ^{0}C	20.920	519	0.084
600 ^{0}C	20.337	1999	0.207
Reference	29.105	5315	0.136
300 ^{0}C	29.109	3948	0.144
400 ^{0}C	29.120	6141	0.144
700 ^{0}C	28.500	898	0.245
700 ^{0}C	29.099	5655	0.125
800 ^{0}C	28.459	5345	0.552
800 ^{0}C	29.039	13687	0.149
900 ^{0}C	29.044	9278	0.177
Reference	31.714	847	0.249
300 ^{0}C	31.730	626	0.231
400 ^{0}C	31.740	503	0.238
700 ^{0}C	32.971	639	0.185
700 ^{0}C	54.654	6489	0.306
700 ^{0}C	55.539	2888	0.948
800 ^{0}C	53.090	22432	0.296
800 ^{0}C	54.685	11743	0.480

Table 4-1: *The V_2O_5 annealed under H_2/Ar gas shows the change in intensity and FWHM.*

4.3.1 SEM and EDS characterization of samples treated with CO/CO_2.

Scanning electron microscopy was used to evaluate the surface morphology and growth mechanism in each of these reactions. The thin films which were prepared from the CVD method (as-deposited) and the films which were reduced in the presence of CO/CO_2 were found to have similar morphologies (Figure 4-4a and 4-4b) of agglomerated particles on the substrate surface. However, the rods were obtained from pre-heated sample as well as the annealed sample. From the images, it is seen that the rods for asdeposited sample were broken down from micro-rods to nano-rods. This shows that temperature has an effect on surface morphology the V_2O_5 film. The rods of the as-deposited sample were found to have varying diameters in nanometers: 437, 304, 323, 372, 434, 350, 250, 291, and 335 with varying length in micro meters: 1.8, 1.4, 1.9, 2.0, 1.8, 1.3, 1.2, and 704 nm, 567 nm.

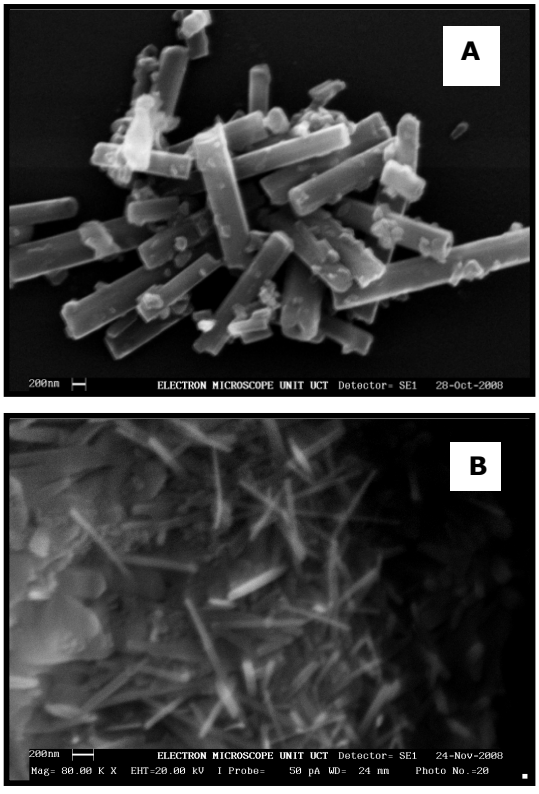

Figure 4-4: *(a) The asdeposited V_2O_5 on a glass substrate (b) the annealed V_2O_5 sample at 600^0C.*

In this research, the EDS which is interfaced with scanning electron microscopy was used for the atomic composition analysis. This technique was also use to find out whether there were impurities present in the film. The EDS spectrum in Figure 4-4 showing the *K-beta* and *K-alpha* peaks of vanadium and they are determined with the corresponding atomic weight in table 4-2. The sharp peak of *K-alpha* is showing that the sample has vanadium (V) and its atomic percent was determined as 74.14. However, oxygen (O) is also there in the sample but EDS did not extract any information due to technological problems of EDS detectors. Carbon (C) is the following element to have high atomic percentage of about 23.60. It comes from the sample since pure glass is non-conducting it had to be coated with carbon. Silicon (Si) and calcium (Ca) is probably comes from the glass substrate

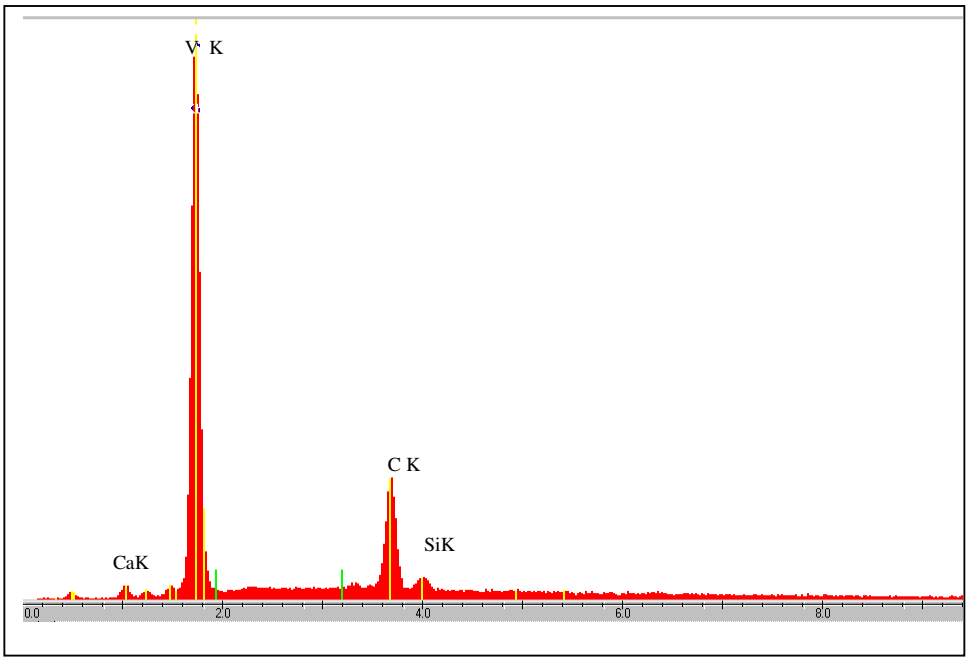

Figure 4-5: *EDS spectrum showing the vanadium main peaks*.

Element		Line	Weight %	Error k-Ratio	Atomic %
C	Ka	6.87	1.290	0.0276	23.60
O	Ka	0.00	0.000	0.0000	0.00
Si	Ka	1.30	0.042	0.0087	1.91
Ca	Ka	0.33	0.018	0.0040	0.34
V	Ka	91.50	0.384	0.8964	74.14

Table 4-2: *The information of the heated V_2O_5 sample taken from the EDS spectrum*.

4.3.2 AFM characterization of CO/CO_2-treated samples.

The AFM technique was used to study the surface morphology of the film. Both CO/CO_2 treated and non-treated V_2O_5 images were studied further to see the shape of the crystals and determine the influence of temperature on these crystals. Corning glass was the only substrate used for the deposition of the film in this experiment. Figure 4-6a is a typical AFM image of the non-treated sample, Figure 4-6b is the sample annealed at 450 ^{0}C and Figure 4-6c is the annealed sample at 600 ^{0}C for 20 minutes, respectively. This thin film exhibits the morphology of polycrystallites which shows nano-structures such as nanorods. The increase in these grains also increases the surface roughness (root mean square, RMS) of the film. The roughness of the pre-heated sample of V_2O_5 on glass was determined as 11.8 nm and the roughness of the annealed sample of V_2O_5 on a glass at 600 ^{0}C was determined as 14.8 nm. Therefore, the roughness increases as the heating time of the film increases. The increase in annealing time can change the surface structure and it is possible for the crystal structure to also change.

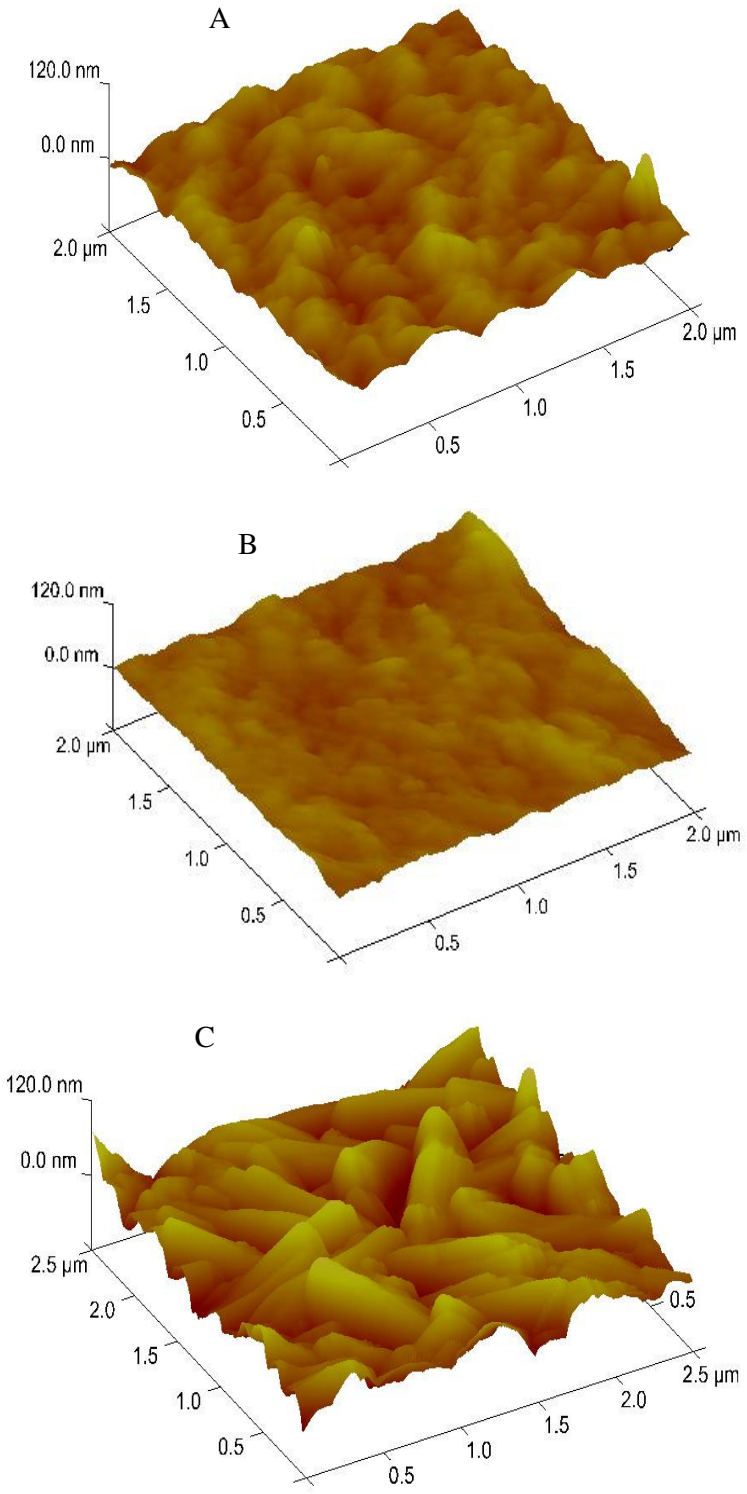

Figure 4-6: *The AFM images of the annealed samples for 20 minutes under CO/CO_2 gas. (a) Non-heated V_2O_5 deposited on a corning glass, (b) heated V_2O_5 at 450 ^0C and (c) The heated V_2O_5 at 600 ^0C.*

(a)

4.4 Crystallography of CO/CO_2 sample using XRD technique

X-ray diffraction (XRD) was used to characterize the films from all reactions and indicated the production of monoclinic vanadium dioxide from orthorhombic vanadium pent-oxide (see Figure 4-7).The identification of phases was firstly done on the 95 ^{0}C pre-heated pure V_2O_5 on a glass. The XRD results showed four peak of pure V_2O_5: [200], [001], [400], and [002]. As can be seen in the figure, the 001 reflection is the strongest peak and it was confirmed by XRD pdf file. The lattice parameters *a* and *c* were calculated from the equation (4.4) using the spectrum above. The results were: *a*= 11.5 Å and *c*=4.350 Å, which is the lattice parameter of the orthorhombic V_2O_5 **[66]**. According to the XRD pdf file, the space group of the crystal structure is P_{mn21}.

The spectra in Figure 4-8 are the heated V_2O_5 samples under the mixture of carbon monoxide with carbon dioxide. The substrate used for these samples was corning glass. These samples were annealed for 20 minutes each. Temperature was varied from 400 ^{0}C to 600 ^{0}C and flow rate of the gas was fixed at 4.5 litres per minutes. The V_2O_5 peak is diminishing directly proportional with the increase in temperature. The decrease in peak height shows that the intensity is also decreasing. As the heat treatment has been performed to the sample, V_6O_{13} and V_3O_7 peaks are starting to appear.

The spectrum in Fig. 4-9 shows the sample which was heated at 350 ^{0}C. This sample was annealed in the presence of CO/CO_2 (50:50 %) with the flow rate of 57 ml/min. According to some published papers the annealing time for V_2O_5 to form VO_2 is approximately 2 hours depending on the flow rate of gas during reduction process **[43]**. It can be seen from the spectrum that the V_2O_5 peak has totally disappeared at 350 ^{0}C and the orientation (002) of V_6O_{13} starts

dominating. The other Magneli phases such as V_3O_7 and V_4O_9 appeared at 350 ^{0}C. This phenomenon shows that oxygen began to escape from the crystal. The VO_2 signal was obtained in (-202) and (402) planes, which was confirmed by XRD pdf. file. The main V_6O_{13} peak can affect the VO_2 hysteresis which can cause poor metal-semiconductor properties. According to the spectrum the peaks are different, some are sharp and some are broad. If the peak is sharp it means FWHM is small and the grain size is large. Once the peak is broad this means the grain size is small. Therefore, the film has the mixture of large and small grains (see equation 2.5).

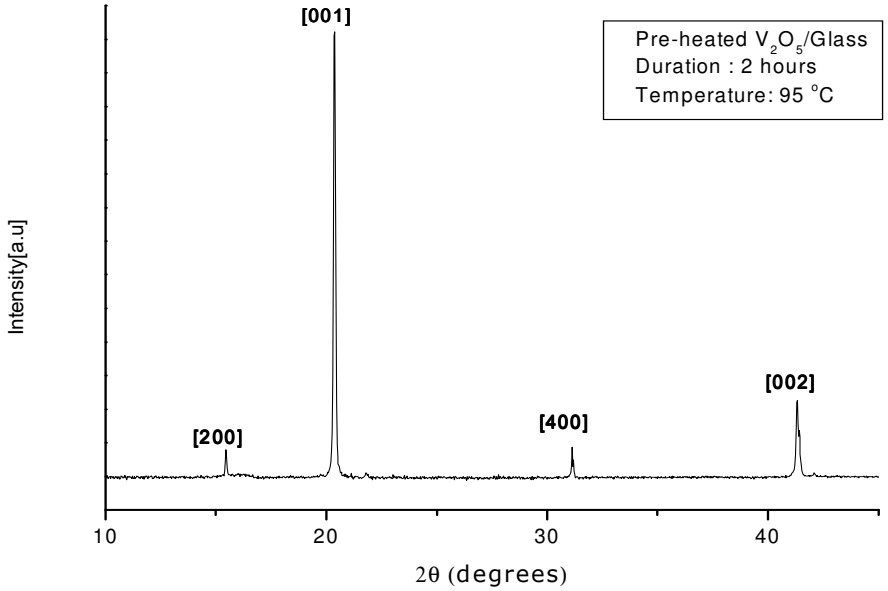

Figure 4-7: *The XRD spectrum of V_2O_5 deposited on glass substrate.*

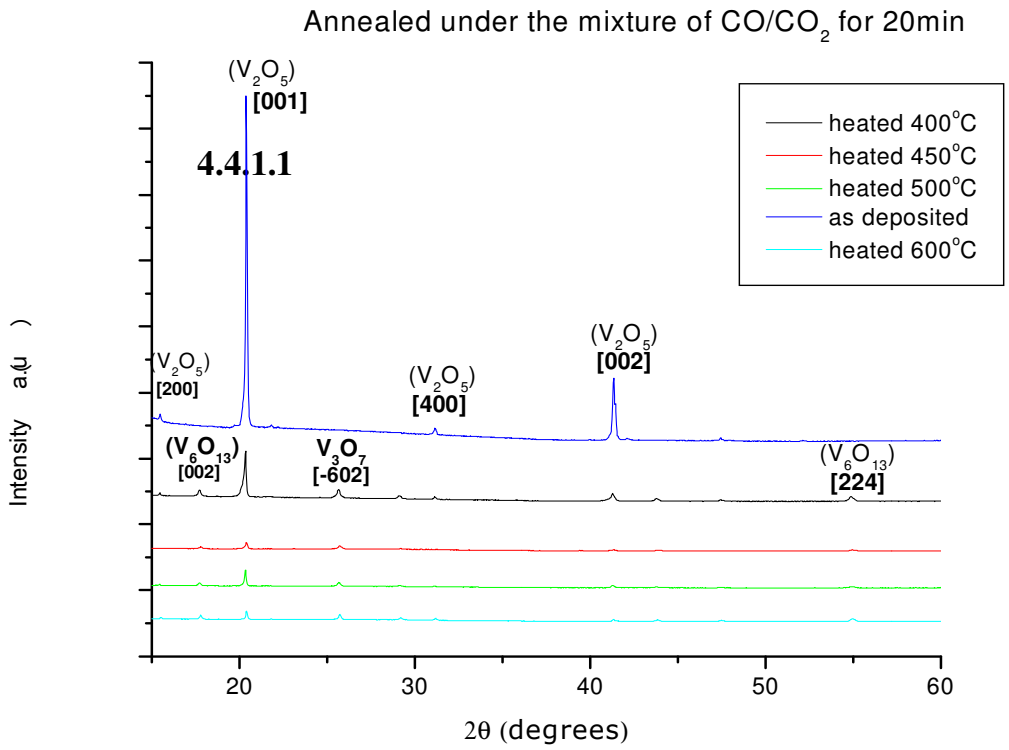

Figure 4-8: *The annealed V_2O_5/glass under the mixture of CO/CO_2.annealing time is 20 minutes.*

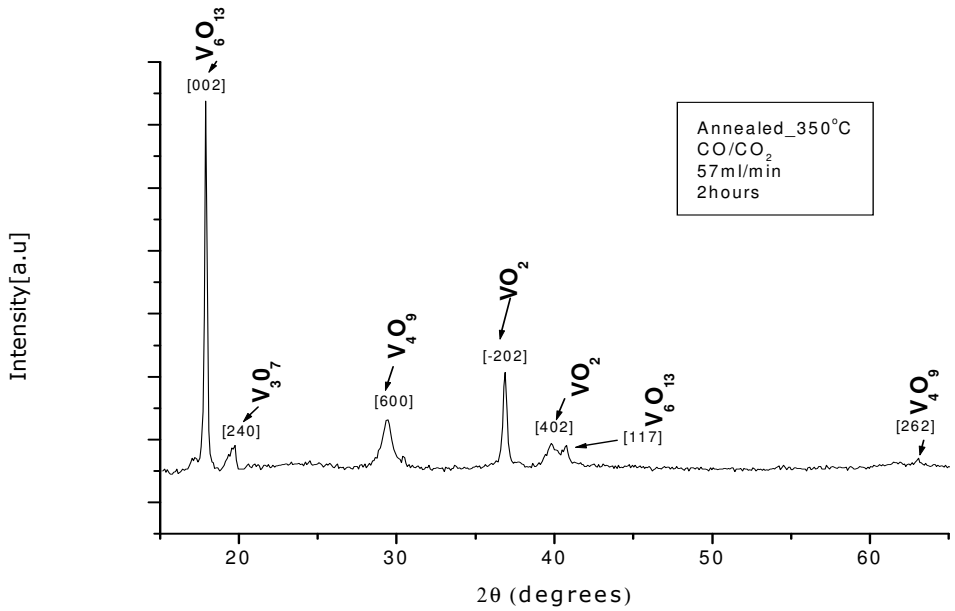

Figure 4-9: *The V_2O_5 sample, which was annealed at 350 ^{0}C under CO-CO_2.*

4.5 UV-Vis characterization of heated V_2O_5 under CO/CO_2

This kind of technique was used to study the optical behavior of the CO/CO_2 reduced sample in the visible region. By performing optical measurement using UV-Vis spectroscopy, the film can show semiconducting VO_2 behavior regardless of what is seen through XRD. In Fig 4-10, shows the UV-Visible spectra of the samples which were annealed for 20 minutes in the presence of CO/CO_2 mixture. The film is absorbing in the ultra violet region and starts to transmit in the visible range. The non-heated sample is transmitting about 8 % which indicating that the non-CO/CO_2 treated film was too thick. The transmittance of the film starts to decrease as the heat treatment was performed. The decrease in transmittance shows that the film has become rough, thus increasing its diffuse reflectance. In the absorption cut-off, there is a shift with respect to the heat treatment. This results in the change of band gap as calculated in table 4-3. Theoretical, if VO_2 is a Mott insulator there should be spin expectations below the charge-excitation gap of 0.6 eV [67]. Nevertheless, the calculated band gap shows that our film does not contain VO_2.

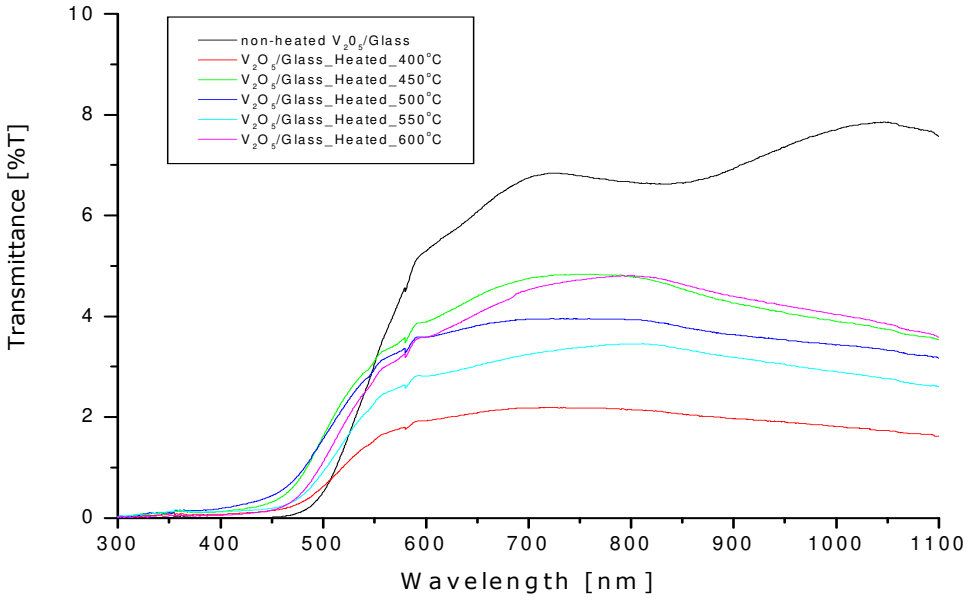

Figure 4-10: *UV-Vis spectra of the samples annealed under CO/CO_2 gas.*

Temperature (^{0}C)	λ (nm)	Eg (eV)
Non-heated	566	2.2
400	631	2.0
450	612	2.0
500	641	1.9
550	637	1.9
600	599	2.1

Table 4-3: *Calculated band gap of the annealed V_2O_5 under CO/CO_2 gas.*

4.5.1 FTIR-optical characterization of the CO/CO_2 treated V_2O_5

The FTIR was used to observe the behavior of the treated film in the infrared region. This technique was also used to determine the stretching of bonds in the infrared .In Fig. 4-11, the V_2O_5 samples were annealed for 400 ^{0}C, 450 ^{0}C, 500 ^{0}C, 550 ^{0}C, 600 ^{0}C. The annealing time was fixed for two hours under the mixture of CO/CO_2. The exponential increase of transmittance starts approximately from the wavenumber of 2000 cm^{-1}. According to theoretical V-O FTIR spectrum, stretching in V=O bond is found at the range of 400-1800 cm^{-1} and V-O-V stretching is found at 650-800 cm^{-1} **[68]**. In our spectrum V-O bound is not found since the glass substrate is absorbing a lot of visible light and infrared. According to the table of infrared data interpretation in table 4-1, C-H stretching bond is found at A= 2848 cm^{-1} and B= 2921 cm^{-1} which could be the contamination from the reducing gas. The stretching in O-H bond due to V_2O_5 sol-gel is found at the wavenumber of C=3520 cm^{-1}. The non-heated film transmits the light of about 14% and after annealing the transmittance drops to 7 %T and below.

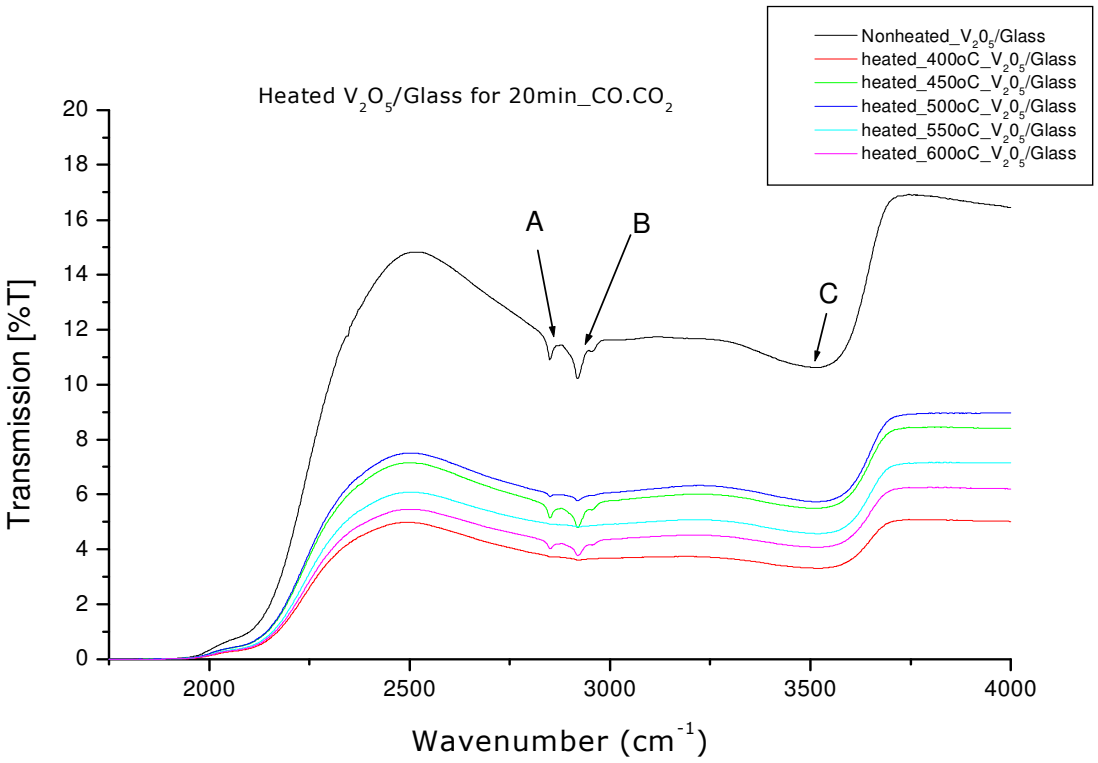

Figure 4-11: *The FTIR spectra of the annealed V_2O_5 film for 20 minutes. It was observed that temperature has influence in transmittance of the annealed film.*

4.5.2 Raman results

In this research, Raman spectroscopy was used to determine the stretching of V-O bonds and to determine the vibration modes of V_2O_5 and VO_2. It was also used to determine influence of temperature to the intensity and full width at half maximum (FWHM). The normal Raman measurements were performed to the samples which were calcined under CO/CO_2 (shown in Figure 4-12). The model used in this characterization was Horiba HR800 with the power of 5.1 mW and a wavelength of 514.5 nm.

In contrast, a shoulder with a relatively weak intensity is observed at low frequency between 200 and 450cm $^{-1}$, which is associated with the bending vibration modes of the V_3–O, V_2–O and V=O. The Raman spectra of the as-

deposited films show two broad peaks around at 496 and 535 cm^{-1}, due to the stretching modes of the V–O–V and V_3–O bonds, respectively. The shift in peaks is observed from 722 to 696 cm^{-1} and 1570 to 1137 cm^{-1}, the broadness of the peaks is also decreasing, which could be caused by the breaking of V-O bonds. The band appearing at 975 and 1020 cm^{-1} corresponds to the V (vanadium)-O_v (vanadyl oxygen) stretching mode. The band between 700 and 900 cm^{-1} is assigned to the anti-symmetric stretching vibration of the V-O_b-V group (Ob: bridge oxygen). The group of bands present at <600 cm-1 wavenumber correspond to the edge-shearing 3V-O_c stretching and the bridging V-O_b-V deformations [69-71].

When the reduction of V^{5+} ions to V^{4+} ions with the insertion of CO/CO_2 converts the V^{5+}=O bonds to V^{4+}=O bonds, it's also possible to expect the conversion of V^{5+}–O–V^{5+} single bonds to V^{4+}–O–V^{4+} single bonds. Based on these experimental results, we propose that the V^{4+}=O bonds are generated by two different mechanisms. The first mechanism is the direct conversion of V^{5+}=O bonds to V^{4+}=O bonds with CO/CO_2 insertion. The second mechanism is the breaking of V^{4+}–O–V^{4+} single bonds. When the V^{5+}–O–V^{5+} single bonds are reduced to the V^{4+}– O–V^{4+} bonds by reducing oxygen content with the insertion of CO/CO_2, the distances between V and O become longer due to the weaker coulomb interaction and these bonds can be broken, thus creating the V^{4+}=O bonds [69-71]. We believe that this second process generates a more disordered amorphous structure due to the breaking of bonds. This increased state of amorphization also can be evidenced in the V_2O_5 films deposited in decreased oxygen partial pressures. As shown in the Raman spectra of Fig. 4-12, increased oxygen deficiency (more reduced state) leads to more structural disorder in the vanadium oxide thin films.

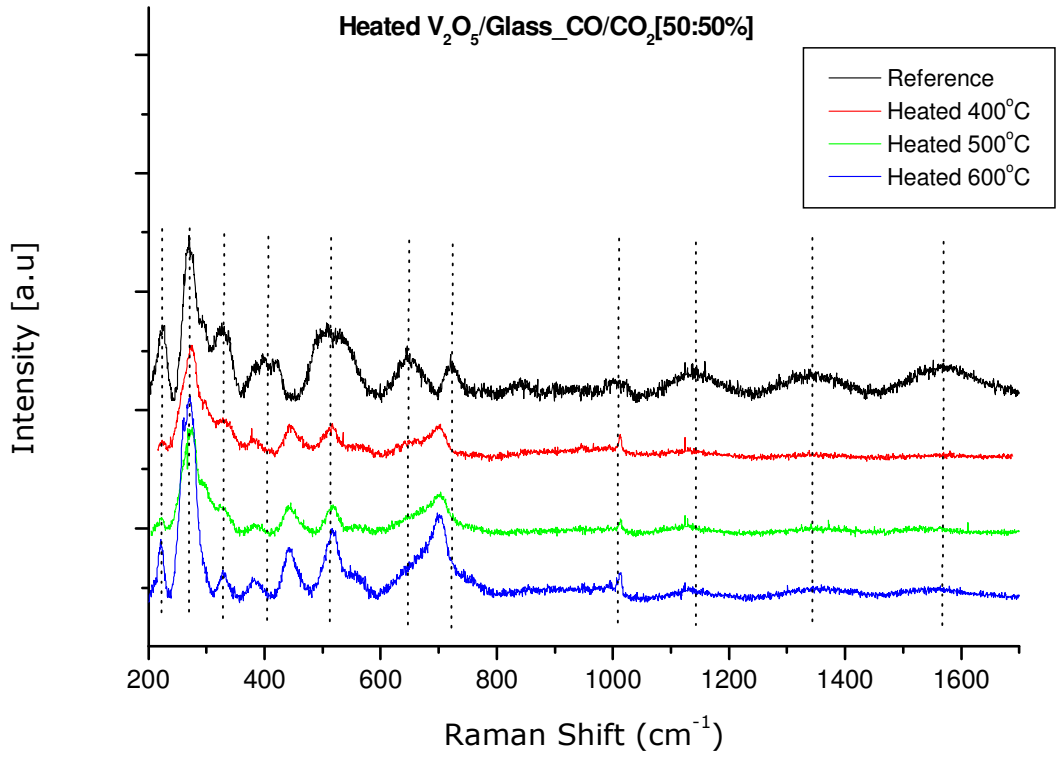

Figure 4-12: *Raman measurements of the annealed samples under CO/CO_2 gas.*

4.6 Study of surface morphology using SEM

This technique was used to study the effect of laser irradiation on the V_2O_5 film. The films which were prepared from the CVD reaction showed the images rods from samples reduced by CO/CO_2 gas. After laser irradiation, Figure 4-13a and Figure 4-13b showed similar images of spheres which seem to be hollow. The spheres which were obtained from laser irradiation had diameters in nanometers: 733, 688, 681, 650, 666, 629, 621, 615, and 591 nm. The increase in hollow spheres affects the optical properties of the film which will be studied by UV-visible spectrometer in 4.10.

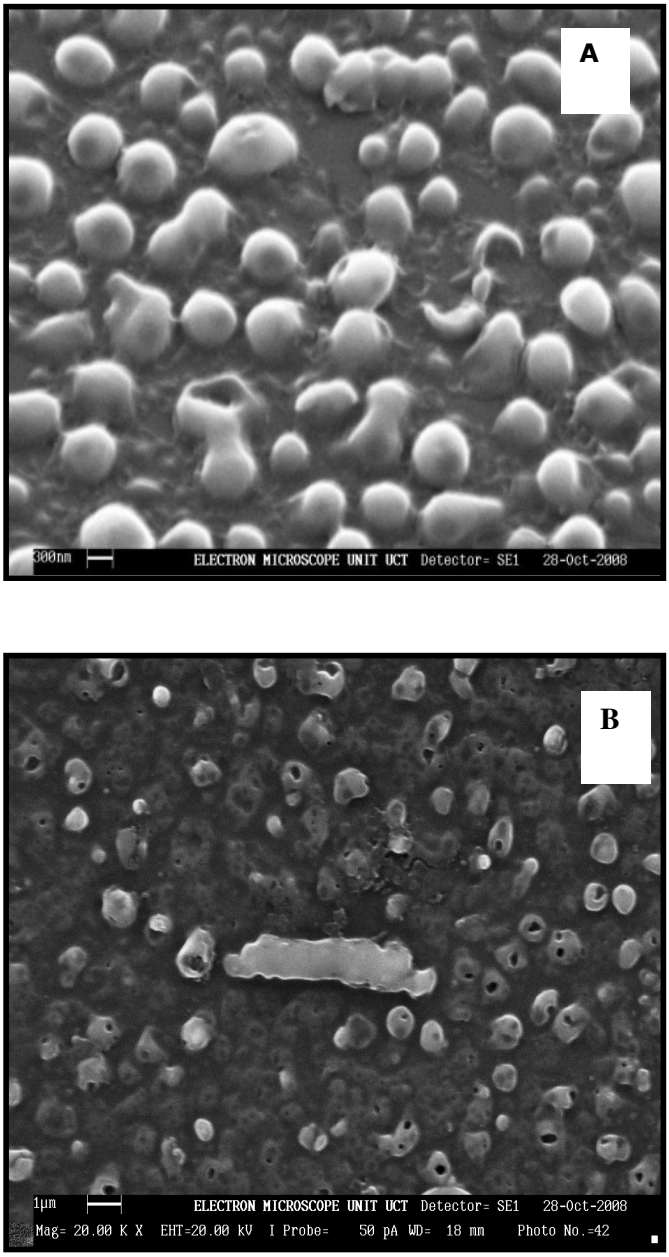

Figure 4-13: (*a) laser irradiated sample-5 shots (b) laser irradiated sample 100 shots*

4.6.1 Surface Morphology of the irradiated V_2O_5 samples

The deposited V_2O_5 samples (see Figure 4-14a) were irradiated with a laser of wavelength 514.5 nm. It was observed that, the increasing of crystals also increases the root mean square roughness of the film as shown in Fig. (4-14b). Using Nanoscope software, the average roughness of the film was calculated. Before laser irradiation, the average root mean square roughness of the non-heated V_2O_5 film was determined as 16.7 nm. After the irradiation of five shots the average roughness root mean square roughness was determined as 103 nm. The film was also irradiated with 100 shots and showed the decrease in average root mean square roughness of 41.6 nm. Therefore, heat treatment of the film can be also done by sending the laser beam through the sample. The increase in number of shots to the film also increases the number of grains on the film surface. As in the number of shots increases, the vibration of atoms in crystal lattice and results in changing the crystal structure.

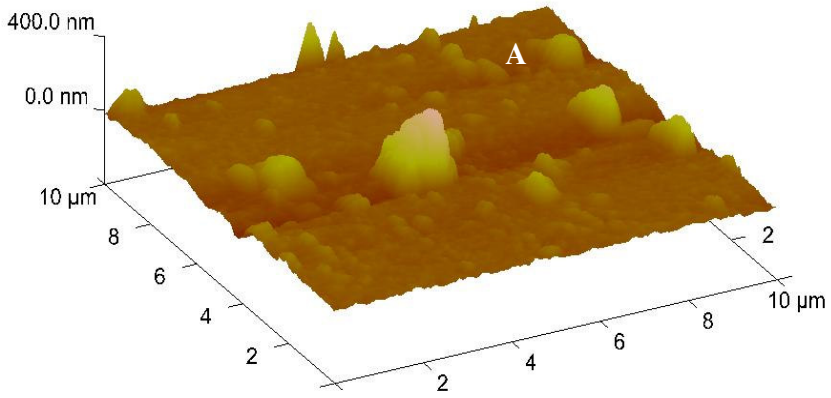

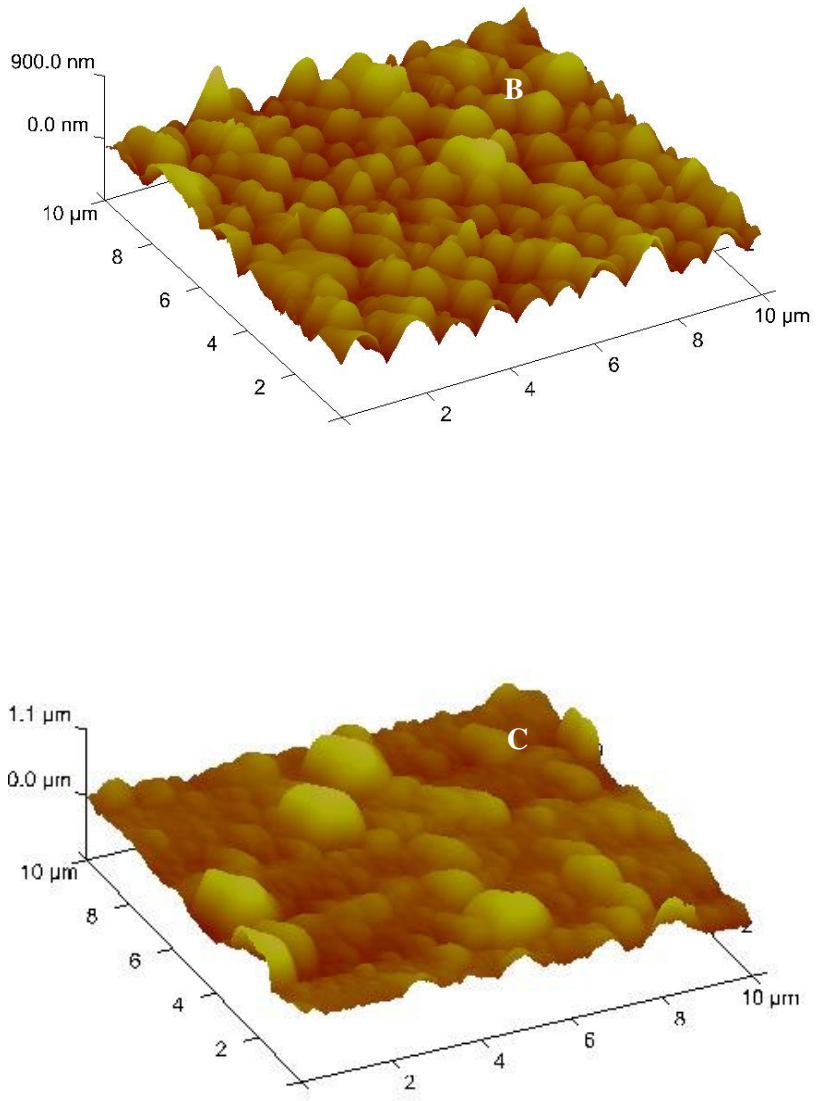

Figure 4-14: *(c) Non-heated V_2O_5 on a glass. (b) Laser irradiation of V_2O_5 film with 5 shots (c) Laser irradiation of V_2O_5 film with 100 shots*

4.7 Identification of phases using XRD technique

The XRD technique was once more used to study the crystallography of the laser irradiated samples and study the effect of shots as the function of phases. Fig. 4-15 shows a typical XRD spectrum of the sample which was irradiated with different shots: 1 shot, 2 shots, 5 shots, 10 shots, 25 shots and 100 shots.

The samples of V_2O_5 deposited on a glass, which were irradiated with the wavelength of 514.5 nm shows a phase shift in peaks compared to the non-irradiated sample. In the spectrum the shift is not uniform, is not shifting in one direction which could be due to the different doses into amorphous sample. It is also obtained that intensity and FWHM have no standard pattern but fluctuating increase. Using equation 2.6, the grain size was calculated in nano-meters as shown in Table 4-4 and 4-5.

During irradiation, the laser strikes the film which causes the vibration in atoms. This can change the crystal structure of the material. The phase shift can be seen from the magnified XRD peaks in Fig. 4-15. The sending of laser to the film is knocking atoms and heating the film at the same time. The V-O bond becomes loose which really change the crystal structure. The XRD pdf file showed that the V_2O_5 orthorhombic structure changes to tetragonal structure as the pure V_2O_5 is irradiated [72-74].

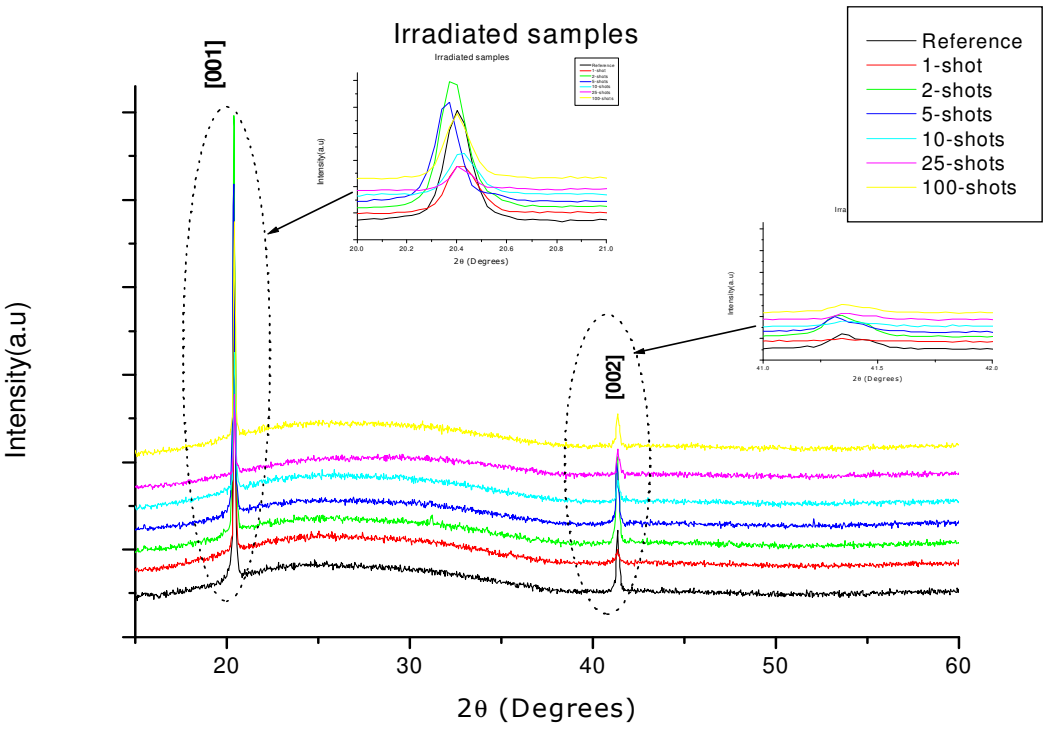

Figure 4-15: *XRD measurements in the 20 minutes annealed samples.*

[001] Peak

Shots	2θ (⁰)	intensity (a.u)	FWHM	Grain size (nm)
0	20.41	9712	0.132	22
1	20.42	4666	0.176	16
2	20.38	10889	0.127	23
5	20.36	8594	0.118	24
10	20.42	3611	0.139	20
25	20.42	1981	0.112	26
100	20.40	5550	0.130	22

Table 4-4: *laser irradiated V_2O_5 film with the calculated grain size of (001) peak.*

[002] Peak				
Shots	**2θ (0)**	**intensity (a.u)**	**FWHM**	**Grain size**
0	41.3	1434	0.128	12
0	41.4	568	0.109	14
1	41.3	195	0.085	18
1	41.4	40	0.469	3
2	41.4	932	0.161	9
2	41.3	1770	0.133	11
5	41.4	526	0.112	14
5	41.3	1322	0.111	14
10	41.3	506	0.139	11
10	41.5	189	0.119	13
25	41.4	646	0.103	15
25	41.5	345	0.152	10
100	41.4	811	0.164	9
100	41.5	290	0.080	19

Table 4-5: *laser irradiated V_2O_5 film with the calculated grain size of (002) peak.*

4.8 Raman results for the laser irradiated samples

The normal Raman measurements were performed to the samples which were heated with excimer laser (see Figure 4-16). This technique was used to see the effect of shots in the broadness and the intensity of the peaks.

At a first glance, the normal Raman spectra of our pure V_2O_5 films exhibit sharp peaks in a way similar to the CO/CO_2 treated V_2O_5 film. The intensity of these films is quite low; this fact can be explained by the small amount of deposited material and the low laser irradiation used. In addition, a luminescence background must be taken into account. The phase shift in peaks of the irradiated samples was observed, which was also observed by XRD. The full width at half maximum of the peaks was observed to be very broad although there were some few sharp peaks. However, the broadness of the bands can be due to the amorphous state of the film or caused by small crystals in the sample.

The peaks located between 487 and 303 cm^{-1} are assigned to the bending vibrations of the bridging V–O–V (doubly coordinated oxygen), and the triply coordinated oxygen (V_3–O) bonds, respectively. Two more low-frequency Raman peaks at 165 and 122 cm^{-1} can be distinguished which correspond to the lattice vibration. These two peaks are strongly associated with the layered structure. There are two broad peaks at 645 and 712 cm^{-1} due to the stretching vibration modes of the V_3–O and V_2–O bonds in a disordered V–O–V framework, respectively. These peaks appear as different two peaks at the asdeposited sample, 2 shots, 5shots and 10 shots, and appear as single peak at 25 shot and 100 shots. This real shows that laser heated the sample as a result of breaking of V-O bonds [69-71].

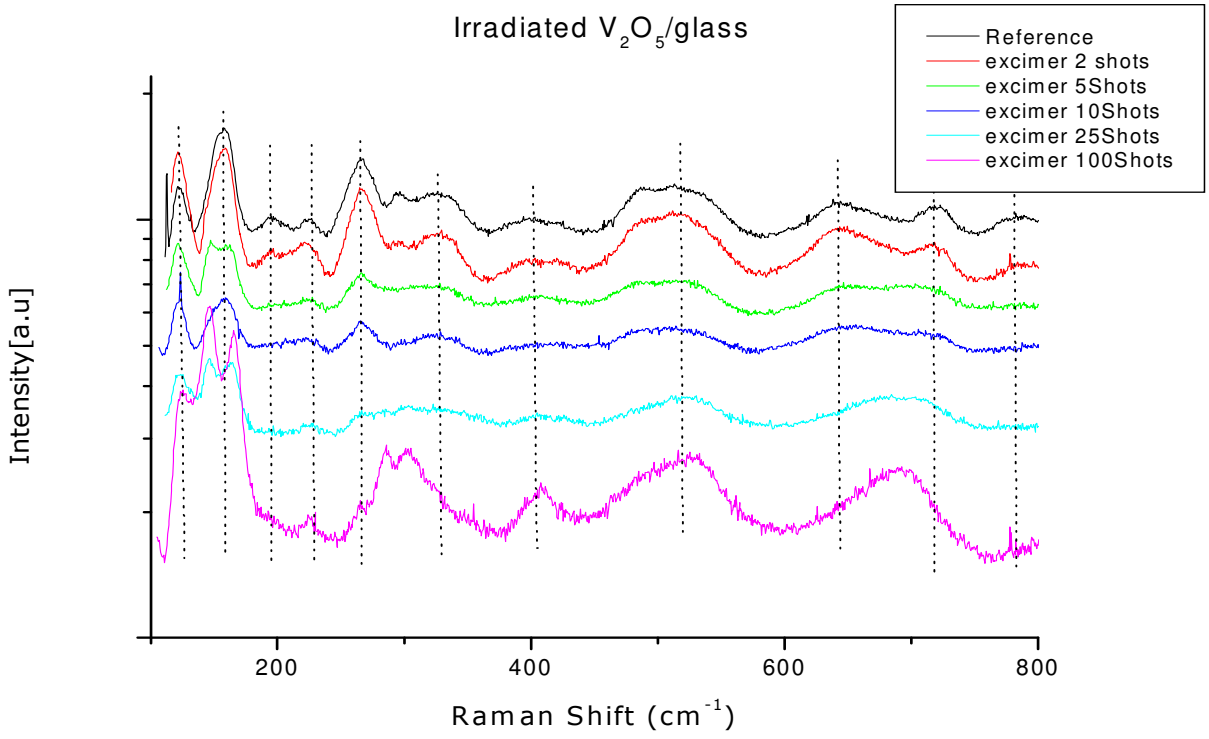

Figure 4-16: *The Raman spectra of the samples irradiated with the excimer laser.*

4.9 Optical properties of laser irradiated samples by FTIR

The FTIR measurements were also performed on the irradiated samples (see Figure 4-17). In order to compared the effect of laser in V_2O_5 film, the V_2O_5 film was irradiated with different doses including 1 shot, 2 shots, 5 shots, 10 shots, 25 shots and 100 shots. The first three irradiations (1, 2 and 5 shots) were from the film of the same deposition standard. The last three irradiations (10, 25 and 100 shots) were performed from the different asdeposited as the first three irradiations. Therefore the two different asdeposited films showed different transmittance due to the different thickness. The different reference samples come from the fact there was no standard tool to deposit uniform film. The samples also start transmitting exponential approximately from 2000 cm^{-1}. The highest transmittance of the sample is around 9 %T. The stretching of bonds was determined at A=2872 cm^{-1} and B=3497 cm^{-1}, which is C-H and O-H bonds, respectively. According to theoretical V-O FTIR spectrum, stretching in V=O bond is found at the range of 400-1800 cm^{-1} and V-O-V stretching is found at 650-800 cm^{-1} [68].

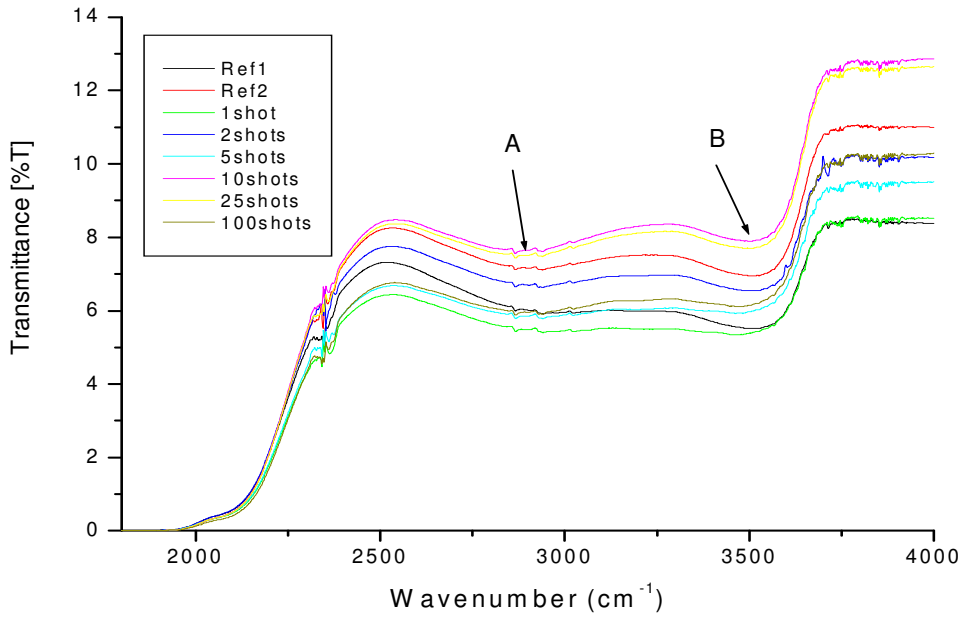

Figure 4-17: *The FTIR spectra for the laser irradiated V_2O_5 film.*

4.10 Optical properties of laser irradiated samples by UV-Vis

This technique was used to study the effect of laser doses on the V_2O_5 film. Figure 4-17 are the spectra of the laser irradiated samples for 1 shot, 2 shots, 5 shots, 10 shots, 25 shots and 100 shots. The irradiation was done in two different, pre-fabricated films. This was done such that the two films were fabricated in different thicknesses. According to the observations in the spectrum, the irradiated V_2O_5 coating is transmitting in the visible light as well as infrared region of the EM wave spectrum. The maximum transmittance of the non-calcined is approximately 31 %, which could be due to the thickness of the film or the formation of the crystals on the surface of the film.

The absorption cut-off is shifting proportional to the increase of laser doses. The slightly change in band gap calculated in table 4-6, which confirms XRD results of changing in crystal structure (orthorhombic to tetragonal). The calculated band gap of the non-heated V_2O_5 film is 3.3 eV and the theoretical band gap is 3.35 eV. In conclusion, the band gap of the laser irradiated V_2O_5 film is depending on the wavelength of absorbance.

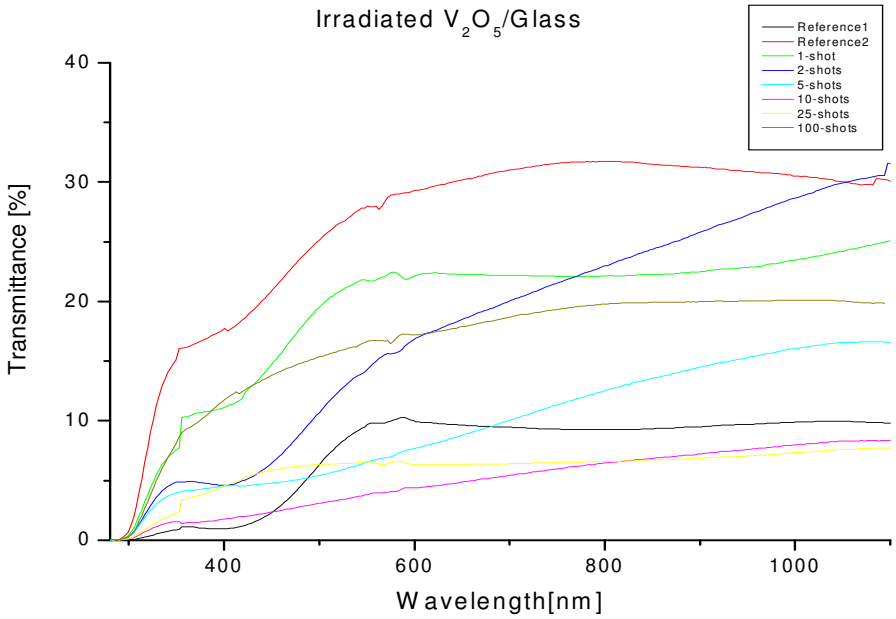

Figure 4-18: *UV-Vis measurements of the laser irradiated film.*

No. of shots	λ (nm)	Eg (eV)
Non-irradiated	371	3.4
1	337	3.7
2	350	3.5
5	335	3.7
10	359	3.5
25	328	3.8
100	345	3.6

Table 4-6: *Calculated band gap of the laser irradiated V_2O_5 film.*

4.10.1 Determination of composition and thickness of film by RBS

In order for the thickness and the composition of the film to be known, the RBS measurements were performed. This technique was also use to determine the impurities present in the film. The machine was calibrated using standard materials such as platinum (Pt), palladium (Pd), titanium (Ti), silicon (Si), silicon dioxide (SiO_2) and carbon (C). During calibration (see Fig. 4-19), the slope and offset were determined as 3.899 KeV/Channel and 69.308 KeV, respectively. The simulation (see Fig. 4-20) was done in layers; layer one was the film consisting of vanadium, oxygen and carbon. The concentration was determined as v = 0.36, o = 1 and c = 0.02. The thickness of the first layer (film) determined using RUMP program was 2010 x 10^{15} at/cm^2. The calculated thickness using SRIM program was determined as 318 nm. The second layer was the corning glass substrate consisting of silicon, oxygen calcium, magnesium, aluminum and sodium. During simulation, the concentration was determined as Si = 0.18, O = 0.45, Ca = 0.035, Mg = 0.023 and Al = 0.002.

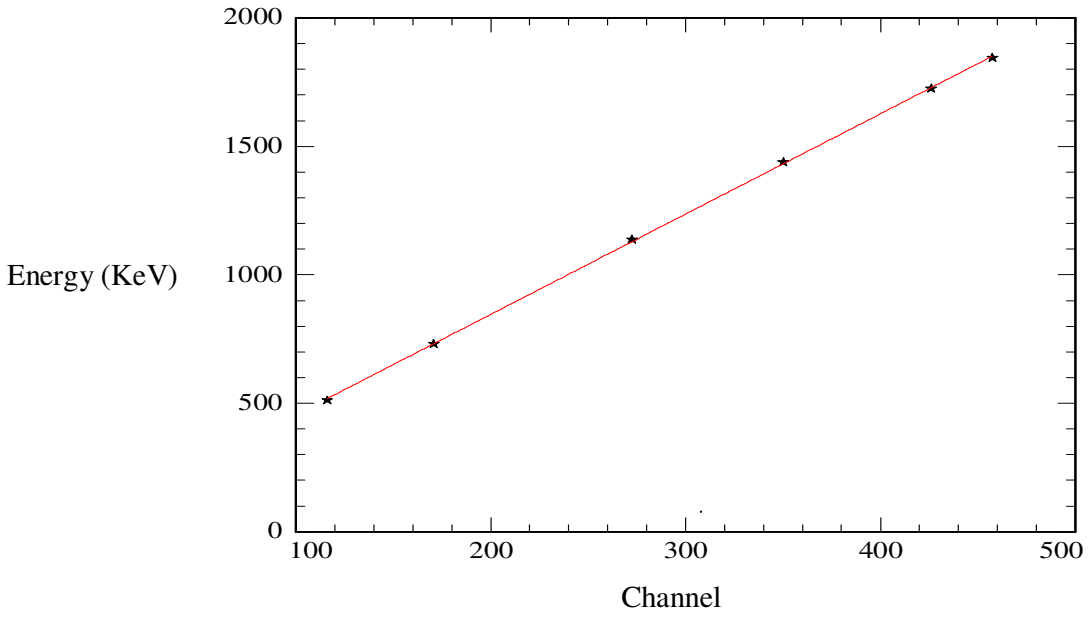

Figure 4-19: *The calibration of RBS technique*

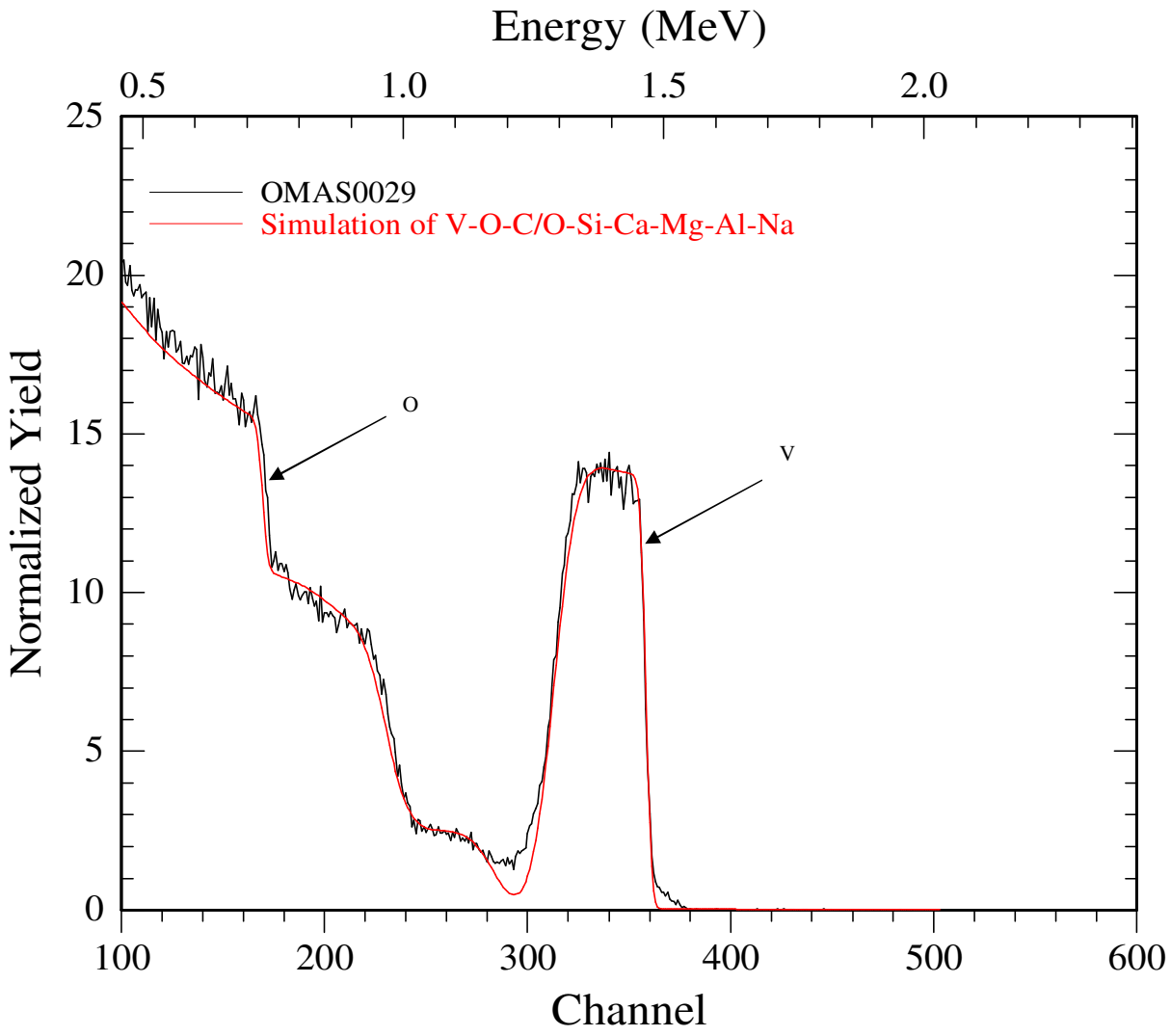

Figure 4-20: *The simulated RBS spectrum showing the thickness of the film.*

4.10.2 Determination of hydrogen concentration using ERDA technique

The ERDA is interfaced with RBS, i.e. they are using same beam in the microprobe. These ERDA measurements were performed in order to determine the hydrogen concentration present in the V_2O_5 film since it is from V_2O_5 sol-gel. During the striking of positive ions to solid target (V_2O_5 film on a substrate), enough energy is transferred from the incident ion to the target nucleus. There is an energy loss (from scattered particles) which is determined between the initial beam energy and the final beam.

In this experiment, Mylar foil was used to block only the heavy ions and allow only light element such as hydrogen to pass through and get detected. The Kapton material ($C_{22}H_{10}N_2O_5$) was used as the standard material for calibration. This material has a tendency of releasing more hydrogen ions. Its hydrogen concentration is approximately 30 at %. This material was bombarded with ion beam of different energies (3 MeV, 2.5 MeV, and 2 MeV). The hydrogen concentration of prepared V_2O_5 samples was calculated using SIMNRA program. The calculations were done in layer form and they showed that H-concentration is decreasing as the channel and energy are decreasing. The average concentration of hydrogen was determined as 0.896%. During simulation (see figure 4-21), some crucial parameters for calibration such as the offset and slope were calculated. The offset and slope were calculated as 42.5 and 2.3, respectively. These parameters were calculated using RUMP program which is normally used for RBS simulation. The thickness of the film was determined as $3000x10^{15}$ Atoms/cm^2. The collected charge used was $1.48x10^{-3}$ μC and the detector solid angle of $1.48x10^{-3}$ sr.

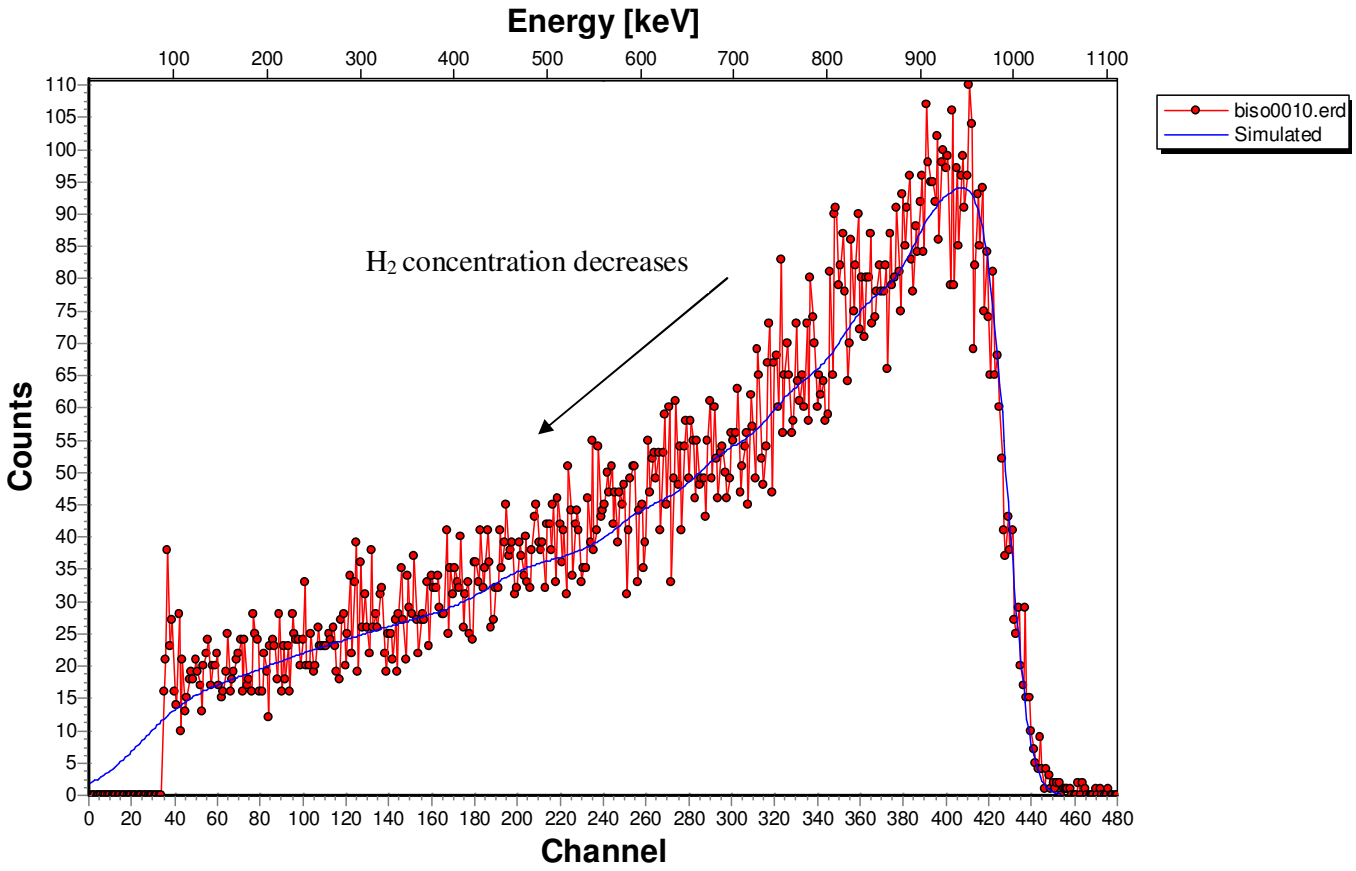

Figure 4-21: *The simulated ERDA spectrum for hydrogen concentration.*

CHAPTER 5 -Conclusion

5.1 Summary and conclusion

In this project, the reduction and characterization of heated V_2O_5 to form VO_2 has been carried out. All the reduction of V_2O_5 sol-gel was done in three different techniques namely: H_2/Ar gas, CO/CO_2 gas and laser ablation. After the analysis of the samples was done, there are some conclusions drawn up from the obtained results.

Summary of reduced V_2O_5 samples under H_2/Ar gas:

The surface morphology which was studied using SEM showed the increase in number of grains after heating the sample. The crystals obtained after heat treatment at high temperature were rod-like shape. The AFM results also confirmed the increase of crystals on the surface of the film. According the AFM results, maximum roughness and the average root mean square roughness are decreasing as the film is heated at high temperature. The crystallography analysis of heat-treatment of the film was studied with XRD technique and showed the slightly reduction of V_2O_5 to V_6O_{13} by H_2/Ar gas. The intensity of V_2O_5 diminishing as the heat treatment is done at high temperatures. The optical results were not presented since silicon wafer is not transmitting in visible light region.

Summary of reduced V_2O_5 samples under CO/CO_2 gas:

The CO/CO_2 gas was effectively employed to reduce V_2O_5 to VO_2 thin films. The both as-deposited and the heated samples under this reducing gas were studied their surface morphology using SEM. The SEM images showed grains on a surface of the film before and after the heat-treatment. It was found that the as-deposited and the 600^0C heated samples have similar morphologies of agglomerated particles on the film surface. In measurements it showed that the rods found in the as-deposited film were in the scale of microns and after sample

has been annealed at 600^0C, the rods were in the scale of nanometers. The EDS analysis was also done since EDS is interface with SEM. The EDS spectrum showed the *K-beta* and *K-alpha* peaks of vanadium and their corresponding atomic weight. The AFM results confirmed the SEM results, after heat-treatment at low temperature 450^0C, the number of grains increases and forms rods at temperature of 600^0C. The roughness of the film also increased after annealing from 8.24nm to 11.8nm.

The crystallography of these samples were studied using XRD technique, it was found that the as deposited sample is pure orthorhombic V_2O_5 with the space group of P_{mn21}. The lattice parameter were calculated as a= 11.5 Å and c=4.350 Å. The XRD revealed that 3500C is a promising temperature of reducing V_2O_5 to VO_2. This sample was found to have two VO_2 peaks: (-202) and (402).

The optical measurements were done by UV-Visible and the film showed the low transmittance. The low transmittance is due to the thickness of the film and the non-oriented particles on the film. It is also shown that the absorption cut-off is shifting with respect to the annealing temperature. However, this phenomenon shows the presence of different phases with different band gaps. The FTIR which was used to study optical properties and the stretching of bonds showed the less transmittance due to thickness of the film, and the stretching of C-H bond approximately 2846 and 2920 cm^{-1}. The Raman was also used to find the stretching bonds. The weak intensity was observed at low frequency between 200 and 450cm^{-1}, which is associated with the bending vibration modes of the V_3–O, V_2–O and V=O. The Raman spectrum of asdeposited film shows two broad peaks around at 496 and 535 cm^{-1}, due to the stretching modes of the V–O–V and V_3–O bonds, respectively.

Summary of reduced V_2O_5 samples reduced by laser irradiation:

In this reduction technique, the SEM images showed the interesting surface morphology of V_2O_5 rods changing into V_2O_5 hollow spheres after laser irradiation. The AFM images also confirmed the dramatic change of V_2O_5 rods to V_2O_5 hollow spheres. However, the hollow spheres were not clearly under AFM as the SEM images. The crystallography was studied using XRD; the results showed the shift in phases after laser irradiation. This phenomenon shows the stretching of V-O bonds during laser heating, which causes the crystal lattice to vibrate. The vibration of atoms also causes the change in crystal structure as it was found that orthorhombic V_2O_5 changed to tetragonal structure.

The UV-Vis showed that the film transmittance decreasing as the heat treatment as has been performed to the film. In the results showed by UV-Vis measurements, the absorption cut-off is shifting with respect to the annealing temperature. This can be caused by the variation of the band gap or not being uniform of the film. The optical properties, vibration modes and the stretching of V-O bonds were studied using FTIR. The irradiated film is transmitting very low in the IR region due to film thickness and the increase of hollow spheres. It was also found the similarities of irradiated film with the CO/CO_2 sample, it was observed that the absorption cut-off shifting with respect to number of doses. The stretching in O-H bond was determined between 3600 and 3200 cm^{-1} due to the V_2O_5 sol-gel. The stretching of C-H bond was also found at at 2863 cm^{-1} and 2936 cm^{-1}.

The vibration modes and stretching of V-O bond was studied using Raman. The peaks located between 487 and 303 cm^{-1} were assigned to the bending vibrations of the bridging V–O–V and V_3–O bonds, respectively. The broad peaks were found at 645 and 712 cm^{-1} due to the stretching vibration modes of the V_3–O and V_2–O bonds in a disordered V–O–V framework, respectively.

The RUMP program was used to analyze RBS measurements which showed exactly the elements present in our film. This type of program also showed which elements is the substrate was made of. Determination of thickness of the film was using RUMP was very important to pursue with other calculations.

The SIMNRA program was used to analyze the ERDA measurements. The aim for these measurements was the determine hydrogen concentration since the film was from V_2O_5 sol-gel. In the measurements, hydrogen concentration was seen decreasing as the channel decreases. This was seen as directly proportional to the decrease in energy.

In comparison of the three V_2O_5-VO_2 reduction techniques, the CO/CO_2 is the promising to reduce V_2O_5 to VO_2 thin films. The three vital parameters in this technique are; temperature, time and flow rate of the reducing gas. The heat treatment is also promising with the slightly reduction of V_2O_5 to VO_2 film. Laser irradiation is long process to reduce V_2O_5 to VO_2 thin films. The further research of VO_2 coatings should be studied to improve too dark colour and unappealing of the film. A deeper scientific understanding of how thermochromics work is still required and some of the processes used to make VO_2 coatings are not easy to control.

REFERENCES

[1] H. Cui, V. Teixeira, L. Meng , R. Wang , J. Gao , E. Fortunato. Thermochromic properties of vanadium oxide films prepared by dc reactive magnetron sputtering. Thin Solid Films 516 (2008) 1484–1488

[2] D. Vernardou, M.E. Pemble, D.W. Sheel, Vanadium oxides prepared by liquid injection MOCVD using vanadyl acetylacetonate. 188–189 (2004) 250– 254

[3] Y. Kim, S. Gopukumar, K. Kim, B. Cho, Performance of electrostatic spray-deposited vanadium pentoxide in lithium secondary cells. 117 (2003) 110–117

[4] S. Mickevicˇius, V. Bondarenka , S. Grebinskij , H. Tvardauskas, M. Andriulevicˇius , S. Tamulevicˇius , S. Kacˇiulis, The metals chemical states in hydrated vanadium oxides. 40 (2009) 126–129

[5] J. ´Swiatowska-Mrowiecka , F. Martin , V. Maurice , S. Zanna, Klein, J. Castle, P. Marcus, The distribution of lithium intercalated in V_2O_5 thin films studied by XPS and ToF-SIMS. 53 (2008) 4257–4266

[6] E. Shouji 1, D. A. Buttry, EQCM measurements of solvent transport during Li^+ intercalation in V_2O_5 xerogel films. 45 (2000) 3757–3764

[7] T. Maruyama, Y Ikuta, J. Mater. Sci. 28 (1993) 5073-5078

[8] L.A. Ryabova, A. Serbinov, A.S. Darevsky. J. Electrochem. Soc. 119 (1972) 427-429

[9] M.B. Sahana, M.S. Dharmaprakash, S.A. Shivashankar. J. Mater. Chem. 12 (2002) 333-338

[10] I. Takahashi, M.Hibino, T. Kudo, Jap. J. Appl. Phys. 35 (1996) L438-L440

[11] I. Takahashi, M. Hibino, K. Tetsuichi, Jap. J. Appl. Phys. 40 (2001) 1391-1395

[12] I.P. Parkin, Troy D. Manning, Intelligent Thermochromic Windows. 83 (2006) 393-400

[13] H.K. Pulker, Coatings on Glass (Second Edition), 1999, Pages 103-317

[14] F. Béteille, F.J. Livage. J. Sol-Gel Sci. Technol. 13 (1998) 915-921

[15] F. Béteille, F. Livage. J. Mater. Res.Bull. 32 (1997) 1109-1117

[16] S.W Lu, L.S. Hou, F.X. Gan, J. Mater. Sci.Lett. 15 (1996) 856-857

[17] E. Cavanna, J.P. Segaud, F. Livage, J.Mater.Res.Bull. 34 (1999) 167-177

[18] T.J. Hanlon, J.A. Coath, M.A Richardson. Thin Solid Films 436 (2003) 269- 272

[19] F. Béteille, F.J. Livage. J. Sol-Gel Sci. Technol. 13 (1998) 915-921

[20] V. Keppens, D. Mandrus, L.A. Boatner. Chemical and Sonochemical Approaches to the formation of VO_2 and VO_2-impregnated materials. 495 (1998) 439

[21] A. Block-Bolten, J. M. Bertrand, S. N. Flengas. Oxidation of CO to CO_2 in Melts Containing V_zO_s and Alkali Oxides. 52 (1974) 2068

[22] G. Guzman, F. Béteille, R. Morineau, J. Livage. J. Mater. Chem. 6 (1996) 505-506

[23] C.Q. Feng, S.Y.Wang, R. Zeng, Z.P. Guo, K. Konstantinov, H.K. Liu, Synthesis of spherical porous vanadium pentoxide and its electrochemical properties. 184 (2008) 485–488

[24] A. Cao, J. Hu, H. Liang, L. Wan, Self-Assembled Vanadium Pentoxide (V_2O_5) Hollow Microspheres from Nanorods and Their Application in Lithium-Ion Batteries. 44 (2005) 4391-4394

[25] C.V. Ramana, O.M. Hussain, B. Srinivasulu Naidu, P.J. Reddy, Spectroscopic characterization of electron-beam evaporated V_20_5 thin films. 305 (1997) 219-226

[26] A. Chakrabarti, K. Hermann, R. Druzinic, M. Witko, F. Wagner, M. Petersen, Geometric and electronic structure of vanadium pentoxide:A density functional bulk and surface study. 59 (1999) 583-590

[27] Y. Ningyi, L. Jinhua, L. Chenglu: Valence reduction process from sol-gel V_2O_5 to VO_2 thin films. 191 (2002) 176-180

[28] J.B. Kana Kana. Reversible Tunability in Novel Utrafast Nanoplasmonics Synthesis and Characterization of Au-VO_2 Nanophotonics. PHD Thesis (2008) 1-98

[29] C.B. Greenberg. Thin Solid Films. 110 (1983) 73-82

[30] Y. Takahshi, M. Kanamori, H. Hashimoto, Y. Moritani, Y. Masudi. J. Mater. Sci. 24 (1989) 192-198

[31] Optical Properties and Spectroscopy of Nanomaterials**.** available online (16/10/2009)
http://www.worldscibooks.com/etextbook/7093/7093_chap01.pdf

[32] D. Johansson, VO_2 films as active infrared shutters. MSc Thesis (2006). Available online (01/06/2009)
www.ifm.liu.se/ar/2006.pdf

[33] M.N. Field, I.P. Parkin. J. Mater. Chem. 10 (2000) 1863-1866

[34] F. Guinneton, L. Sauques, J. Valmalette, F. Cros, J Gavarri Optimized infrared switching properties in thermochromic vanadium dioxide thin films: role of deposition process and microstructure. 446 (2004) 287–295

[35] F. Guinnetona,b, L. Sauquesb, J. Valmalettea, F. Crosb, J. Gavarria, Role of surface defects and microstructure in infrared optical properties of thermochromic VO_2 materials. 66 (2005) 63–73

[36] Y.L. Wang , M.C. Li, L.C. Zhao, The effects of vacuum annealing on the structure of VO_2 thin films. 201 (2007) 6772–6776

[37] H. Wang, X. Yi, Y. Li, Fabrication of VO_2 films with low transition temperature for optical switching applications. 256 (2005) 305–309

[38] C. Piccirillo, R.l Binions, I.P. Parkin, Synthesis and characterisation of W-doped VO_2 by Aerosol Assisted Chemical Vapour Deposition. 516 (2008) 1992–1997

[39] J. Shi, S. Zhou, B You, L. Wu, Preparation and thermochromic property of tungsten-doped vanadium dioxide particles. 91 (2007) 1856–1862

[40] J.B. MacChesney, J.F. Potter, H.J. Guggenheim. J Electrochem. Soc. Solid State Sci. 115 (1968) 52-55

[41] F. Béteille, F. Livage. J. Mater. Res.Bull. 32 (1997) 1109-1117

[42] W. Burkhardt, T. Christmann, B.K. Meyer, W. Niessner, D. Schalch, A. Scharmann. Thin Solid Films 345 (1999) 229-235

[43] P. Jin, S. Nakao, S. Tanemura. Thin Solid Films. 324 (1998) 151-158

[44] P. Jin, S. Tanemura. Jap.J.Appl.Phys. 34 (1995) 2459-2460

[45] T.E Phillips, R.A Murray, T.O. Poehler. Mater. Res.Bull. 22 (1987) 1113-1123

[46] G. Golan, A. Axelevitch, B. Sigalov, B. Gorenstein, Metal–insulator phase transition in vanadium oxides films. 34 (2003) 255–258

[47] B.D. Cullity, Elements of X-ray diffraction, 2nd Edition, pp 81-99 (Addison-Wesley publishing company, 1978)

[48] J. R. Connolly. Introduction to X-Ray Powder Diffraction, spring 2003 (available online, 03/07/2008)

epswww.unm.edu/xrd/xrdclass/01-XRD-Intro.pdf

[49] S. Hussain, Investigation of Structural and Optical Properties of Nanocrystalline Zn, MSc. Thesis. (Available online, 04/11/2009)

www.google.com

[50] G. Binning, C.F. Quate, Ch. Geber, Atomic Force Microscope, Phys. Rev. Letters, 56 (1986) 930

[51] H. Hoper, T. Gesang, W. Possart, O.D. Hennemann, and S. Boseck,Optimizing AC-Mode Atomic Force Microscopy, Scanning, 18 (1996) 339-343

[52] A. Ulcinas, V. Snitka, Intermittent contact AFM using the higher modes of weak cantilever, Ultramicroscopy. 86 (2001) 217-222

[53] Y. Martin, C.C. Williams, H.k. Wickramasinghe, Atomic Force Microscopy-force mapping and profiling on a sub 100 scale, J. Appl. Phys. 61 (10) 4723

[54] M.T. P Postek, K.S. Howard, A.T. Johnson, K.L. McMiche, Scanning Electron Microscopy (Ladd Research Industries, 83 Holly court, Williston, Vermont, 2001)

[55] P.J. Goodhew, T. Humpreys, R. Branland, Electron Miscroscopy& analysis Third edition, pp 122-166-(Taylor & Francis Group, Jan 2001)

[56] L.C. Feldman, J.W Mayer, S.T. Picraux, Materials Analysis by Ion Channeling. (Academic Press, 1982)

[57] C.P. Hobbs, J.W McMillan, D.W. Palmer, "The effects of surface topography in nuclear microprobe Rutherford backscattering analysis". Nucl. Inst. and Meth. 30 (1988) 342–348

[58] L.C. Feldman and J.W. Mayer, Fundamentals of surface and thin film Analysis pp 13-38 (Elserivier Science Publishing Company, 1986)

[59] J. Tirira, Y. Serruys and P. Trocellier, Forward Recoil Spectrometry (Plenum Press, New York, 1996)

[60] G. Boudreault, accurate beam analysis, 33 (2002) 478

[61] A. Richardson and J. Messman, Calibration and Validation of UV-VIS Absorption Spectrophotometers. 10 (1997) 7

[62] R. Mavrodineanu and R. Burke, "Chemical Calibration Standards for Molecular Absorption Spectrometry," Advances in Standards and Methodology in Spectrophotometry, C. Burgess and K.D. Mielenz, Eds. (Elsevier Science Publishers B.V, Amsterdam, The Netherlands), 1987, pp 125-174.

[63] C.P. Sherman Hsu, Infrared Spectroscopy, Chapter 15 (Available online, 24/10/2009)

www.prenhall.com/settle/**chapter**s/ch15.pdf

[64] F.A. Settle, Handbook of Instrumental Techniques for Analytical Chemistry. Chap. 16 93(1997) 481-495

[65] P. D. Simonson, an Introduction to Raman Spectroscopy and the Development of SERS. (Online 24 /01/ 2009).

www.google.com

[66] W. Lambrecht, B. Sjafari-Rouhani , J. Vennik, J. Phys. C: Solid State Phys., 19 (1986) 369.

[67] R.M. Wentzcovitch, VO_2: Peierls or Mott-Hubbard? A View from Band Theory. 72 (1994) 3389-3392

[68] Y.L. Wang, M.C. Li, L.C. Zhao The effects of vacuum annealing on the structure of VO_2 thin films. 201 (2007) 6772–6776

[69] S. Lee, H. M. Cheong, M. J. Seong, P. Liu, C. E. Tracy, A. Mascarenhas, J. R. Pitts, S. K. Deb, Raman spectroscopic studies of amorphous vanadium oxide thin films. 165 (2003) 111 – 116

[70] Q. Su, C.K. Huang, Y.Wang, Y.C. Fan, B.A. Lu,W. Lan, Y.Y.Wang, X.Q. Liu, Formation of vanadium oxides with various morphologies by chemical Vapor deposition. 475 (2009) 518–523

[71] V. V. Fomichev, P.I. Ukrainskaya, T. M. Ilyin, "Vibrational spectra and electrostatic fields of V_2O_5 and lithium vanadium bronzes", Spectrochimica Acta part A 53 (1997) 1833-1837.

[72] Z. Liu, G. Fang, Y. Wang, Y. Bai and K. Yao, Laser-induced colouration of V_2O_5, 33 (2000) 2327-2332

[73] A. Surca, B. Orel, Electrochimica Acta 44 (1999) 3051-3057

[74] X. J. Wang, H. D. Li, Y.J. Fei, X. Wang, Y. Y. Xiong, Y. X. Nie, K. A. Feng, "XRD and Raman study of vanadium oxide thin films deposited on fused silica substrates by RF magnetron sputtering", Appl. Surf. Sci., 177 (2001) 8-14